Title
The Role of Dendrites in the Organization of Functional Neural Circuits for Motion Detection in the Retina

Author
El-Quessny, Malak

Publication Date
2021

Peer reviewed|Thesis/dissertation

The Role of Dendrites in the Organization of Functional Neural Circuits for Motion Detection in the Retina

By

Malak Yasser El-Quessny

A dissertation submitted in partial satisfaction of the

requirements for the degree of

Doctor of Philosophy

in

Neuroscience

in the

Graduate Division

of the

University of California, Berkeley

Committee in charge:
Professor Marla B. Feller, Chair
Professor Ehud Isacoff
Professor Teresa Puthussery
Professor Hillel Adesnik

Spring 2021

The Role of Dendrites in the Organization of Functional Neural Circuits for Motion Detection in the Retina

Abstract

The Role of Dendrites in the Organization of Functional Neural Circuits for Motion Detection in the Retina

By

Malak Yasser El-Quessny

Doctor of Philosophy in Neuroscience

University of California, Berkeley

Professor Marla B. Feller, Chair

Retinal ganglion cells (RGCs) represent the output computations of the visual world. In the mouse, they represent >30 parallel channels of visual processing, encoding both image-forming and non-image forming features. The dendrites of RGCs are considered essential in ensuring that the downstream visual system receives a full depiction of the sampled visual field. Different retinal ganglion cell types have evolved a multitude of dendritic arbor architectures that allow them to efficiently encode the spatial and temporal features of the visual scene that they are tuned to. Despite this fundamental role of dendritic morphology, there are relatively few studies that directly test whether different dendritic morphologies lead to variations in the wiring and resulting computations within a neural circuit.

This main body of this work has aimed to address this question in a well-defined neural circuit in the retina that is responsible for our ability to detect the direction an object moves in the visual world. Direction selectivity is a neural computation where a directionally selective retinal ganglion cell (DSGC), one of the output neurons of the retina whose axons comprise the optic nerve, fire more action potentials in response to motion in one direction, versus motion in the opposite direction. Multiple presynaptic mechanisms involving the specific wiring of excitatory and inhibitory inputs onto DSGC dendrites have been postulated to contribute to the direction selectivity computation. Additionally, postsynaptic computations within the DSGC dendrites have been postulated to sharpen their directional tuning

Here, we explore how DSGC dendrites contribute to both the presynaptic organization of excitatory and inhibitory inputs, and the postsynaptic contribution to directional tuning. First, we show that visual experience influences the dendritic orientation in a population of asymmetric ventral preferring DSGCs (vDSGCs) whose dendrites point ventrally. By comparing the tuning of normally versus dark-reared vDSGCs, we find that their tuning to ventral motion is preserved regardless of their dendritic orientation. This is due to the persistence of asymmetric wiring of inhibition in dark-reared vDSGCs. However, we find that the ventral orientation of vDSGC dendrites is necessary for their postsynaptic directional computation, which occurs in the absence of inhibitory input. Hence, in vDSGCs, dendritic morphology dictates postsynaptic but not presynaptic mechanisms for directional computation.

Second, we show that dendritic morphology, across two distinct populations of DSGCs, does not determine the organization of presynaptic inputs. By comparing the excitatory and inhibitory receptive fields across two morphologically distinct DSGC subtypes, we find that although asymmetric DSGCs exhibit greater tuning of their inhibitory input in response to a moving stimulus, compared to symmetric DSGCs, the synaptic organization of excitation relative to inhibition is comparable across cell types. Hence, DSGC dendritic morphology does not dictate the organization of excitatory and inhibitory synaptic inputs relative to each other.

Dedication

This work is dedicated to my incredible family:
my parents, Amira and Yasser
and my other parents, my siblings, Mariam and Moe.
Nothing will ever separate us.

To my nephew and nieces: Taha, Karima and (little) Amira.
For bringing me the purest form of joy.
Whose infinite curiosity reminds me why I live to learn about nature.

And finally, again and again and again
To the one whose voice forever echoes in my heart
My mom: the architect, the mother, the daughter, the sister
who dreamed and loved and never stopped doing so.
My best friend and confidant.
I dedicate this work, my life, and all other accomplishments to you, mammy.

I hope you are always smiling upon me.

TABLE OF CONTENTS

CHAPTER 3: Spatially Offset Inhibition does not Determine Retinal Direction Selectivity and is not Organized by Dendrites

CHAPTER 4: Conclusions and future directions

CHAPTER 1:
Introduction to the role of dendrites in retinal direction selectivity.

Since Santiago Ramón y Cajal's observation of Golgi-stained brain tissue, scientists have marveled at the intricacy and diversity exhibited by the branches emanating from a neuron's cell body: their dendrites. Within and across neuronal types, dendrites vary in their shape, their size, asymmetry, orientation and branching complexity. Like the branches of a tree determine their exposure to sunlight and rainwater, dendritic shape is thought to determine the locations from which a neuron receives its synaptic inputs, the number of synaptic inputs it receives, and the types of synapses that will form.

How does dendritic morphology affect its function within a neural circuit? The shape of a neuron's dendritic tree determines its function by influencing how synaptic information is received and inegrated (Stuart & Spruston, 2015). This relationship is perhaps seen most clearly in neurons of sensory systems, where the shape of the dendritic arbor is the primary determinant of the shape of the receptive field. The dendritic arbor of a neuron is thought to define the region of the world from which it receives input, either directly from sensory receptors or indirectly via synapses (Peichl & Wässle, 1983). A second aspect of dendritic shape, the arbor's branching pattern, determines the density with which a neuron samples this field. Complex dendrites with high branch number and branching frequency can capture inputs from numerous presynaptic partners, whereas simple arbors sample more sparsely. Features such as dendrite diameter, distance from the soma, and the number of branches also determine function by influencing the probability that an excitatory postsynaptic potential (EPSP) produced at a given synapse will contribute to the firing of the neuron (Magee, 2000). Furthermore, nonlinear effects on synaptic efficacy arise from having multiple inputs on the same dendritic branch (London & Häusser, 2005; Spruston, 2008), further implicating dendritic morphology in influencing the organization of synaptic inputs and sampling of the sensory world.

How, in turn, does circuit function affect dendritic morphology? Afferent signaling is of particular importance to the process of dendritic growth and patterning. First, the timing of afferent innervation and synapse formation coincides with the period of maximum growth and dendritic remodeling. Second, neurotransmission, evoked either spontaneously or by sensory input, triggers changes in intracellular calcium levels that affect the dendritic cytoskeleton (Lefebvre et al., 2015). For example, severing afferent inputs to the nucleus laminaris (NL) of the chick auditory brainstem, or spike suppression by TTX application, leads to NL neurons with smaller dendritic tufts (Deitch & Rubel, 1984; Wang & Rubel, 2012). Conversely, unilateral removal of a cricket's auditory organ leads postsynaptic neurons to sprout dendrites to the contralateral organ (Hoy et al., 1985). Third, afferent inputs use a variety of molecular signals in addition to neurotransmitters to communicate with postsynaptic dendrites. One important category of signals involved in dendritic growth are neurotrophins. The neurotrophin family of molecules have been implicated in regulating dendrite elaboration in a variety of cell types, influencing both the shape and size of the dendritic arbor (Liu et al., 2009; Lom & Cohen-cory, 1999; Mcallister et al., 1995). For example, in the mouse cerebellum, parallel fiber afferents onto purkinje cells secrete Neurotrophin-3, which signals through TrkC receptors on the purkinje cell dendrites, promoting the expansion of its dendritic arbor (Joo et al., 2014), such that neighboring purkinje cells with less TrkC receptor expression exhibit diminished dendritic arbor territories.

Hence, neural circuit function is correlated with changes in the dendritic morphology of neurons across the nervous system.

Though a great deal of progress has been made in characterizing the development of dendrites (Lefebvre et al., 2015) and dendritic spines (Alvarez & Sabatini, 2007), we still know relatively little about how a neuron's specific morphology is influenced by its function within a circuit or how its morphology contributes its function at the circuit level.
By elucidating the developmental mechanisms that coordinate the wiring of neural circuits with distinct dendritic structures, we can learn more about what dendrites do and how their dendritic fields organize into functional circuits.

To this end, the mammalian retina has served as an excellent system for the investigation of the role of activity, both spontaneous and visually evoked, in the development of dendritic arbor morphology, synaptic specificity and neural circuit computations. Retinal circuits assemble in various configurations such that current estimates indicate that incoming visual signals are processed by 30 parallel processing streams within 30 separate (Baden & Euler, 2016; Sanes & Masland, 2015). Within each retinal circuit, distinct subsets of the five retinal cell types (Figure 1) selectively assemble to detect distinct visual features like luminance, contrast and motion. The diversity of retinal circuit connectivity is highlighted one of the retina's synaptic layers, the inner plexiform layer (IPL), where the visual signal diverges from 12-14 bipolar cell types to 30-50 amacrine and ~40-50 ganglion cell types (Baden et al., 2016; Franke et al., 2017; Helmstaedter et al., n.d.; Sanes & Masland, 2015).

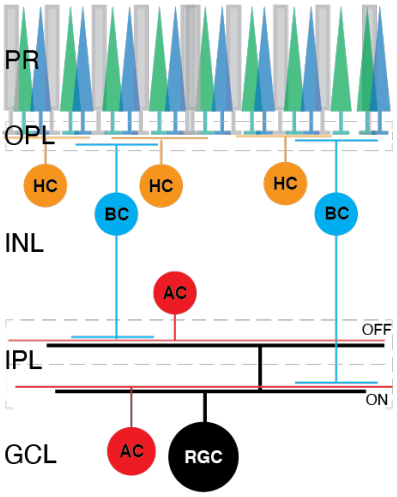

Figure1: Simplified schematic of the retinal circuit. PR: photoreceptor layer, INL: Inner nuclear layer, IPL: Inner Plexiform Layer, GCL: Ganglion Cell Layer. Grey boxes indicate synaptic layers. ON and OFF sublamina of

In this thesis, I explore the role of dendritic morphology in organization of a distinct retinal circuit that selectively encodes the direction of motion and is called the direction-selective (DS) circuit.

Direction selectivity in the retina

When we navigate through our natural environment, light projects images from the outside world through our pupils, where they are focused by our lenses and then onto the retina. During this motion, the images projected onto the retina are constantly updating due to a combination of self-motion, resulting from our own head and eye movements, and object motion in the visual field. In order to achieve appropriate visual reflexes, perception and visually guided behavior necessary to navigate our environments, the visual system has evolved an essential function of motion detection - a neural computation which starts in the retina.

The main body of work on retinal motion processing investigates one of these distinct retinal circuits that selectively encodes the direction of motion and is called the direction-selective (DS)

circuit. In the mammalian visual system, direction selectivity was first observed in the spiking pattern of direction-selective ganglion cells (DSGCs) by Barlow, Hill and Levick (Barlow & Hill, 1963; Barlow & Levick, 1964), where DSGCs are maximally activated by light moving in one direction, termed their "preferred" direction, and suppressed by light moving in the opposite or "null" direction. DSGCs comprise 20-40% of ganglion cells in the mouse retina (Bos et al., 2016; Chen et al., 2014), and the discovery of different DSGC subtypes has prompted fine scale investigations of their various output properties (Morrie & Feller, 2016; Vaney et al., 2012; Wei, 2018; Wei et al., 2011). Based on their very distinct morphologies and spiking properties, ON and ON-OFF DSGCs were the first motion sensors to be studied in the retina.

Classification of DSGCs

ON DSGCs have a sustained firing pattern in response only to increments of moving light (positive motion contrast). They have large receptive field centers and large mono-stratified dendrites that co-stratify with ON amacrine cell processes and ON bipolar cell terminals. The combination of their large receptive fields, their weak surround suppression and their preferential tuning to slow velocities of motion supports their role in detecting global motion and gaze stabilization (Oyster, 1968; Sivyer et al., 2010; Wyatt & Daw, 1975). Anterograde labeling of ON-DSGCs in various transgenic animals revealed that their central projections specifically target the accessory optic system (AOS) (Simpson, 1984; Yonehara et al., 2009), an area implicated visual-oculomotor and -vestibular events such as optokinetic nystagmus (Giolli et al., 1985), supporting the hypothesis that ON DSGCs contribute to the optokinetic reflex and non-image-forming perception.

Compared to ON-DSGCs, ON-OFF DSGCs have more transient firing patterns in response to both increments and decrements of moving light (positive and negative motion contrasts, respectively). They have smaller receptive field centers and smaller bi-stratified dendrites that co-stratify with ON and OFF amacrine and bipolar cell subtypes. Population calcium imaging has revealed that ON-OFF DSGCs cluster into four subtypes: in the central retina, they cluster around the four cardinal axes of visual space: dorsal, ventral, nasal and temporal, and the clusters gradually skew towards the peripheral retina, following the axes of horizontal and vertical optic flow (Bos et al., 2016; Sabbah et al., 2017). Additionally, ON-OFF DSGCs are tuned to a broad range of image velocities and display complex receptive field properties that allow them to multiplex visual information like encoding image interruption, broad ranges of velocity, image position in visual space as well as direction (Dhande et al., 2013; Ding et al., 2021; Trenholm, Schwab, et al., 2013). This invariance to image features classifies ON-OFF DSGCs as excellent detectors of local or object motion in the visual field. In this thesis, I specifically focus my studies on ON-OFF DSGCs.

ON-OFF DSCGs mainly project to the superior colliculus (SC) and the dorsal lateral geniculate nucleus of the (dLGN) thalamus (Huberman et al., 2009; Kay et al., 2011; Rivlin-Etzion et al., 2011). Retrograde labeling of the SC combined with functional imaging of labeled RGCs, has revealed a direct inheritance of directional tuning in the SC from ON-OFF DSGCs (Shi et al., 2017). However, calcium imaging of DSGC boutons in the dLGN have revealed that dLGN neurons integrate information from multiple ganglion cell types to generate new "combined" feature representations (Liang et al., 2018; Seabrook et al., 2017). In this way, the features

encoded by an ON-OFF DSGCs are demultiplexed by being pooled with other ganglion cell outputs. The computational outcome of this step is still under investigation.

Advancements in studies of the genetic fingerprint that is postulated to exist for each ON-OFF DSGC subtype, have identified various DSGC subpopulations in transgenic animals (Morrie & Feller, 2016). Microarray expression profiling identified follastinn-like 4 (Fstl-4) as a gene that is specifically expressed in ventral motion preferring DSGCs (BD-RGCs), matrix metalloprotease 17 (MMP17) expressed in nasal preferring DSGCs, while cadherin-6 (Cdh6) and collagen25a1 (Col24a1) are expressed in vertical motion (dorsal and ventral) preferring DSGCs (Kay et al., 2011). Additionally, functional investigations of RGCs labeled in BAC transgenic mouse lines revealed a subtype of ventral preferring DSGCs expressing GFP under the Homeobox 9 (Hb9) promoter and has asymmetric ventrally pointing dendrites (Trenholm et al., 2011); two different subtypes of nasal preferring DSGCs expressing GFP under the dopamine receptor D_4 (Drd4) (Huberman et al., 2009) and the thyrotropin releasing hormone receptor (Trhr) promoters (Rivlin-Etzion et al., 2011). The extent of overlap of some of the different cellular identities is under active investigation. Nevertheless, they have offered scientists a unique tool to extensively study the genetic, molecular and physiological characteristics of the parallel DS circuits, along with their pre- and postsynaptic mechanisms for tuning.

Presynaptic mechanisms mediating direction selectivity

The direction selective computation is performed using two mechanisms: the first relies on the tuning of presynaptic excitatory and inhibitory inputs onto the DSGC; and the second relies on the postsynaptic dendritic processing properties of the DSGC itself.

To understand the role of the retinal circuit that is presynaptic to the DSGC in generating the directional computation, researchers have performed detailed characterization of the tuning of the output of each cell-type. Indeed, retinal information flows via excitatory glutamatergic synapses from the photoreceptors onto the bipolar, and from bipolar to ganglion cell synapses. Since photoreceptors encode light intensity at fixed points in the visual field, they are insufficient for motion processing since they cannot correlate these distinct points in space. There has been some debate regarding the role of bipolar cell feedforward excitation in tuning the DS circuit since calcium imaging of bipolar cell terminals indicated symmetric glutamate release to all directions of motion (Yonehara et al., 2013), while recent glutamate imaging experiments (Matsumoto et al., 2019) have supported the hypothesis that glutamatergic release from bipolar cell terminals displays directional tuning. Despite this debate, the most well-characterized synaptic mechanism underlying directional tuning is mediated by inhibition.
The first, well-studied, example of directionally tuned output in the retina is in the dendrites of starburst amacrine cells (SACs), aptly named for their radially symmetric, “starburst” like morphology (Euler et al., 2002). Each dendritic branch of a SAC forms a distinct computational unit, with its own electrotonically isolated inputs and outputs, responding robustly to outward (centrifugal) motion and weakly to inward (centripetal) motion (Euler et al., 2002; Vlasits et al., 2016). SACs also constitute the only cell type in the retina which co-releases two neurotransmitters: GABA and acetylcholine (ACh) (Lee et al., 2010; Sethuramanujam et al., 2016) though only GABA release has been shown to be directional, while ACh is released via a paracrine mechanism (Sethuramanujam et al., 2018; Wei, 2018).

The role of tuned inhibition in the DS computation:

Retinal direction selectivity is mediated primarily by inhibition through multiple, non-mutually exclusive, models (W. R. Taylor & Vaney, 2002). The canonical synaptic mechanism meditating direction tuning in the retina is tuned asymmetric inhibition (Barlow & Levick, 1964) whereby null direction motion leads to greater inhibitory input onto the DSGC, compared to preferred direction motion. This tuned asymmetric inhibition is provided by SACs through two mechanisms. The first mechanism is due to asymmetric SAC-DSGC wiring (Figure 2A), which was revealed though paired voltage clamp recordings between DSGCs and SACs and quantal analysis, indicating that DSGCs form more inhibitory GABAergic synapses with SACs on their null side, compared to SACs on their preferred side (Morrie & Feller, 2015; Wei et al., 2011). The second mechanism mediating asymmetric inhibition is the SAC's centrifugal motion (outward along it's dendrites) tuning (Figure 2B), combined with the wiring specificity of null-direction oriented SAC dendrites and DSGCs revealed through serial block face electron microscope (SBEM) reconstructions (Briggman et al., 2011).

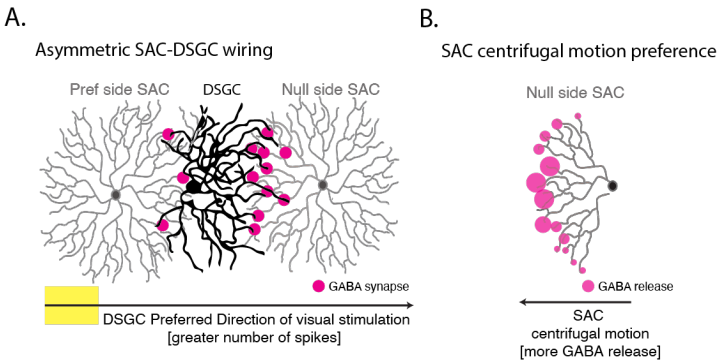

Figure2: Components of Tuned Asymmetric Inhibition. A) Asymmetric wiring. B) Centrifugal motion preference in SAC dendrites.

The mechanisms mediating the wiring specificity between DSGCs and null-side SACs are still under intense investigation. Recently, a study revealed that the genetic knockout of FRMD7, a gene implicated in human congenital nystagmus, leads to a loss in horizontal (nasal and temporal) motion tuning in the retina (Yonehara et al., 2016). A loss in asymmetric wiring between SACs and horizontally tuned DSGCs was found to underly this loss in DSGC tuning, pointing to a role for molecular recognition in mediating targeted horizontal axis asymmetric wiring. However, the mechanisms mediating asymmetric wiring along the vertical axis and the four cardinal directions remains unknown.

The role of excitation in the DS computation:

DSGCs receive excitatory input from glutamatergic bipolar cells, which synapse directly onto their dendrites, and cholinergic input from SACs which have processes that stratify laterally in the inner plexiform layer (IPL) of the retina (Famiglietti, 1983; Tauchi & Masland, 1985; Vaney, 1984). Though the role of excitatory input in tuning the DS circuit is well established in the rabbit (Fried et al., 2002), its role in tuning DSGCs in mouse has been under debate. Thus far, paired SAC-DSGC recordings show that cholinergic input onto DSGCs is symmetric (Lee et al., 2010) and single-cell voltage clamp recordings, combined with glutamate imaging has shown that glutamatergic excitatory input is untuned in DSGCs (Park et al., 2015).

More recently, transgenic mice in which SACs lack GABA release ($Vgat^{flx/flx}$ x ChAT-Cre), revealed that DSGCs retained half of their directional tuning, pointing to a contribution for excitation in tuning DSGC output (Pei et al., 2015). Additionally, in a reduced circuit using optogenetic stimulation of SACs in transgenic animals where SACs lack directional GABAergic output, it was revealed that cholinergic excitation contributes to DS tuning by temporally preceding inhibition during preferred direction motion (Hanson et al., 2019)). In wildtype mice, however, cholinergic excitation contributes to directional tuning during only low contrast stimulation (Sethuramanujam et al., 2016), while glutamatergic inputs enhance DSGC output during noisy stimuli via NMDA receptor-mediated symmetric, multiplicative scaling (Poleg-Polsky & Diamond, 2016b). Accordingly, this DS wiring scheme, where inhibitory input is asymmetric and spatially offset from the dendritic field, while bipolar cell excitatory input is centered on the DSGC dendritic field, is postulated to enhance the directional tuning of DSGCs, though has not been experimentally assessed in mice.

The role of spatially offset inhibition in the DS computation:

Another well-established mechanism for DS tuning is based on spatially offset inhibition (Fried et al., 2002; Hubel & Wiesel, 1962; Lien & Scanziani, 2018; Priebe & Ferster, 2005; W. R. Taylor & Vaney, 2002), with the timing of synaptic inputs during a moving stimulus being the predominant parameter: during preferred direction motion, the excitatory response is elicited before the stimulus enters the inhibitory receptive field, thus a temporal delay is introduced into the inhibitory response (Figure 3). During null direction motion, the inhibitory response is elicited before the stimulus enters the excitatory receptive field, thus a temporal delay is introduced to the excitatory response and the inhibitory input effectively suppresses spiking output. Spatially offset inhibition is the classical mechanism postulated to underly direction selective responses in both the rabbit retina and in the mammalian visual cortex ((Fried et al., 2002; Hubel & Wiesel, 1959, 1962; Lien & Scanziani, 2018; Priebe & Ferster, 2005; Rossi et al., 2020; W. R. Taylor & Vaney, 2002)

In the mammalian visual cortex, many neurons show directional tuning. In primates and carnivores, directional tuning of cortical neurons is postulated to arise de novo whereby neurons extract directional information by combining inputs that respond with different temporal delays to stimuli that are present in different locations in visual space. These tuning properties are refined with visual experience following eye opening (Li et al., 2006, 2008; Richards & Van Hooser, 2018; Roy et al., 2020). This follows the Hassanstein-Reichart correlator model, also displayed in fly retinal DS neurons, positing that excitatory input combined with built-in temporal delays enable neurons to detect motion direction.

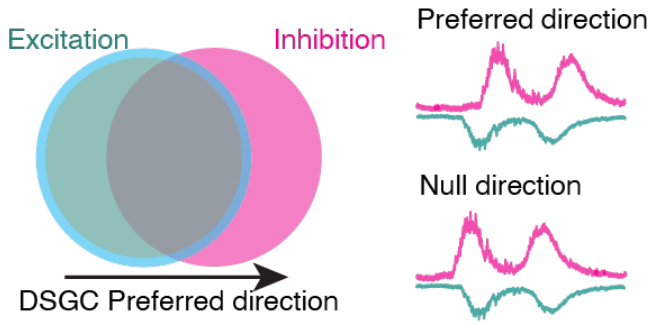

Figure 3: Schematic of spatially offset inhibition. Left: Organization of the DSGC's excitatory (green) and inhibitory (magenta) receptive field relative to its preferred direction. Right: Temporal offsets in excitatory and inhibitory input during preferred and null direction stimulation

In the mouse visual cortex, directional tuning has been shown to originate in the retina (Cruz-Martín et al., 2014). Whole-cell voltage clamp recordings have revealed a strong tuned excitation of thalamic inputs onto layer 4 (thalamo-recipient) neurons of the mouse primary visual cortex (Niell & Stryker, 2010) via both amplitude modulation and temporal delays (Lien & Scanziani, 2018). However, the tuning of the thalamic axons that synapse onto an individual L4 neuron showed uncorrelated feature tuning, indicating that at least some of the cortical directional selectivity seems to arise from spatiotemporal delays in thalamic excitation (Lien & Scanziani, 2018), combined with intracortical excitation and inhibition which sharpen cortical DS tuning.

This was also displayed in vivo in the L4 neurons of cat visual cortical neurons where excitatory and inhibitory inputs are tuned to the same preferred direction but are temporally out of phase (Priebe & Ferster, 2005). A linear combination of excitatory and inhibitory synaptic inputs followed by a nonlinearity step is postulated to mediate this tuned directional output. This nonlinearity could either be the spiking threshold (Priebe & Ferster, 2005) or shunting inhibition (Barlow & Levick, 1964; Monier et al., 2003) whereby null direction motion nonlinearly suppresses excitatory input. In the mouse visual cortex, in vivo whole cell voltage clamp recordings of L4 neurons in V1 show that DS neurons receive tuned thalamic excitation and untuned intracortical inhibition, though the skewness of excitation changed with stimulus direction thereby creating a spatially offset E to I receptive field (Lien & Scanziani, 2018). More recently, Rossi et al. (2020) combined functional imaging of L2/3 neurons of V1 with rabies virus tracing of presynaptic intracortical connections to show that the direction selectivity of the postsynaptic neuron is unrelated to the selectivity of the presynaptic neurons but is correlated to the spatial offset of the excitatory and inhibitory receptive fields relative to each other.

In the mouse retina, several studies have revealed that temporal delays between the excitatory and inhibitory synaptic inputs, consistent with spatially offset inhibition, play a role in the DS computation (Hanson et al., 2019; Pei et al., 2015). However, whether these temporal offsets in excitation and inhibition represent a spatial offset in synaptic distribution has not been investigated.

In my thesis, I explore the spatial organization of excitatory and inhibitory synapses in two DSGC subtypes that have very distinct dendritic morphologies. Multielectrode array data has shown that the spiking output of both DSGCs possesses similar directional tuning under bright stimulus conditions (Yao et al., 2018). In chapter 3, I show that the relative tuning of inhibition is different across cell types, which warrants an investigation into the relative role of spatially offset inhibition across cell types. To answer this question, I conduct two-photon guided voltage clamp recordings of GFP-tagged DSGCs to isolate the excitatory and inhibitory synaptic inputs while stimulating the circuit with a static light distributed across their receptive field. Surprisingly, I find that both cell types exhibit similar excitatory and inhibitory receptive field organizations. We show that SAC directional tuning and SAC-DSGC wiring specificity remains to be the most pivotal element of directional tuning. Regardless of the location of the SACs that maximally inhibit a DSGC, we find that a combination of the high coverage factor of SAC processes (Morrie & Feller, 2018)and the molecularly determined null-oriented SAC-DSGC wiring specificity (Briggman et al., 2011) determines asymmetric inhibition and directional tuning, regardless of cell type or spatial displacement of excitation and inhibition.

Postsynaptic mechanisms for mediating direction selectivity

Postsynaptic nonlinearities

Weakly tuned presynaptic inputs can generate robust DSGC tuning after amplification via a number of postsynaptic mechanisms. In the rabbit retina, asymmetric excitation and inhibition constitute the presynaptic mechanisms mediating directional tuning in DSGCs (W. Taylor et al., 2000). The postsynaptic mechanisms mediating DS tuning in rabbit DSGCs were revealed upon blockade of voltage gated sodium channels, via tetrodotoxin (TTX) application, whereby the tuning of synaptic inputs significantly decreased (Oesch et al., 2005) implicating DSGC spike generation in sharpening its DS tuning. Further investigations using simultaneous multi-site current clamp recordings of ON-OFF DSGC somas and dendrites revealed a strong contribution of dendritic spikes to axonal action potentials (Sivyer et al., 2010) primarily driven by cholinergic excitation from SACs (Brombas et al., 2017). These studies indicate that nonlinear conductances, due to voltage-gated ion channels, sharpen tuning by generating dendritic spikes, and thus slightly larger depolarizations for preferred versus null direction motion, which can produce substantially different spiking outputs (Wei, 2018). Additionally, computational modelling revealed that dendrites are electrotonically isolated due to their highly branching dendritic morphology allowing strong input resistance at the distal dendrites, along with a high density of voltage-gated sodium channels on more proximal dendrites allowing efficient nonlinear integration of weakly tuned excitatory input onto DSGC dendrites (Schachter et al., 2010).

Similarly, in the mouse retina, nonlinear conductances maintain directional tuning in the absence of inhibitory input (Trenholm et al., 2011). For example, in a subtype of ventral motion preferring DSGCs (vDSGC), whose asymmetric dendrites point towards its preferred direction, pharmacological blockade of $GABA_A$ receptors results in the loss of inhibitory input, but not a loss in directional tuning. Computational modeling experiments show that voltage gated sodium channels on the distal dendrites of vDSGCs enable efficient integration of excitatory input in a reverse Rall method (Rall et al. 1967), whereby visual stimulation from the soma to the dendrite leads to more efficient integration of excitatory inputs than that from the dendrites towards the soma (Trenholm et al., 2011). Paired current clamp recordings of vDSGCs, along with tracer coupling experiments reveal that homologous gap junction coupling of vDSGCs contribute to excitatory subthreshold junctional potentials, with observed functional rectification that enables lateral propagation of excitatory input along the preferred direction (Trenholm et al., 2014; Trenholm, McLaughlin, et al., 2013). Additionally, vDSGCs are the only known DSGC to form a network of homologously gap-junction coupled cells, thus promoting dendritic spiking as well as accurate encoding of the position of moving objects (Trenholm et al., 2014; Trenholm, McLaughlin, et al., 2013; Trenholm, Schwab, et al., 2013; Yao et al., 2018).

Another way in which nonlinear conductances contribute to DSGC directional tuning, is revealed under noisy stimulus conditions (Poleg-Polsky & Diamond, 2016b) whereby DSGC selectivity is maintained across input conditions, specifically across stimuli of varying contrasts, by multiplicative scaling of synaptic inputs. Hence, preferred direction depolarizations remain larger than null depolarizations by the same proportion. This is achieved by a combination of tuned

inhibition shunting null direction excitation and voltage-dependent NMDA receptor conductances (Poleg-Polsky & Diamond, 2016a; Sethuramanujam et al., 2016).

Dendritic morphology

The dendritic asymmetry of vDSGCs, and its morphological alignment with its preferred direction further promotes its postsynaptic mechanism for directional tuning. In Chapter 2 of this thesis, we show that dark-reared vDSGCs lose their ventral dendritic orientation and although their gap junction network is intact, their inhibition independent directional tuning is severely attenuated (El-Quessny et al., 2020). Additionally, previous studies stimulating half of the dendritic tree of symmetric DSGCs in their preferred direction in the presence $GABA_A$ receptor blockers, have shown that all DSGCs possess nonlinear conductances that enable inhibition-independent directional tuning (Trenholm et al., 2011). Together, these studies provide strong evidence that the dendritic morphology of DSGCs provides a postsynaptic mechanism for directional tuning that is independent of inhibitory input tuning.

Dendritic asymmetries also contribute to DS tuning in a subset of DSGCs and are present in all noncanonical RGCs (Kim et al., 2008; Rousso et al., 2016; Trenholm et al., 2011). For example, asymmetric ventrally-oriented RGCs labelled under the JAM-B-Cre mouse line (J-RGCs), stratify in a narrow band of the IPL between ON and OFF SAC processes (Kim et al., 2008), thus not cofasciculating with SAC processes. However, J-RGCs exhibit asymmetric spike responses to ventral motion (along their dendrites) of negative contrast. Rather than relying on SAC mediated inhibition, J-RGCs exhibit a slanted space-time organization of their excitatory receptive field along their dendrites, towards the ventral axis, thereby facilitating the efficient summation of excitatory input along their preferred direction. Further work has shown that this receptive field structure of J-RGCs also enable color opponency, whereby stimulation with green light leads to greater action potential firing than UV light in dorsal retina and vice versa in ventral retina (Joesch & Meister, 2016).

Local Dendritic Processing in directional tuning

The mechanisms mediating the tuning of synaptic inputs onto DSGCs have been extensively studied though the postsynaptic computations that occur within RGC dendrites remain under investigation. A recent study using simultaneous calcium imaging and dense noise stimulation to examine the dendritic receptive fields of four types of OFF RGCs (tOff alpha, tOff mini, sOff and F-mini^{Off}), revealed subtype-specific variations in dendritic integration properties (Ran et al., 2020). By analyzing the receptive fields within ROIs distributed across the dendritic field, the study found that some RGCs exhibited synchronous dendritic computations (tOff mini, sOff and F-mini^{Off}), where different ROIs had similar/overlapping receptive fields, while the other subtype (tOFF alpha) exhibited more local computations, where different ROIs had more distinct receptive fields. This indicates that different subtypes of RGCs compute balances of excitation and inhibition in a localized fashion, which differ across the dendritic field.

Similar studies in DSGCs indicate that local directional computations are performed within the dendritic tree (Jain et al., 2020). Computational modeling showed that nonlinear conductance within the dendritic tree promotes a multi-compartmental model, allowing local interactions

between excitation and inhibition to shape dendritic DS, while SAC ablation abolished DS. This indicates that direction selectivity is computed via the tight alignment of cholinergic and GABAergic inputs, which ensure shunting of null direction excitation.

In conclusion, the retinal direction selective computation relies on a combination of pre and postsynaptic mechanisms. In chapter 2 of this thesis, we show that dendritic morphology facilitates the postsynaptic mechanism of DS, whereby DSGCs whose dendrites are unoriented along their preferred direction exhibit reduced inhibition-independent tuning relative to DSGCs with oriented dendrites. In chapter 3 of this thesis, we show that DSGCs with asymmetric morphology exhibit greater tuning of inhibitory inputs compared to DSGCs with symmetric morphologies, though distinct morphologies of these two subsets of DSGCs does not contribute to the organization of their presynaptic inputs. Hence, DSGC dendritic morphology contributes to postsynaptic mechanisms for DS and increases the likelihood of stronger asymmetric wiring of inhibition but does not contribute to the organization of its presynaptic inputs.

REFERENCES

Alvarez, V. A., & Sabatini, B. L. (2007). *Anatomical and Physiological Plasticity of Dendritic Spines*. https://doi.org/10.1146/annurev.neuro.30.051606.094222

Baden, T., Berens, P., Franke, K., Román Rosón, M., Bethge, M., & Euler, T. (2016). The functional diversity of retinal ganglion cells in the mouse. *Nature*. https://doi.org/10.1038/nature16468

Baden, T., & Euler, T. (2016). Retinal Physiology: Non-Bipolar-Cell Excitatory Drive in the Inner Retina. In *Current Biology*. https://doi.org/10.1016/j.cub.2016.03.065

Barlow, H. B., & Hill, R. M. (1963). Evidence for a physiological explanation of the waterfall phenomenon and figural after-effects. *Nature*, *2*.

Barlow, H. B., & Levick, W. R. (1964). Retinal Ganglion Cells Responding Selectively to Direction and Speed of Image Motion in the Rabbit. *Journal of Physiology*, 377–407.

Bos, R., Gainer, C., & Feller, M. B. (2016). Role for visual experience in the development of direction-selective circuits. *Current Biology*. https://doi.org/10.1016/j.cub.2016.03.073

Briggman, K. L., Helmstaedter, M., & Denk, W. (2011). Wiring specificity in the direction-selectivity circuit of the retina. *Nature*. https://doi.org/10.1038/nature09818

Brombas, A., Kalita-De Croft, S., Cooper-Williams, E. J., & Williams, S. R. (2017). Dendro-dendritic cholinergic excitation controls dendritic spike initiation in retinal ganglion cells. *Nature Communications*, *8*, 1–14. https://doi.org/10.1038/ncomms15683

Chen, M., Lee, S., Park, S. J. H., Looger, L. L., & Zhou, Z. J. (2014). Receptive field properties of bipolar cell axon terminals in direction-selective sublaminas of the mouse retina. *Journal of Neurophysiology*. https://doi.org/10.1152/jn.00283.2014

Cruz-Martín, A., El-Danaf, R. N., Osakada, F., Sriram, B., Dhande, O. S., Nguyen, P. L., Callaway, E. M., Ghosh, A., & Huberman, A. D. (2014). A dedicated circuit links direction-selective retinal ganglion cells to the primary visual cortex. *Nature*. https://doi.org/10.1038/nature12989

Deitch, J. S., & Rubel, E. W. (1984). Afferent Influences on Brain Stem Auditory Nuclei of the Chicken: Time Course and Specificity of Dendritic Atrophy Following Deafferentation. *Journal of Comparative Neurology*, *79*, 66–79.

Dhande, O. S., Estevez, M. E., Quattrochi, L. E., El-danaf, R. N., Nguyen, P. L., Berson, D. M., & Huberman, A. D. (2013). *Genetic Dissection of Retinal Inputs to Brainstem Nuclei Controlling Image Stabilization*. *33*(45), 17797–17813. https://doi.org/10.1523/JNEUROSCI.2778-13.2013

Ding, J., Chen, A., Chung, J., Acaron Ledesma, H., Wu, M., Berson, D. M., Palmer, S. E., & Wei, W. (2021). Spatially displaced excitation contributes to the encoding of interrupted motion by the retinal direction-selective circuit. *BioRxiv*, 1–38.

El-Quessny, M., Maanum, K., & Feller, M. B. (2020). Visual Experience Influences Dendritic Orientation but Is Not Required for Asymmetric Wiring of the Retinal Direction Selective Circuit. *Cell Reports*, *31*(13), 107844. https://doi.org/10.1016/j.celrep.2020.107844

Euler, T., Detwiler, P. B., & Denk, W. (2002). Directionally selective calcium signals in dendrites of starburst amacrine cells. *Nature*, *418*(6900), 845–852. https://doi.org/10.1038/nature00931

Famiglietti, E. V. (1983). On and OFF Patheats through Amacrine Cells in Mammalian Retina: The Synaptic Connections of "Starburst" Amacrine Cells. *Vision Research*.

Franke, K., Berens, P., Schubert, T., Bethge, M., Euler, T., & Baden, T. (2017). Inhibition

decorrelates visual feature representations in the inner retina. *Nature*, *542*(7642), 439–444. https://doi.org/10.1038/nature21394

Fried, S. I., Mü nch, T. A., & Werblin, F. S. (2002). *Mechanisms and circuitry underlying directional selectivity in the retina*. www.nature.com/nature

Giolli, R. A., Blanks, R. H. I., Torigoe, Y., & Williams, D. D. (1985). Projections of Medial Terminal Accessory Optic Nucleus , Ventral Tegmental Nuclei , and Substantia Nigra of Rabbit and Rat as Studied by Retrograde Axonal Transport of Horseradish Peroxidase. *Journal of Comparative Neurology*, *116*.

Hanson, L., Sethuramanujam, S., de Rosenroll, G., Jain, V., & Awatramani, G. B. (2019). Retinal direction selectivity in the absence of asymmetric starburst amacrine cell responses. *ELife*, *8*. https://doi.org/10.7554/eLife.42392

Helmstaedter, M., Briggman, K. L., Turaga, S. C., Jain, V., Seung, H. S., & Denk, W. (n.d.). Connectomic reconstruction of the inner plexiform layer in the mouse retina. *Nature*. https://doi.org/10.1038/nature12346

Hoy, R. R., Nolen, T. G., & Casaday, G. C. (1985). Dendritic sprouting and compensatory synaptogenesis in an identified interneuron following auditory deprivation in a cricket. *Proceedings of the National Academy of Sciences*, *82*(November), 7772–7776.

Hubel, D. H., & Wiesel, T. (1959). Receptive fields of single neurons in the cat's striate cortex. *Journal of Physiology*, 574–591.

Hubel, D. H., & Wiesel, T. (1962). Receptive Fields, Binocular Interaction and Functional Architecture in the cat's visual cortex. *Journal of Physiology*, 106–154.

Huberman, A. D., Wei, W., Elstrott, J., Stafford, B. K., Feller, M. B., & Barres, B. A. (2009). Report Genetic Identification of an On-Off Direction- Selective Retinal Ganglion Cell Subtype Reveals a Layer-Specific Subcortical Map of Posterior Motion. *Neuron*, *62*(3), 327–334. https://doi.org/10.1016/j.neuron.2009.04.014

Jain, V., Murphy-Baum, B. L., DeRosenroll, G., Sethuramanujam, S., Delsey, M., Delaney, K., & Awatramani, G. B. (2020). The functional organization of excitation and inhibition in the dendritic arbors of retinal direction-selective ganglion cells. *ELife*, 1–23. https://doi.org/10.1101/718783

Joesch, M., & Meister, M. (2016). A neuronal circuit for colour vision based on rod-cone opponency. *Nature*. https://doi.org/10.1038/nature17158

Joo, W., Hippenmeyer, S., & Luo, L. (2014). *Dendrite morphogenesis depends on relative levels of NT-3/TrkC signaling*. *346*(6209), 721–723.

Kay, J. N., De la Huerta, I., Kim, I.-J., Zhang, Y., Yamagata, M., Chu, M. W., Meister, M., & Sanes, J. R. (2011). Retinal Ganglion Cells with Distinct Directional Preferences Differ in Molecular Identity, Structure, and Central Projections. *Journal of Neuroscience*, *31*(21), 7753–7762. https://doi.org/10.1523/JNEUROSCI.0907-11.2011

Kim, I., Zhang, Y., Yamagata, M., Meister, M., & Sanes, J. R. (2008). *Molecular identification of a retinal cell type that responds to upward motion*. *452*(March). https://doi.org/10.1038/nature06739

Lee, S., Kim, K., & Zhou, Z. J. (2010). Role of ACh-GABA Cotransmission in Detecting Image Motion and Motion Direction. *Neuron*. https://doi.org/10.1016/j.neuron.2010.11.031

Lefebvre, J. L., Sanes, J. R., & Kay, J. N. (2015). Development of Dendritic Form and Function. *Annual Review of Cell and Developmental Biology*. https://doi.org/10.1146/annurev-cellbio-100913-013020

Li, Y., Fitzpatrick, D., & White, L. E. (2006). The development of direction selectivity in ferret

visual cortex requires early visual experience. *Nature Neuroscience*, *9*(5), 676–681. https://doi.org/10.1038/nn1684

Li, Y., Van Hooser, S. D., Mazurek, M., White, L. E., & Fitzpatrick, D. (2008). Experience with moving visual stimuli drives the early development of cortical direction selectivity. *Nature*, *456*(7224), 952–956. https://doi.org/10.1038/nature07417

Liang, L., Fratzl, A., Goldey, G., Ramesh, R. N., Sugden, A. U., Morgan, J. L., Chen, C., & Andermann, M. L. (2018). A Fine-Scale Functional Logic to Convergence from Retina to Thalamus. *Cell*, *173*(6), 1343-1355.e24. https://doi.org/10.1016/j.cell.2018.04.041

Lien, A. D., & Scanziani, M. (2018). Cortical direction selectivity emerges at convergence of thalamic synapses. *Nature*, *558*(7708), 80–86. https://doi.org/10.1038/s41586-018-0148-5

Liu, X., Robinson, M. L., Schreiber, A. N. N. M., Wu, V., Lavail, M. M., Cang, J., & Copenhagen, D. R. (2009). *Regulation of Neonatal Development of Retinal Ganglion Cell Dendrites by Neurotrophin-3 Overexpression*. *458*(February), 449–458. https://doi.org/10.1002/cne.22016

Lom, B., & Cohen-cory, S. (1999). *Brain-Derived Neurotrophic Factor Differentially Regulates Retinal Ganglion Cell Dendritic and Axonal Arborization In Vivo*. *19*(22), 9928–9938.

London, M., & Häusser, M. (2005). *Dendritic Computation*. https://doi.org/10.1146/annurev.neuro.28.061604.135703

Magee, J. C. (2000). Dendritic integration of excitatory synaptic input. *Nature Reviews Neuroscience*, *1*.

Matsumoto, A., Briggman, K. L., & Yonehara, K. (2019). Spatiotemporally Asymmetric Excitation Supports Mammalian Retinal Motion Sensitivity. *Current Biology*, *29*(19), 3277-3288.e5. https://doi.org/10.1016/j.cub.2019.08.048

Mcallister, A. K., Lo, D. C., Katz, L. C., & Carolina, N. (1995). *Neurotrophins Regulate Dendritic Growth in Developing Visual Codex*. *15*(Figure 1), 791–803.

Monier, C., Baudot, P., Graham, L. J., & Fre, Y. (2003). *Orientation and Direction Selectivity of Synaptic Inputs in Visual Cortical Neurons : A Diversity of Combinations Produces Spike Tuning*. *37*, 663–680.

Morrie, R. D., & Feller, M. B. (2015). An Asymmetric Increase in Inhibitory Synapse Number Underlies the Development of a Direction Selective Circuit in the Retina. *Journal of Neuroscience*. https://doi.org/10.1523/JNEUROSCI.0670-15.2015

Morrie, R. D., & Feller, M. B. (2016). Development of synaptic connectivity in the retinal direction selective circuit. In *Current Opinion in Neurobiology*. https://doi.org/10.1016/j.conb.2016.06.009

Morrie, R. D., & Feller, M. B. (2018). A Dense Starburst Plexus Is Critical for Generating Direction Selectivity. *Current Biology*, *28*(8), 1204-1212.e5. https://doi.org/10.1016/j.cub.2018.03.001

Niell, C. M., & Stryker, M. P. (2010). Modulation of Visual Responses by Behavioral State in Mouse Visual Cortex. *Neuron*. https://doi.org/10.1016/j.neuron.2010.01.033

Oesch, N., Euler, T., & Taylor, W. R. (2005). Direction-selective dendritic action potentials in rabbit retina. *Neuron*, *47*(5), 739–750. https://doi.org/10.1016/j.neuron.2005.06.036

Oyster, C. W. (1968). The Analysis of Image Motion by the Rabbit Retina. *Journal of Physiology*, 613–635.

Park, S. J. H., Borghuis, B. G., Rahmani, P., Zeng, Q., Kim, I. J., & Demb, J. B. (2015). Function and circuitry of VIP+ interneurons in the mouse retina. *Journal of Neuroscience*, *35*(30), 10685–10700. https://doi.org/10.1523/JNEUROSCI.0222-15.2015

Pei, Z., Chen, Q., Koren, D., Giammarinaro, B., Acaron Ledesma, H., & Wei, W. (2015). Conditional Knock-Out of Vesicular GABA Transporter Gene from Starburst Amacrine Cells Reveals the Contributions of Multiple Synaptic Mechanisms Underlying Direction Selectivity in the Retina. *The Journal of Neuroscience : The Official Journal of the Society for Neuroscience*, *35*(38), 13219–13232. https://doi.org/10.1523/JNEUROSCI.0933-15.2015

Peichl, L., & Wässle, H. (1983). The Structural Correlate of The Receptive Field Centre of Alpha Ganglion Cells in the Cat Retina. *Journal of Physiology*, 309–324.

Poleg-Polsky, A., & Diamond, J. S. (2016a). NMDA Receptors Multiplicatively Scale Visual Signals and Enhance Directional Motion Discrimination in Retinal Ganglion Cells. *Neuron*. https://doi.org/10.1016/j.neuron.2016.02.013

Poleg-Polsky, A., & Diamond, J. S. (2016b). Retinal circuitry balances contrast tuning of excitation and inhibition to enable reliable computation of direction selectivity. *Journal of Neuroscience*, *36*(21), 5861–5876. https://doi.org/10.1523/JNEUROSCI.4013-15.2016

Priebe, N. J., & Ferster, D. (2005). Direction selectivity of excitation and inhibition in simple cells of the cat primary visual cortex. *Neuron*, *45*(1), 133–145. https://doi.org/10.1016/j.neuron.2004.12.024

Ran, Y., Huang, Z., Baden, T., Schubert, T., Baayen, H., Berens, P., Franke, K., & Euler, T. (2020). Type-specific dendritic integration in mouse retinal ganglion cells. *Nature Communications*, *11*(1), 1–15. https://doi.org/10.1038/s41467-020-15867-9

Richards, S. E. V., & Van Hooser, S. D. (2018). Neural architecture: From cells to circuits. In *Journal of Neurophysiology* (Vol. 120, Issue 2, pp. 854–866). American Physiological Society. https://doi.org/10.1152/jn.00044.2018

Rivlin-Etzion, M., Zhou, K., Wei, W., Elstrott, J., Nguyen, P. L., Barres, B. A., Huberman, A. D., & Feller, M. B. (2011). Transgenic Mice Reveal Unexpected Diversity of On-Off Direction-Selective Retinal Ganglion Cell Subtypes and Brain Structures Involved in Motion Processing. *Journal of Neuroscience*. https://doi.org/10.1523/JNEUROSCI.0564-11.2011

Rossi, L. F., Harris, K. D., & Carandini, M. (2020). Spatial connectivity matches direction selectivity in visual cortex. *Nature*, *2019*(January 2019). https://doi.org/10.1038/s41586-020-2894-4

Rousso, D. L., Qiao, M., Kagan, R. D., Yamagata, M., Palmiter, R. D., & Sanes, J. R. (2016). Two Pairs of ON and OFF Retinal Ganglion Cells Are Defined by Intersectional Patterns of Transcription Factor Expression. *Cell Reports*. https://doi.org/10.1016/j.celrep.2016.04.069

Roy, A., Osik, J. J., Meschede-Krasa, B., Alford, W., Leman, D. P., & Van Hooser, S. D. (2020). Synaptic and intrinsic mechanisms underlying development of cortical direction selectivity. *ELife*, *9*, 1–52. https://doi.org/10.7554/eLife.58509

Sabbah, S., Gemmer, J. A., Bhatia-Lin, A., Manoff, G., Castro, G., Siegel, J. K., Jeffery, N., & Berson, D. M. (2017). A retinal code for motion along the gravitational and body axes. *Nature*. https://doi.org/10.1038/nature22818

Sanes, J. R., & Masland, R. H. (2015). *The Types of Retinal Ganglion Cells : Current Status and Implications for Neuronal Classification*. 221–248. https://doi.org/10.1146/annurev-neuro-071714-034120

Schachter, M. J., Oesch, N., Smith, R. G., & Rowland Taylor, W. (2010). Dendritic spikes amplify the synaptic signal to enhance detection of motion in a simulation of the direction-selective ganglion cell. *PLoS Computational Biology*, *6*(8).

https://doi.org/10.1371/journal.pcbi.1000899
Seabrook, T. A., Burbridge, T. J., Crair, M. C., & Huberman, A. D. (2017). *Assembly of the Mouse Visual System*.
Sethuramanujam, S., Awatramani, G. B., & Slaughter, M. M. (2018). Cholinergic excitation complements glutamate in coding visual information in retinal ganglion cells. *Journal of Physiology*, *596*(16), 3709–3724. https://doi.org/10.1113/JP275073
Sethuramanujam, S., McLaughlin, A. J., deRosenroll, G., Hoggarth, A., Schwab, D. J., & Awatramani, G. B. (2016). A Central Role for Mixed Acetylcholine/GABA Transmission in Direction Coding in the Retina. *Neuron*. https://doi.org/10.1016/j.neuron.2016.04.041
Shi, X., Barchini, J., Ledesma, H. A., Koren, D., Jin, Y., Liu, X., Wei, W., & Cang, J. (2017). *Retinal origin of direction selectivity in the superior colliculus*. *20*(4). https://doi.org/10.1038/nn.4498
Simpson, J. I. (1984). The accessory optic system. *Annual Review of Neuroscience*, 13–41.
Sivyer, B., van Wyk, M., Vaney, D. I., & Taylor, W. R. (2010). Synaptic inputs and timing underlying the velocity tuning of direction-selective ganglion cells in rabbit retina. *Journal of Physiology*, *588*(17), 3243–3253. https://doi.org/10.1113/jphysiol.2010.192716
Spruston, N. (2008). *Pyramidal neurons : dendritic structure and synaptic integration*. *9*(march), 206–221. https://doi.org/10.1038/nrn2286
Stuart, G. J., & Spruston, N. (2015). *review Dendritic integration : 60 years of progress*. *18*(12). https://doi.org/10.1038/nn.4157
Tauchi, M., & Masland, R. H. (1985). Local Order among the Dendrites of an Amacrine Cell Population. *Journal of Neuroscience*, 2494–2501.
Taylor, W., He, S., Levick, W. R., & Vaney, D. I. (2000). Dendritic Computation of Direction Selectivity by Retinal Ganglion Cells. *Science*.
Taylor, W. R., & Vaney, D. I. (2002). Diverse synaptic mechanisms generate direction selectivity in the rabbit retina. *The Journal of Neuroscience : The Official Journal of the Society for Neuroscience*, *22*(17), 7712–7720. https://doi.org/22/17/7712 [pii]
Trenholm, S., Johnson, K., Li, X., Smith, R. G., & Awatramani, G. B. (2011). Parallel mechanisms encode direction in the retina. *Neuron*. https://doi.org/10.1016/j.neuron.2011.06.020
Trenholm, S., McLaughlin, A. J., Schwab, D. J., & Awatramani, G. B. (2013). Dynamic Tuning of Electrical and Chemical Synaptic Transmission in a Network of Motion Coding Retinal Neurons. *Journal of Neuroscience*. https://doi.org/10.1523/JNEUROSCI.0808-13.2013
Trenholm, S., McLaughlin, A. J., Schwab, D. J., Turner, M. H., Smith, R. G., Rieke, F., & Awatramani, G. B. (2014). Nonlinear dendritic integration of electrical and chemical synaptic inputs drives fine-scale correlations. *Nature Neuroscience*. https://doi.org/10.1038/nn.3851
Trenholm, S., Schwab, D. J., Balasubramanian, V., & Awatramani, G. B. (2013). Lag normalization in an electrically coupled neural network. *Nature Neuroscience*. https://doi.org/10.1038/nn.3308
Vaney, D. I. (1984). ‘ Coronate ’ amacrine cells in the rabbit retina have the ‘ starburst ’ dendritic morphology. *Proceedings of the Royal Society of London*, *Masland 1983*.
Vaney, D. I., Sivyer, B., & Taylor, W. R. (2012). Direction selectivity in the retina: Symmetry and asymmetry in structure and function. *Nature Reviews Neuroscience*. https://doi.org/10.1038/nrn3165
Vlasits, A. L., Morrie, R. D., Tran-Van-Minh, A., Bleckert, A., Gainer, C. F., DiGregorio, D. A.,

& Feller, M. B. (2016). A Role for Synaptic Input Distribution in a Dendritic Computation of Motion Direction in the Retina. *Neuron*. https://doi.org/10.1016/j.neuron.2016.02.020

Wang, Y., & Rubel, E. W. (2012). *In Vivo Reversible Regulation of Dendritic Patterning by Afferent Input in Bipolar Auditory Neurons*. *32*(33), 11495–11504. https://doi.org/10.1523/JNEUROSCI.1737-12.2012

Wei, W. (2018). Neural mechanisms of motion processing in the mammalian retina. *Annual Review of Vision Science*, *4*, 165–192. https://doi.org/10.1146/annurev-vision-091517-034048

Wei, W., Hamby, A. M., Zhou, K., & Feller, M. B. (2011). Development of asymmetric inhibition underlying direction selectivity in the retina. *Nature*. https://doi.org/10.1038/nature09600

Wyatt, H. J., & Daw, W. (1975). Directionally Sensitive Ganglion Cells in the Rabbit Retina : Specificity for Stimulus Direction, Size and Speed. *Journal of Physiology*, *6*.

Yao, X., Cafaro, J., McLaughlin, A. J., Postma, F. R., Paul, D. L., Awatramani, G., & Field, G. D. (2018). Gap Junctions Contribute to Differential Light Adaptation across Direction-Selective Retinal Ganglion Cells. *Neuron*, *100*(1), 216-228.e6. https://doi.org/10.1016/j.neuron.2018.08.021

Yonehara, K., Farrow, K., Ghanem, A., Hillier, D., Balint, K., Teixeira, M., Jüttner, J., Noda, M., Neve, R., Conzelmann, K. K., & Roska, B. (2013). The first stage of cardinal direction selectivity is localized to the dendrites of retinal ganglion cells. *Neuron*. https://doi.org/10.1016/j.neuron.2013.08.005

Yonehara, K., Fiscella, M., Drinnenberg, A., Esposti, F., Trenholm, S., Krol, J., Franke, F., Scherf, B. G., Kusnyerik, A., Müller, J., Szabo, A., Jüttner, J., Cordoba, F., Reddy, A. P., Németh, J., Nagy, Z. Z., Munier, F., Hierlemann, A., & Roska, B. (2016). Congenital Nystagmus Gene FRMD7 Is Necessary for Establishing a Neuronal Circuit Asymmetry for Direction Selectivity. *Neuron*. https://doi.org/10.1016/j.neuron.2015.11.032

Yonehara, K., Ishikane, H., Sakuta, H., Shintani, T., Nakamura-, K., Kamiji, N. L., Usui, S., & Noda, M. (2009). *Identification of Retinal Ganglion Cells and Their Projections Involved in Central Transmission of Information about Upward and Downward Image Motion*. *4*(1). https://doi.org/10.1371/journal.pone.0004320

CHAPTER 2: Visual Experience Influences Dendritic Orientation but is not Required for Asymmetric Wiring of the Retinal Direction Selective Circuit

Publication related to this work:
This chapter is a full reprint of El-Quessny, Maanum and Feller, Cell Reports (2020), of which I was the primary author. This work is included with permission from all authors.

El-Quessny, M., Maanum, K. & Feller, M.B. (2020). Visual Experience Influences Dendritic Orientation but is not Required for Asymmetric Wiring of the Retinal Direction Selective Circuit. Cell Reports,

SUMMARY

Changes in dendritic morphology in response to activity have long been thought to be a critical component of how neural circuits develop to properly encode sensory information. Ventral-preferring direction-selective ganglion cell (vDSGC) have asymmetric dendrites oriented along their preferred direction, which has been hypothesized to play a critical role in their tuning. Here we report the surprising result that visual experience is critical for the alignment of vDSGC dendrites to their preferred direction. Interestingly, vDSGCS in dark-reared mice lose their inhibition-independent dendritic contribution to direction selective tuning while maintaining asymmetric inhibitory input. These data indicate that different mechanisms of a cell's computational abilities can be constructed over development through divergent mechanisms.

INTRODUCTION

Neural computations rely upon the precise wiring, which emerges during development. A classic example of such a computation is direction selectivity (DS). In the retina, direction selective ganglion cells (DSGCs) fire many action potentials in response to stimuli moving in a preferred direction (PD) and few to no action potentials in response to stimuli moving in the opposite, or null direction (ND) (Barlow and Levick, 1965). The DS computation is based primarily on the asymmetric wiring of an inhibitory interneuron, the starburst amacrine cell (SAC), onto DSGCs such that motion in the DSGC's null direction generates more inhibition than motion in the preferred direction (Vaney and Taylor, 2002; Demb, 2007). This asymmetric wiring is present as early as postnatal day 10 (P10), a few days prior to eye opening (Wei *et al.*, 2011; Yonehara *et al.*, 2011) and is a consequence of DSGCs preferentially forming synapses with SACs located on their null side, relative to their preferred side (Morrie and Feller, 2015).

What instructs this asymmetric wiring? The establishment of wiring specificity in the nervous system is a complex process involving an interplay between molecular cues dictating synaptic specificity and activity-dependent synaptic strengthening/weakening (Leighton and Lohmann, 2016). In addition, it is thought that form instructs function, i.e. that the morphology of axons and dendrites and their relative spatial organization dictate the location of synapses (Wong and Ghosh, 2002; Richards and Van Hooser, 2018). In the retinal DS circuit, the relative roles of molecular specification, neural activity, and the spatial organization of presynaptic (SAC) relative to postsynaptic (DSGC) cells in instructing this wiring remains a mystery.

A few studies implicate the morphology of SACs in instructing asymmetric wiring. SACs have radially symmetric processes and serial EM reconstructions show that the orientation of individual SAC process is tightly correlated with the null direction of the DSGCs that receive synaptic input from them (Briggman, Helmstaedter and Denk, 2011; Ding *et al.*, 2016; Bae *et al.*, 2018). SAC-specific genetic deletion of the cell-adhesion protein Protocadherin G (Pcdhg) (Lefebvre *et al.*, 2012; Kostadinov and Sanes, 2015) or the axon guidance protein Semaphorin 6A (Sema6A)(Sun *et al.*, 2013) both of which alter SAC radial morphology, eliminate directional tuning of DSGCs. However, in the case of Sema6A, loss of DS is due to a reduction in asymmetric inhibition while asymmetric wiring is maintained (Morrie and Feller, 2018). Interestingly, a hypo-morphic mutation in the FRMD7 gene, which is associated with congenital nystagmus in humans, abolishes direction selectivity along the horizontal axis without impacting SAC morphology (Yonehara *et al.*, 2016). The mechanism by which FRMD7 or other molecules expressed by SACs instruct the selective wiring to different subtypes of DSGCs remains unknown.

An alternative hypothesis is that the postsynaptic DSGC dendrites influence asymmetric wiring. DSGCs that encode motion in different directions have distinct molecular profiles and morphological characteristics (Kay *et al.*, 2011; Trenholm *et al.*, 2011). Across the nervous system, the shape of a dendrite has implications for the organization of synaptic inputs as well as its functional role within a circuit (Wong and Ghosh, 2002; Richards and Van Hooser, 2018). Indeed, a recent study indicated that the relative orientation of dendrites and axons were more important than molecular identity in instructing synapse specificity in spinal cord sensory motor circuits (Balaskas *et al.*, 2019).

One way to investigate the role of DSGC morphology in the wiring of DS circuits would be to alter the morphology of the DSGC and assess its consequences on DS tuning and synaptic wiring. To do this, we used the Hb9-GFP mouse line, which expresses GFP in ON-OFF ventral-preferring DSGCs (vDSGCs). Uniquely among DSGCs, vDSGC's dendritic fields are asymmetric and oriented in their preferred directions (Trenholm *et al.*, 2011; Sabbah *et al.*, 2017) making them more likely to form synapses with SACs on their null side, a hypothesis based on serial EM reconstructions of SAC and DSGC dendrites (Briggman, Helmstaedter and Denk, 2011). We found that in mice that were dark-reared from birth to adulthood, dendrites of vDSGCs were not oriented towards the ventral direction. Though dark-rearing prevented the establishment of inhibition-independent direction selectivity, these dramatic changes in dendritic morphology did not alter the asymmetric wiring of inhibition or alter the overall vDGSCs direction selectivity.

RESULTS

Asymmetric dendrites of ventral preferring DSGCs are not ventrally oriented at eye opening or in dark-reared adults

Dark rearing had a dramatic impact on the dendritic organization of vDSGCs. To characterize the impact of dark-rearing on the dendritic morphology of vDSGCs, we filled Hb9-GFP+ cells in retinas dissected from normally-reared (NR - 12 hr dark/light cycle) and dark-reared (DR - 24 hr dark) adult mice and from mice that had just opened their eyes (P13/14 - 12 hr dark/light cycle) (Figure 1a). Dendritic morphology was independently characterized for ON and OFF arbors by a vector pointing from the soma to the dendritic center of mass (dCOM) whose magnitude (ρ) corresponded to the degree of dendritic asymmetry and whose angle (Θ) corresponded to dendritic orientation (Figure S1 and Methods).

As described previously (Trenholm *et al.*, 2011), NR adult vDSGC dendrites were asymmetric, and both ON and OFF dendrites were oriented ventrally (Figures 1a and 1b). NR adult vDSGC ON and OFF dendrites were oriented ventrally and within 45 degrees of each other (Figures 1a and 1b). At P13/14, vDSGC ON and OFF dendrites were asymmetric (Figure 1c), but they were not preferentially oriented towards the ventral direction (Figure 1d) and displayed some variability in their alignment with each other (Figure 1e). Surprisingly, in mice that were dark-reared (DR), the orientation of vDSGCs' ON and OFF dendrites were similar to the eye opening distribution: asymmetric (Figure 1c) and their orientation deviated significantly from the ventral direction (Figures 1d, S1 and Table S1). Hence, visual experience is necessary for the alignment of ON and OFF vDSGC dendrites to the ventral axis of the retina.

We also examined other features of vDSGC dendrites after dark-rearing. First, we found that dark-rearing increased the dendritic field size of OFF-stratifying dendrites (Figure 1f), similar to the impact of dark rearing on OFF-stratifying asymmetric J-RGCs (Elias *et al.*, 2018). Second, dark-rearing had no impact on mosaic organization of vDSGCs (Figure S2), indicating that their spacing may not be set by homotypic interactions between dendritic segments (Rockhill, Euler and Masland, 2000; Kay, Chu and Sanes, 2012).

One unique property of vDSGCs among DSGCs is that they are gap junction coupled and have been shown to retain their gap junction coupling into adulthood (Trenholm *et al.*, 2013). Coupling broadens their directional tuning at low/scotopic light levels (Yao *et al.*, 2018). Recent data indicates that the extent of coupling is influenced by visual experience (Zhang, Wu and Zhang, 2020). To address whether dark-rearing influences vDSGC coupling in adulthood, we conducted tracer coupling experiments on normally-reared and dark-reared adult vDSGCs (Figure S3a). In dark reared mice, the pattern of tracer-coupled vDSGCs did not change relative to normally-reared mice (Figures S3b). Interestingly, dark-reared mice showed a small but significant increase in the number of tracer-coupled cells (Figures S3c and S3d), though the proportion of GFP+ cells to which they were coupled did not change (Figure S3e). Hence changes in coupling between vDSGCs are not likely to mediate the increased variability of dendritic orientation in dark-reared mice.

Ventral motion preference is preserved in dark-reared vDSGCs despite altered dendritic morphology

Does function follow form? In NR mice, vDSGC dendrites are oriented in the same direction as their motion preference. This orientation potentially influences at least two different mechanisms that contribute to their DS computation. First, DSGCs receive stronger null direction inhibition from SACs located on the null side of the DSGC soma (Briggman, Helmstaedter and Denk, 2011; Morrie and Feller, 2015; Ding *et al.*, 2016; Bae *et al.*, 2018). For vDSGCs, this preferential wiring is potentially facilitated by the ventral orientation of their dendrites. Second, unlike other DSGCs, vDSGCs retain some directional tuning in the absence of inhibitory input (Trenholm *et al.*, 2011), a feature attributed to their asymmetric dendrites. Modeling experiments suggest that this postsynaptic mechanism of directional tuning is mediated by nonlinear conductances at the distal dendrites of vDSGCs, which allow them to integrate excitatory input along the soma-to-dendrite ventral direction more efficiently than in the opposite dorsal direction (Trenholm *et al.*, 2011, 2013).

To determine the impact of development and visual experience on DS tuning of vDSGCs, we conducted cell-attached recordings of spikes in response to drifting bars moving in 8 different directions in NR adult and P13/14, as well as DR adult animals (Figure 2a). Surprisingly, we observed no differences in the strength of DS tuning in any of the experimental groups (Figure 2b and Table S2). Note that OFF responses were less tuned at eye opening (Figure 2c), consistent with findings that OFF DS circuits mature later than ON circuits (Hoon *et al.*, 2014; Rosa *et al.*, 2016). Thus, we only analyzed ON spike tuning for P13/14. We found a significant increase in the variance of the preferred direction of spiking relative to the ventral axis (PDΔv) for OFF responses (Figure S4b), similar to what was observed using population imaging of direct selective responses (Bos et al, 2016). Note a direct comparison with this previous study (Bos et al, 2016) is not possible since the responses of Hb9-GFP cells, which comprise only a subset of ventral preferring DSGCs (Sabbah et al ,2017), were not analyzed separately.

The preservation of ventral motion preference in P13/14 and adult DR vDSGCs (Figures 2d and S4a) resulted in a strong dissociation of dendritic orientation ($dCOM_{\Theta}$) and spiking preferred direction (PD_{Θ}) (Figure 2d). Moreover, there was no correlation between the relative dendritic

orientation and the preferred direction ($|dCOM_{\Theta}\text{-}PD_{\Theta}|$) and the tuning of the spike responses (Figures 2d, S4). Hence, direction selective tuning of vDSGCs appears to be independent of the orientation of the dendrites.

Dendritic alignment is critical for inhibition-independent tuning of vDSGCs.

The asymmetric morphology of vDSGCs, along with the alignment of their dendritic arbor and preferred direction, has been postulated to underlie their ability to retain some directional tuning in the absence of inhibitory input (Trenholm *et al.*, 2011). Modeling experiments suggest that this postsynaptic mechanism of directional tuning is mediated by nonlinear conductances at the distal dendrites of vDSGCs, which allow them to integrate excitatory input along the ventral or centrifugal direction (i.e. soma-to-dendrite) more efficiently than in the dorsal or centripetal direction (dendrite to soma). However, the relationship between dendritic orientation and postsynaptic, inhibition-independent mechanisms of directional tuning has not been fully explored.

To establish whether there is a correlation between dendritic morphology and inhibition-independent tuning, we conducted both cell attached and current clamp recordings from vDSGCs in normally-reared adults in the presence of a $GABA_A$ receptor blocker, gabazine (50 μM) (Figure 3a). For these experiments we used slower stimulation velocities to enhance the postsynaptic contributions to directional tuning (Trenholm *et al.*, 2011). Consistent with previous findings, both ON and OFF responses retained some of their directional tuning in the absence of inhibitory input (Figures 3c and S5c). Interestingly, while both ON and OFF responses remain tuned, the direction of ON tuning deviated from the ventral axis (Figure 3c, Figure S5e and Table S2).

We next compared dendritic morphology and inhibition-independent tuning on a cell-by-cell basis. The strength of the tuning of both ON and OFF responses were only weakly correlated with the magnitude of dendritic asymmetry (Figure S5f). However, we observed a correlation between the relative alignment of the OFF dendrite & OFF preferred direction ($|dCOM_{\Theta}\text{-}PD_{\Theta}|$) with the strength of tuning (Figures 3d and S5e, right), though this correlation was lacking for ON responses (Figure 3d and Figure S5e, left). These data indicate that ON and OFF dendrites of vDSGCs may utilize different mechanisms of synaptic integration. Hence, in normally-reared animals, dendritic alignment along the ventral axis influences the contribution of inhibition-independent tuning to the overall directional tuning of the cell, specifically for the OFF pathway.

Interestingly, we observed a significant decrease in both ON and OFF inhibition-independent tuning in vDGSC recorded from dark-reared mice as measured by the vector sum (Figures 3b, 3c, and Figure S5d), though this difference did not reach significance when comparing DSI across rearing conditions.(Note given the large amount of spiking of DSGCS in the presence of gabazine, the vector sum was a less variable measure of tuning). Hence, visual experience is critical for the maturation of the inhibition-independent mechanism of direction selectivity. We postulate that since this reduction in inhibition-independent tuning is not associated with a loss of dendritic asymmetry, that dark-rearing may disrupt the location and or strength of the nonlinearity that underlies the dendritic computation of direction selectivity

Asymmetric inhibition from null side starburst cells is preserved in dark-reared vDSGCs despite altered dendritic morphology.

Since ventral motion preference is preserved in DR vDSGCs, we assessed the impact of dark-rearing on the directional tuning of both inhibitory (Figure 4 and Table S3) and excitatory (Figure S6) synaptic inputs using the whole cell voltage clamp technique. Inhibitory synaptic input was highest for dorsal motion (Figures 4a and 4b) and had similar directional tuning strength (Figure 4c) and tuning angle deviation from the dorsal axis (Figure 4d) in vDSGCs from NR adult, P13/14, and DR adult mice. Hence, asymmetric inhibition in response to null direction motion is independent of visual experience and vDSGC dendritic orientation. In NR and DR adults, we observed small EPSC tuning in the preferred direction, which was absent at P13/14 (Figure S6c).

A feature of the direction selective circuit in the retina is the presence of spatially offset inhibition (Fried et al., 2002; Hanson et al., 2019; Pei et al., 2015; Sivyer et al., 2010). For vDSGCS, this indicates that SACs located on the ventral side of the vDSGC will provide more inhibitory input (Figure 4e). To determine whether directionally tuned IPSCs were generated by SACs located on the null side of vDSGCs, we mapped the excitatory and inhibitory receptive fields of NR and DR adult vDSGCs by recording synaptic currents evoked by squares of light sequentially presented at 100 block-shuffled locations within a soma-centered grid. We calculated the vector from the soma to the center of the inhibitory and excitatory receptive fields (Figures 5a and 5b), using the magnitude (ρ) of the vector to indicate receptive field displacement, and the angle of the vector (Θ) to indicate receptive field orientation. We found that in both NR and DR adult vDSGCs, the inhibitory receptive fields were similarly oriented toward the ventral direction relative to the soma (Figure 5c). We then computed the vector from the excitatory to the inhibitory receptive field centers and observed that the magnitude of their displacement from each other was similar across rearing conditions (Figure 5d). Moreover, the angle of the vector was similarly aligned to the ventral axis ($\Delta\Theta_V$) (Figure 5e). Hence, although DR vDSGCs have displaced dendrites, they still receive spatially offset inhibition from SACs located on their null side. These data indicate that the location of dendrites does not influence their direction selectivity of their presynaptic partners (Figure 4e).

DISCUSSION

Form-function studies to date have observed that the shape of a dendrite influences its role within a circuit, and that the diversity of dendritic morphologies is necessary to fulfill a wide range of neural computations (Wong and Ghosh, 2002; Lefebvre, Sanes and Kay, 2015). This study demonstrates that the precise asymmetric wiring of synaptic circuits that mediate direction selectivity is independent of the orientation of the DSGC dendrites. Visual experience following eye opening is required for asymmetric vDSGCs to orient their dendrites ventrally, and that proper orientation is prevented by dark-rearing. Though dark rearing reduced the inhibition-independent contribution to directional tuning, the tuning and spatial distribution of excitatory and inhibitory synaptic inputs were intact and, as a result, dark-reared vDSGCs retained their normal directional tuning. Hence, the maturation of dendritic morphology appears to be dictated by the functional circuit rather than the traditional view that dendritic morphology dictates circuit function.

Activity influences dendritic morphology

We found that dark-rearing had a dramatic but specific effect on the dendrites of vDSGCs – it prevented the orientation of vDSGC dendrites in the ventral direction and, in a subset of vDSGCs, prevented the alignment of ON with OFF dendrites (Figure 1). This finding indicates that visual experience is necessary for vDSGC dendrites to orient themselves along their preferred direction. This counters our initial hypothesis that the orientation of DSGC dendrites along their preferred direction optimizes antiparallel wiring with null side SAC dendrites. Rather, we postulate that the orientation of the dendrites along their preferred direction is instead necessary for the establishment of inhibition-independent mechanisms for DS. Here we consider these findings in the context of other systems where afferent activity plays a role in asymmetric dendritic development.

How might visual experience influence vDSGC dendrite orientation? One clue comes from examples of neurons whose asymmetric dendritic arbors are oriented towards their presynaptic partners, including ganglion cells in the zebrafish retina (Choi *et al.*, 2010), layer IV Stellate cells in the somatosensory cortex (Woolsey and Van der Loos, 1970; Greenough and Chang, 1988; Nakazawa, Mizuno and Iwasato, 2018), mitral cells of the rodent olfactory bulb (Hinds and Ruffett, 1973; Blanchart, De Carlos and López-Mascaraque, 2006), among others (*for review see* Wong and Ghosh, 2002). In developing zebrafish, retinal ganglion cells (RGCs) initially have both apical and basal dendrites pointing both toward and away from the inner plexiform layer. Upon contact with bipolar cells, RGCs basal dendrites reorient toward the apical side to form functional synapses (Choi *et al.*, 2010). In the *heart-and-soul (has)* mutant zebrafish, RGCs are displaced to the other side of bipolar cells, leading to an increase in basal orientation. This indicates that the location of the RGC dendrites relative to bipolar cell afferents instructs their orientation. In layer IV spiny stellate neurons in barrel cortex, activity-dependent pruning eliminates inactive dendrites oriented away from barrel centers while sparing active dendrites oriented toward the barrel center, which elaborate and stabilize (Harris and Woolsey, 1981; Narboux-Nême *et al.*, 2012; Li *et al.*, 2013). When thalamocortical axon input is silenced via infraorbital nerve cut, or via postsynaptic NMDA receptor knockout, spiny stellate neuron

dendrites misalign with respect to barrel centers (Mizuno *et al.*, 2014, 2018). This suggests that dendrites are oriented toward afferent activity.

Sensory experience may be required for the establishment of dendritic orientation through mechanisms that influence gene transcription. In situ hybridization revealed that the transcription factor BTBD3 is highly localized to the barrels of somatosensory cortex during development and that activity-dependent nuclear translocation of BTBD3 is required for the orientation of stellate neuron dendrites towards the barrel hollows. Similarly, BTBD3 is implicated in the orientation of dendrites in ferret visual cortex towards the center of ocular dominance columns whereby monocular enucleation and BTBD3 shRNA knock-down lead to misorientation of layer IV excitatory neuron dendrites (Matsui *et al.*, 2013).

How does visual experience instruct vDSGCs to orient towards their preferred direction? One possibility is that bipolar cell inputs on the preferred side are stronger and therefore dendrites on the preferred side are stabilized while dendrites on the non-preferred side are pruned. Such asymmetric wiring of bipolar cells was recently reported in ON DSGCs (Matsumoto, Briggman and Yonehara, 2019). However, serial EM reconstructions of symmetric ON-OFF DSGCs (Ding *et al.*, 2016) do not indicate such a bias, though this reconstruction has not been conducted for vDSGCs.

Another clue comes from understanding the specific aspects of visual experience that might influence the direction selective network. First, trained visual experience paradigms, where animals only experience upward (preferred direction) motion leads to increased gap junctional coupling of vDSGCs and synchronizes population spike responses (Zhang, Wu and Zhang, 2020). Null direction training had no effect on coupling, and neither did changing contrast, luminance and temporal frequency regimes of the training stimulus. Second, gap junction networks between vDSGCs are hypothesized to enable motion detection at scotopic light levels and motion discrimination at high light levels (Yao *et al.*, 2018). Although we find that gap junction coupling between vDSGCs are unchanged in dark-reared animals, this suggests that structured visual experience and synchronized network function, provided by sequential activation of gap junction networks and presynaptic inputs may play a key role in mediating the orientation of vDSGC dendrites towards their preferred direction.

Our finding that dark-rearing did not impact stratification differs from previous studies where visual deprivation prevented the stratification of some ganglion cell dendrites (Tian and Copenhagen, 2001) via a process dependent on Brain Derived Neurotrophic Factor (BDNF) activation of TrkC receptors (Liu *et al.*, 2007). Interestingly, this activity dependent stratification does not appear to be dictated by glutamate release from bipolar cells, since vDSGC ON dendrite stratification has been shown to rely on the expression of the adhesion molecule Contactin 5 and its co-receptor Caspr4 for proper stratification, which is expressed by ON SACs (Peng *et al.*, 2017), and since stratification was normal in mice lacking release from ON bipolar cells (Kerschensteiner *et al.*, 2009).

***Implications for postsynaptic, inhibition-independent contributions to DS*:**

Thus far, ventral preferring asymmetric DSGCs (vDSGCs) are the only DSGC subtype to exhibit directional tuning in the absence of inhibitory input (Trenholm *et al.*, 2011). In the presence of the $GABA_A$ receptor antagonist gabazine, other subtypes of anterior and posterior preferring DSGCs lose their directional tuning (Ackert et al., 2009; Bos et al., 2016; Rivlin-Etzion et al., 2011; Wei et al., 2011). However, due to the correlation of dendritic orientation and preferred direction in normally-reared adult vDSGCs, it is postulated that they also possess postsynaptic mechanisms for encoding motion direction. Our results in normally-reared adults are consistent with previous findings, where vDSGCs retain some of their tuning in the absence of inhibitory input (Trenholm et al., 2011). By using a bar stimulus in our experiments, we were able to determine both ON and OFF responses were partially retained during blockade of inhibition

Computational modeling experiments have shown that vDSGCs may possess nonlinear conductances, like voltage gated sodium channels, on their distal dendrites allowing them to efficiently encode ventral motion (from soma to distal dendrites) more efficiently than dorsal motion (from dendrites to soma) (Trenholm *et al.*, 2011). Using current clamp recordings, we found that ON and OFF dendrites utilize different mechanisms for integrating excitatory input (Figure 3c), where ON dendrites follow a more passive model of centripetal (dendrite-to-soma) integration (Rall, 1964), whereas OFF dendrites follow a more active model of centrifugal (soma to dendrite) integration in the absence of inhibitory input (Stuart and Spruston, 2015). Dark-rearing significantly reduces this contribution to directional tuning. Since asymmetric dendrites are maintained after dark-rearing, we hypothesize that visual experience is required for establishing the nonlinear conductance or the organization and kinetics of excitatory inputs onto DSGC dendrites (Matsumoto, Briggman and Yonehara, 2019).

Hence for DS cells, it appears that even though the primary computation is set up by an experience-independent molecular program, there can be additional computations set up by experience-dependent processes. This leads to the interesting hypothesis that the alignment of dendrites and the establishment of inhibition-independent tuning requires the presence of the primary computation of directional preference.

ACKNOWLEDGEMENTS

We thank Benjamin E. Smith for the dendritic analysis macro. Alex Tiriac and Mathew M. Summers for their contributions to the revision experiments, and to members of the Feller lab for commenting on the manuscript. M.Q. was supported by the Ruth L. Kirschstein Pre-doctoral National Research Service Award (F31 NS106756), K.M. was supported by UC Berkeley Summer Undergraduate Research Fellowship (SURF) and M.Q. and M.B.F. were supported by NIH R01EY019498, R01EY013528 and P30EY003176.

AUTHOR CONTRIBUTIONS

M.Q. conducted the experiments and analyzed all the data. K.M. conducted mosaic analysis experiments and measured dendritic field size. M.Q. and M.B.F. designed the experiments and wrote the manuscript.

FIGURE CAPTIONS

Figure 1: Dark-rearing prevents orientation of vDSGC dendrites toward the ventral direction.
(A) Example maximum intensity projections (left) and binarized skeletons (right) of filled vDSGCs with ON (magenta) and OFF (green) dendrites segments for normally-reared adults (left, P30-50, NR Adult), at eye opening (middle, NR P13/14) and in adults that are dark-reared from birth (right, P30-50, DR Adult) with ON and OFF dCOM vectors overlaid on dendritic skeleton. Scale bar = 100 μm.
(B) Characterization of dendritic orientation in NR adults (n=25 cells), at eye opening (n=26 cells) and in DR adults (n=35 cells). Left: ON vs. OFF dendrite center of mass vector angle ($dCOM_{\Theta}$). Right: polar plots of ON (magenta) and OFF (green) dendrite center of mass vectors. Blue data points refer to example cell above.
(C) Summary data for dCOM vector magnitude as a measurement of ON (magenta) and OFF (green) dendritic asymmetry. Horizontal bar = mean; error bar = SEM. Significance assessed by Kruskal-Wallis one-way ANOVA, p_{ON} and $p_{OFF}>0.05$.
(D) Summary data for deviation of ON (magenta) and OFF (green) dendritic angle from the ventral (270˚) axis for all three conditions. Horizontal bar = median. Box plots represent variance. Kruskal-Wallis one-way ANOVA, Dunn-Siddak post-hoc test. ****$p<0.0001$
(E) Summary data for absolute difference between ON (magenta) and OFF (green) dendritic angle. Horizontal bar = median. Box plots represent variance. Significance assessed by Levene's test for absolute variance ***$p<0.001$
(F) Summary data for ON and OFF dendritic field size of vDSGCs in three conditions. horizontal bar = mean; error bar = SEM. Significance assessed by One-way ANOVA, $p=8.7x10^{-5}$; Tukey-Kramer post-hoc test. * $p<0.05$

Mean ± Standard deviation values in Table S1.

Figure 2: Ventral motion preference is preserved in dark-reared mice despite altered vDSGC dendritic morphology.
(A) Example dendritic skeletons of normally-reared adult (left), eye opening (middle) and dark-reared adult (right) vDSGCs next to the average spike responses of the same cells. Shaded boxes define windows over which ON (magenta) and OFF (green) responses are assessed. Tuning curves plotted in polar coordinates ON (magenta) and OFF (green) responses. Radius of tuning curve = 60 spikes for adult and 30 spikes for eye opening.
(B) Population data represented as number of spikes fired for null direction (ND) vs. preferred direction (PD) spiking (left) and as vectors in polar plots (middle inset) of normally-reared adult (left, n=39), eye opening (middle, n=21) and dark-reared adult (right, n=32) vDSGCs. Radius of polar plot: Normalized vector sum (VS) of tuning curve = 0.5, Blue data points refer to ON (filled) and OFF (open) responses of example cell above. Comparison of spike tuning using the magnitude of the normalized vector sum of the tuning curve (right inset) at two velocities (lighter shade: 250 μm/s; darker shade: 500 μm/s) for ON (magenta) and OFF (green) responses. Colored horizontal bar =Mean, error bars = SEM. Significance within conditions assessed by unpaired t-test, *$p_{250\mu m/s} = 0.005$, $p_{500\mu m/s} = 0.05$. Significance across conditions assessed by

One-way ANOVA for ON and OFF responses separately, $p_{ON} = 0.08$, $p_{OFF} = 0.02$. Tukey Kramer post-hoc test $p>0.05$
(C) Comparison of spike tuning using direction selectivity index (DSI) at two velocities (lighter shade: 250 μm/s; darker shade: 500 μm/s) for ON (magenta) and OFF (green) responses. Colored horizontal bar =Mean, error bars = SEM. Significance assessed by One-way ANOVA for ON and OFF responses separately, $p_{ON} = 0.11$, $p_{OFF} = 0.0022$. Tukey Kramer post-hoc test * p_{OFF} (NRadult-P13/14) = 0.02.
(D) Comparison of dendritic orientation ($dCOM_{\Theta}$) vs. spiking directional preference (PD_{Θ}) , for normally-reared adult (left, n=12), eye opening (middle, n=18) and dark-reared adult (right, n=16) vDSGCs. X and Y axes centered on ventral axis (V). Top inset: histogram illustrating vDSGC spiking angle. Right inset: histogram illustrating vDSGC dendritic orientation. Note, P13/14 OFF responses were excluded from this analysis due to weak tuning (See Figure 2c).

Mean ± Standard deviation values in Table S2.

Figure 3: Inhibition-independent tuning is attenuated in dark-reared vDSGCs due to their misoriented dendrites.
(A) Left: example dendrite skeletons for ON and OFF dendritic segments for normally-reared adult vDSGCs. Scale bar = 100 μm. Right: example average spike responses of the same cell in the presence of 50 μM gabazine. Shaded boxes define windows over which ON and OFF responses are assessed. Tuning curves plotted in polar ON (magenta) and OFF (green) responses. Radius of tuning curve = 60 spikes.
(B) Left: example dendrite skeletons for ON and OFF dendritic segments for dark-reared adult vDSGCs. Right: example average spike responses of the same cell in the presence of 50 μM gabazine. Tuning curves plotted in polar ON (magenta) and OFF (green) responses. Radius of tuning curve = 120 spikes.
(C) Left: Population data for normally-reared (NR) adult vDSGC (left, n=30) and dark-reared (DR) adult (right, n=10) responses in 50 μM gabazine represented as vectors in polar plots. Data for ON (magenta) and OFF (green) plotted separately. Note, radius of polar plot is the normalized vector sum (VS) of the tuning curve= 0.50 (NR) and 0.25 (DR). Right: Comparison of tuning strength as quantified by the magnitude of the normalized vector sum of the tuning curve in normally-reared (NR - closed circles) and dark-reared (DR - open circles) adult vDSGCs across using a slow velocity stimulus (250 μm/s) in 50 μM gabazine. Data for ON (magenta) and OFF (green) plotted separately. Statistical significance assessed across velocities by Wilcoxin Rank-Sum test. $p_{ON} = 0.03$, $p_{OFF} = 0.02$. *$p<0.05$. Note, Magnitude of vector sum of tuning curve is used here as a measure of tuning strength as we find that it better explains the variance between morphology-physiology alignment for both ON and OFF circuits. (See figure 3d and figure S5c).
(D) Analysis of normally-reared adult vDSGCs in 50 μM gabazine: how the strength of spike tuning measured by both the magnitude of the vector sum of the tuning curve (Vector sum - darker shade) and direction selectivity index (DSI-lighter shade) varies with the degree of alignment of dendritic angle to the preferred direction of spiking. Data for ON (magenta) and OFF(green) plotted separately. R^2 value indicates fraction of the variance in tuning strength that is explained by morphology-physiology alignment and vice-versa. Statistical significance of correlation coefficient assessed by t-test, $p_{ON}>0.05$, $p_{OFF}<0.05$. n=10 cells.

Mean ± Standard Deviation values in Table S2.

Figure 4: Asymmetric inhibition is maintained in dark-reared vDSGCs.
(A) Example dendritic skeletons of normally-reared adult (left), eye opening (middle) and dark-reared adult (right) vDSGCs next to the average inhibitory currents of the same cells. Tuning curves plotted in polar coordinates ON (magenta) and OFF (green) responses. Radius of tuning curve = 1500 pA.
(B) Left inset: population data for normally-reared adult (left, n=23), eye opening (middle, n=22) and dark-reared adult (right, n=13) vDSGCs represented as peak amplitude of IPSC recorded for null direction (ND) vs. preferred direction (PD) stimulation. Right inset: polar plot for normalized vector sums of population IPSC tuning curves. Radius of polar plot: Vector Sum of tuning curve = 0.5. Blue data points refer to ON (filled) and OFF (open) example cell above.
(C) Tuning strength vDSGC inhibitory input, across two stimulus velocities (lighter shade: 250 μm/s; darker shade: 500 μm/s) quantified as the direction selectivity index (DSI) for normally-reared (NR) adult, eye opening (NR P13/14) and dark-reared (DR) adult. Colored horizontal bar = mean, errors bars = SEM. Statistical significance assessed by One-way ANOVA, $p>0.05$.
(D) Summary data for deviation of preferred direction of IPSC tuning of vDSGCs (ND) from the dorsal (90˚) axis for all three conditions. Horizontal bar = median. Box plots represent variance. Kruskal-Wallis test, $p>0.05$.
(E) Antiparallel SAC-vDSGC wiring (Briggman et al. 2011), where vDSGCs preferentially synapse with null side SACs such that SAC preferred direction (PD) is aligned with vDSGC null direction (ND), schematized under two dendritic geometries. Left: vDSGCs with ventrally oriented dendrites synapse with null-side SACs where dendrites are oriented antiparallel to each other, right: vDSGCs with misoriented dendrites synapse with null-side SACs where dendrites are oriented parallel to each other.

Mean ± Standard deviation values in Table S3.

Figure 5: Inhibitory Receptive field is spatially offset from the excitatory receptive field in adult vDSGCs.
(A) Example mean excitatory (left) and inhibitory (right) PSC responses of normally-reared (NR) adult vDSGCs. Peak amplitude of ON (magenta) and OFF (green) responses are fit with a 2-dimensional gaussian. Ellipse radius in X and Y axes = 2 standard deviations of the gaussian fit centered around fit peak. Right: Population data of NR adult vDSGCs represented as polar plots of vectors from the soma to the excitatory (top) and inhibitory (bottom) receptive field fits. Radius of polar plot = 100 μm, center of polar plot = soma location. NR: n= 13, DR: n=9.
(B) Example mean excitatory (left) and inhibitory (right) PSC responses of dark-reared (DR) adult vDSGCs. Peak amplitude of ON (magenta) and OFF (green) responses are fit with a 2-dimensional gaussian. Ellipse radius in X and Y axes = 2 standard deviation of the gaussian fit centered around fit peak. Right: Population data of DR adult vDSGCs represented as polar plots of vectors from the soma to the excitatory (top) and inhibitory (bottom) receptive field fits. Radius of polar plot = 100 μm, center of polar plot = soma location.
(C) Comparison of the orientation of the vector from the soma to the center of the inhibitory receptive field, relative to the ventral axis ($\Delta\Theta v$). One way ANOVA, $p>0.05$.

(D) Left: Population data of NR (top) and DR (bottom) adult vDSGCs represented as polar plots of vectors from the excitatory to the inhibitory receptive field centers. Radius of polar plot = 100 μm, center of polar plot = EPSC receptive field center. Right: Comparison of the spatial offset (the magnitude of the vector) from the center ON (magenta) and OFF (green) excitatory receptive field to the center of the ON and OFF inhibitory receptive field fits (indicated in schematic above, where excitatory receptive field fit is in blue and inhibitory receptive field fit is in red) in NR and DR adult vDSGCs. One way ANOVA, $p > 0.05$.
(E) Comparison of the orientation of the vector from the center of the excitatory receptive field to the center of the inhibitory receptive field, relative to the ventral axis ($\Delta\Theta v$). Statistical significance assessed by One-way ANOVA, $p > 0.05$.

Mean ± Standard deviation values in Table S3.

METHODS

Lead contact

Further information and requests for resources and reagents should be directed to and will be fulfilled by the Lead Contact, Marla Feller (mfeller@berkeley.edu).

Materials Availability

This study did not generate new unique reagents.

Data and Code Availability

All datasets generated during and/or analyzed during the current study and all custom scripts and functions generated or used during the current study are available from the Lead Contact (mfeller@berkeley.edu) on request.

EXPERIMENTAL MODEL AND SUBJECT DETAILS

Mice used in this study were aged from p13-60 and were of both sexes. Animals used in experiments had not previously been involved in other experiments or exposed to any drugs. Animal health was monitored daily and only healthy animals were used in experiments. To target ventral preferring DSGCs, we used Hb9::GFP (Arber *et al.*, 1999) mice, which express GFP in a subset of DSGCs (Trenholm et al., 2011). Normally-reared animals were kept on a 12h:12h dark-light cycle. Dark-reared animals were kept on a 24h:0h dark-light cycle from birth until tissue collection. All experiments involved recording from 1-7 cells from at least 3 animals of either sex. All animal procedures were approved by the UC Berkeley Institutional Animal Care and Use Committee and conformed to the NIH Guide for the Care and Use of Laboratory Animals, the Public Health Service Policy, and the SfN Policy on the Use of Animals in Neuroscience Research.

METHOD DETAILS

Retina Preparation

Mice were anesthetized with isoflurane and decapitated. Retinas were dissected from enucleated eyes in oxygenated (95% O2/5% CO2) Ames' media (Sigma) for light responses or ACSF (in mM, 119 NaCl, 2.5 KCl, 1.3 MgCl2, 1 K2HPO4, 26.2 NaHCO3, 11D-glucose, and 2.5 CaCl2) for paired recordings. Retinal orientation was determined as described previously (Wei, Elstrott and Feller, 2010). Isolated whole retinas were micro-cut at the dorsal and ventral halves to allow flattening, with dorsal and ventral mounted over two 1–2 mm2 hole in nitrocellulose filter paper (Millipore) with the photoreceptor layer side down, and stored in oxygenated Ames' media or ACSF until use (maximum 10 h). All experiments were performed on retinas in which dorsal-ventral orientation was tracked.

Visual Stimulation

For visual stimulation of vDSGCs, broad-band visible light ranging from 470 to 620 nm was generated using an OLED display (SVGA Rev2 OLED-XL; eMagin) displaying custom stimuli created using MATLAB software with the Psychophysics Toolbox. Drifting bars were presented (velocity = 250 and 500 µm/s, length =600 □m width =350 □m over a 700 □m radius circular mask) in 8 block shuffled directions, repeated 3 times, with each presentation lasting 6 s and

followed by 500 ms of grey screen) were projected through the 20X water-immersion objective (Olympus LUMPlanFl/IR 360/1.0 NA) onto the photoreceptor layer through the same 20x objective used to target cells once the cell attached recording configuration was achieved. The illumination radius on the retina was 1.4 mm to limit modulation of DSGC responses by inhibitory wide-field amacrine cells (Chen *et al.*, 2016)
The directionally selective index (DSI) was calculated for spike responses as: PD-NDPD+ND where PD is the number of spikes in the preferred direction and ND is the number of spikes in the null direction. We also used the magnitude of the vector sum of the spike responses as another measurement of directional tuning (Vector Sum = 1-Circular Variance of the spike responses, (Mazurek, Kager and Van Hooser, 2014)).

Two-photon targeted loose patch and whole-cell voltage-clamp recordings
Oriented retinas were placed under the microscope in oxygenated Ames' medium at 32–34□C. Identification and recordings from GFP+ cells were performed as described previously (Wei et al., 2010). In brief, GFP+ cells were identified using a custom-modified two-photon microscope (Fluoview 300; Olympus America) tuned to 920 nm to minimize bleaching of photoreceptors. The inner limiting membrane above the targeted cell was dissected using a glass electrode. Cell attached voltage clamp recordings were performed with a new glass electrode (4-5 MΩ) filled with internal solution containing the following (in mM): 110 CsMeSO4, 2.8 NaCl, 20 HEPES, 4 EGTA, 5 TEA-Cl, 4 Mg-ATP, 0.3 Na_3GTP, 10 Na_2Phosphocreatine, QX-Cl (pH = 7.2 with CsOH, osmolarity = 290, ECl^- = -60 mV). After cell attached recordings of spikes, whole cell recordings were performed with the same pipette after obtaining a GΩ seal. Holding voltages for measuring excitation and inhibition after correction for the liquid junction potential (-10 mV) were 0 mV and -60 mV, respectively. Signals were acquired using Clampex10.4 recording software and a Multiclamp 700A amplifier (Molecular Devices), sampled at 10 kHz, and low-pass filtered at 6 kHz. Current clamp recordings were performed with a new glass electrode (4-5 MΩ) filled with internal solution containing the following (in mM): 115 K^+ gluconate, 9.7 KCl, 1 $MgCl_2$, 0.5 $CaCl_2$, 1.5 EGTA, 10 HEPES, 4 ATP-Mg_2, 0.5 GTP-Na_3, 0.025, Alexa Fluor 594 (pH = 7.2 with KOH, osmolarity = 290). Tracer coupling experiments of GFP+ cells were performed as described previously (Caval-Holme and Feller, 2019).

Two-photon microscopy and morphological reconstruction
After physiological recordings of vDSGCs were completed, Alexa-594-filled vDSGCs in the Hb9–GFP mice were imaged using the two-photon microscope at 700nm. At this wavelength, GFP is not efficiently excited but Alexa 594 is brightly fluorescent. 600 x 600 µm Image stacks were acquired at z intervals of 1.0 µm and resampled fifteen times for each stack using a 20X objective (Olympus LUMPlanFl/IR 2x digital zoom, 1.0 NA) 30kHz resonance scanning mirrors covering the entire dendritic fields of the vDSGCs. Image stacks vDSGCs were then imported to FIJI (NIH) and a custom macro was used to segment ON and OFF dendrites based on their lamination depth in the inner plexiform layer (ON layer 10-30 µm, OFF layer 35-65 µm depth). Following ON and OFF dendritic segmentation, another custom FIJI macro uses the local maximµm values of fluorescent pixels to binarize and skeletonize ON and OFF dendritic segments for morphological analyses.

Receptive field mapping
To map excitatory and inhibitory receptive fields of vDSGCs, visual stimuli were generated using a computer running 420 nm light through a digital micro mirror device (DLI Cel5500) projector with a light emitting diode (LED) light source through a 20X objective (UMPlanFL 0.5NA W). Stimuli (30 μm^2) at an intensity of $4x10^9$ photons/s/μm^2 were presented in a pseudorandom order, in a 10x10 grid, onto a stimulus field of 500 μm^2, with the DSGC soma located in the center of the stimulus field (See Figure 5). Voltage clamp recordings were simultaneously acquired using methods described above.

Pharmacology
For experiments conducted in gabazine (Tocris, SR95531), we diluted 50 μM in AMES media, and allowed it to perfuse for 5-10 mins at a perfusion rate of 1 mL/min.

Retinal Histology
Whole-mount retinas were fixed in 4% PFA for 20 min, then washed in block solution (2% donkey serum, 2%bovine serum albumin, 0.3% Triton X-100 in PBS, 3 times, 16 min). Next, retinas were incubated in primary antibodies (1:1000 rabbit anti-GFP, Invitrogen, Grand Island, NY; 1:500 goat anti-ChAT, Millipore, Billerica, MA) for 1-3 days, and then washed in block solution (3 times, 15 min) and left in block solution at 4°C overnight. The retinas were then incubated in secondary antibody (1:1000 donkey anti-rabbit Alexa Fluor 488, 1:1000 donkey anti-goat Alexa Fluor 568; Invitrogen) at 4°C overnight. Then, they were washed in block solution (5 times, 30 min) and left in PBS overnight. Then, retinas were mounted and cover slipped with Vectashield (Vector Laboratories, Burlingame, CA).

Whole retina morphological analysis
Fixed and stained whole-mounted retinas were imaged on an epifluorescent macroscope (Olympus MV PLAPO 0.63x) within one week of mounting. Exposure and gain were adjusted per retina to maximize GFP signal. Images were then analyzed on FIJI for use in mosaic and nearest neighbor analysis (Figure S2). Whole retina fluorescent images were processed through a custom built MATLAB script and mosaic analysis was conducted on the imaged somas.

QUANTIFICATION AND STATISTICAL ANALYSIS

Statistical Tests
Details of statistical tests, number of replicates, and p values are indicated in the figures and figure captions. P values less than 0.05 were considered significant.

Whole cell recordings
For cell attached vDSGC recordings, spike counts were calculated by bandpass filtering traces (0.08-2 kHz) and manually identifying a threshold value for spikes on the filtered traces. Local minima below threshold that did not violate refractory period criteria (0.001 s) were counted as spikes. ON and OFF responses were defined as spikes occurring within a 1.9 s time window starting right before the presentation of the leading or trailing edge of the stimulus. The average spike counts across the 3 trials were used to calculate the normalized vector sum of the spike responses. Preferred directions for both ON and OFF responses used to calculate average spike

counts and were defined as the angle of the vector sum of spike responses for the ON and the OFF responses.

For voltage clamp recordings, traces were first average across the 3 trials for each direction and inspected to ensure consistency of responses. Average traces were baseline subtracted based on the last 500 ms of recording or a user defined interval after manual inspection. Peak currents were calculated from average baseline subtracted traces and were the maximal (IPSC) or minimal (EPSC) points during the 1.9 s window described above. The peak currents were used to calculate the vector sum of the current responses. Preferred directions for both ON and OFF responses used to calculate peak responses and were defined as 180˚ - the angle of the vector sum of ON and OFF peak IPSCs, or the angle of the vector sum of ON and OFF peak EPSCs if IPSCs were not recorded in that cell.

For current clamp recordings, traces were first average across the 3 trials for each direction and inspected to ensure consistency of responses. Average traces were baseline subtracted based on the last 500 ms of recording or a user defined interval after manual inspection. Peak depolarizations were calculated from average baseline subtracted traces during the 1.9 s window described above. The peak depolarizations were used to calculate the vector sum of the current responses. Preferred directions for both ON and OFF responses used to calculate peak responses and were defined as the angle of the vector sum of ON and OFF peak EPSPs. All current clamp experiments were performed in the presence of 50 μM Gabazine.

Receptive field mapping

To quantify excitatory and inhibitory receptive field sizes for each cell, we first divided each trace into the ON and OFF response based on the stimulus we present. Next, we fit a two-dimensional Gaussian to the post synaptic current (PSC) peak values averaged over three trials. We use the 2x standard deviation of the gaussian fit to display the size of the receptive fields. To compare the size and location of the PSC receptive fields relative to the soma and to each other, we used the standard deviation and peak coordinates of the Gaussian fits, respectively.

Mosaic analysis

GFP+ somas were selected and a mask of the retinal outline was defined. vDSGC somas were manually marked for each retina to create binary masks, and boundaries of each whole mounted retina was manually traced. Using MATLAB, we generated a random array of binary points (equal to the number of somas for each retina) within the boundary mask of every retina. Next, we generated a custom MATLAB script to calculate the nearest neighbor distances (NND) of our masked somas, normalized to the total size of the retina, and compared these distances to the randomly distributed somas. The regularity index (or conformity ratio) was calculated by dividing the mean NND by the standard deviation from the mean (Riemann, 1978). Both NND and regularity index metrics were compared to a random distribution of the same number of somas for each retina.

Single Cell morphological analysis

To calculate dendritic field size, the furthest dendritic extent was determined by adjusting brightness and contrast of individual maximum intensity z-projection images. A polygon was

constructed using individual dendritic tips, and the area of the polygon is used as a measurement of dendritic field size.

To assess morphological alignment of vDSGC dendrites in oriented retinas, we calculated the center of mass of the dendritic pixels from the binarized vDSGC skeleton relative to the soma. Briefly, a FIJI macro was designed to do the following: 1) allow user to localize the soma, record soma coordinates, and then clear/exclude soma pixels from the stack and dendritic analysis 2) creates a maximum intensity projection of the dendritic pixels and measure their center of mass (COM) using the following equation:

$$COM_x = \sum_{i=1}^{N} \frac{m_i x_i}{M}$$

$$COM_y = \sum_{i=1}^{N} \frac{m_i y_i}{M}$$

where N is the total number of image pixels, *x and y* are the coordinate distance of each pixel ,M is the total number of dendritic pixels, , and *m* is the mass of each pixel *i*, which is either 1 or 0. 3) Following COM calculation, the length of the vector from the dendritic COM to the soma coordinates is used as a measurement of dendritic asymmetry, and the angle of the vector from the dendritic COM to the soma coordinates is used as a measurement of dendritic angle.

Note: Dendritic reconstructions shown in figures were obtained by manually tracing example cells using the simple neurite tracer plugin on FIJI. Dendritic skeletons were then rendered and eroded for presentation.

REFERENCES

Arber, S. *et al.* (1999) 'Requirement for the Homeobox Gene Hb9 in the Consolidation of Motor Neuron Identity', *Neuron*, 23, pp. 659–674.

Bae, J. A. *et al.* (2018) 'Digital Museum of Retinal Ganglion Cells with Dense Anatomy and Physiology', *Cell*, 173(5), pp. 1293-1306.e19. doi: 10.1016/j.cell.2018.04.040.

Balaskas, N. *et al.* (2019) 'Positional Strategies for Connection Specificity and Synaptic Organization in Spinal Sensory-Motor Circuits', *Neuron*. Elsevier Inc., 102(6), pp. 1143-1156.e4. doi: 10.1016/j.neuron.2019.04.008.

Barlow, H. B. and Levick, W. R. (1965) *The mechanism of directionally selective units in rabbit's retina.*, *The Journal of Physiology*. doi: 10.1113/jphysiol.1965.sp007638.

Blanchart, A., De Carlos, J. A. and López-Mascaraque, L. (2006) 'Time frame of mitral cell development in the mice olfactory bulb', *Journal Comparative and General Neurology*, 543(August 2006), pp. 496–529. doi: 10.1002/cne.

Briggman, K. L., Helmstaedter, M. and Denk, W. (2011) 'Wiring specificity in the direction-selectivity circuit of the retina.', *Nature*. Nature Publishing Group, 471(7337), pp. 183–188. doi: 10.1038/nature09818.

Caval-Holme, F. and Feller, M. B. (2019) 'Gap Junction Coupling Shapes the Encoding of Light in the Developing Retina', *Current Biology*. Elsevier Ltd., 29(23), pp. 4024-4035.e5. doi: 10.1016/j.cub.2019.10.025.

Chen, Q. *et al.* (2016) 'Stimulus-dependent recruitment of lateral inhibition underlies retinal direction selectivity', *eLife*, 5, pp. 1–19. doi: 10.7554/eLife.21053.

Choi, J. H. *et al.* (2010) 'In vivo development of dendritic orientation in wild-type and mislocalized retinal ganglion cells', *Neural Development*, 5(1). doi: 10.1186/1749-8104-5-29.

Demb, J. B. (2007) 'Cellular Mechanisms for Direction Selectivity in the Retina', *Neuron*, 55(2), pp. 179–186. doi: 10.1016/j.neuron.2007.07.001.

Ding, H. *et al.* (2016) 'Species-specific wiring for direction selectivity in the mammalian retina', *Nature*. Nature Publishing Group, 535(7610), pp. 105–110. doi: 10.1038/nature18609.

Elias, E. *et al.* (2018) 'Glutamate activity regulates and dendritic development of J-RGCs', *Frontiers in Cellular Neuroscience*, 12(August), pp. 1–14. doi: 10.3389/fncel.2018.00249.

Greenough, W. T. and Chang, F. L. F. (1988) 'Dendritic pattern formation involves both oriented regression and oriented growth in the barrels of mouse somatosensory cortex', *Developmental Brain Research*, 43(1), pp. 148–152. doi: 10.1016/0165-3806(88)90160-5.

Harris, R. M. and Woolsey, T. A. (1981) 'Dendritic plasticity in mouse barrel cortex following

postnatal vibrissa follicle damage', *Journal of Comparative Neurology*, 196(3), pp. 357–376. doi: 10.1002/cne.901960302.

Hinds, J. W. and Ruffett, T. L. (1973) 'Mitral cell development in the mouse olfactory bulb: Reorientation of the perikaryon and maturation of the axon initial segment', *Journal of Comparative Neurology*, 151(3), pp. 281–305. doi: 10.1002/cne.901510305.

Hoon, M. *et al.* (2014) 'Functional architecture of the retina: Development and disease', *Progress in Retinal and Eye Research*. Elsevier Ltd, 42, pp. 44–84. doi: 10.1016/j.preteyeres.2014.06.003.

Kay, J. N. *et al.* (2011) 'Retinal Ganglion Cells with Distinct Directional Preferences Differ in Molecular Identity, Structure, and Central Projections', *Journal of Neuroscience*, 31(21), pp. 7753–7762. doi: 10.1523/JNEUROSCI.0907-11.2011.

Kay, J. N., Chu, M. W. and Sanes, J. R. (2012) 'MEGF10 and MEGF11 mediate homotypic interactions required for mosaic spacing of retinal neurons', *Nature*. Nature Publishing Group, 483(7390), pp. 465–469. doi: 10.1038/nature10877.

Kerschensteiner, D. *et al.* (2009) 'Neurotransmission selectively regulates synapse formation in parallel circuits in vivo', *Nature*. Nature Publishing Group, 460(7258), pp. 1016–1020. doi: 10.1038/nature08236.

Kostadinov, D. and Sanes, J. R. (2015) 'Protocadherin-dependent dendritic selfavoidance regulates neural connectivity and circuit function', *eLife*, 4(JULY2015), pp. 1–23. doi: 10.7554/eLife.08964.

Lefebvre, J. L. *et al.* (2012) 'Protocadherins mediate dendritic self-avoidance in the mammalian nervous system', *Nature*. doi: 10.1038/nature11305.

Lefebvre, J. L., Sanes, J. R. and Kay, J. N. (2015) 'Development of Dendritic Form and Function.', *Annual review of cell and developmental biology*, 31(1), pp. 741–77. doi: 10.1146/annurev-cellbio-100913-013020.

Leighton, A. H. and Lohmann, C. (2016) 'The wiring of developing sensory circuits—From patterned spontaneous activity to synaptic plasticity mechanisms', *Frontiers in Neural Circuits*, 10(SEP), pp. 1–13. doi: 10.3389/fncir.2016.00071.

Li, H. *et al.* (2013) 'Laminar and Columnar Development of Barrel Cortex Relies on Thalamocortical Neurotransmission', *Neuron*. Elsevier Inc., 79(5), pp. 970–986. doi: 10.1016/j.neuron.2013.06.043.

Liu, X. *et al.* (2007) 'Brain-derived neurotrophic factor and TrkB modulate visual experience-dependent refinement of neuronal pathways in retina', *J Neurosci*, 27(27), pp. 7256–7267. doi: 10.1523/JNEUROSCI.0779-07.2007.

Matsui, A. *et al.* (2013) 'BTBD3 Controls Dendrite Orientation Toward Active Axons in

Mammalian Neocortex', *Science*, 342(November), pp. 1114–1118.

Matsumoto, A., Briggman, K. L. and Yonehara, K. (2019) 'Spatiotemporally Asymmetric Excitation Supports Mammalian Retinal Motion Sensitivity', *Current Biology*. Elsevier Ltd., 29(19), pp. 3277-3288.e5. doi: 10.1016/j.cub.2019.08.048.

Mazurek, M., Kager, M. and Van Hooser, S. D. (2014) 'Robust quantification of orientation selectivity and direction selectivity', *Frontiers in Neural Circuits*, 8(AUG), pp. 1–17. doi: 10.3389/fncir.2014.00092.

Mizuno, H. *et al.* (2014) 'NMDAR-regulated dynamics of layer 4 neuronal dendrites during thalamocortical reorganization in neonates', *Neuron*. Elsevier Inc., 82(2), pp. 365–379. doi: 10.1016/j.neuron.2014.02.026.

Mizuno, H. *et al.* (2018) 'Patchwork-Type Spontaneous Activity in Neonatal Barrel Cortex Layer 4 Transmitted via Thalamocortical Projections', *Cell Reports*. ElsevierCompany., 22(1), pp. 123–135. doi: 10.1016/j.celrep.2017.12.012.

Morrie, R. D. and Feller, M. B. (2015) 'An Asymmetric Increase in Inhibitory Synapse Number Underlies the Development of a Direction Selective Circuit in the Retina', *Journal of Neuroscience*, 35(25), pp. 9281–9286. doi: 10.1523/JNEUROSCI.0670-15.2015.

Morrie, R. D. and Feller, M. B. (2018) 'A Dense Starburst Plexus Is Critical for Generating Direction Selectivity', *Current Biology*. Elsevier Ltd, 28(8), pp. 1204-1212.e5. doi: 10.1016/j.cub.2018.03.001.

Nakazawa, S., Mizuno, H. and Iwasato, T. (2018) 'Differential dynamics of cortical neuron dendritic trees revealed by long-term in vivo imaging in neonates', *Nature Communications*. Springer US, 9(1). doi: 10.1038/s41467-018-05563-0.

Narboux-Nême, N. *et al.* (2012) 'Neurotransmitter release at the thalamocortical synapse instructs barrel formation but not axon patterning in the somatosensory cortex', *Journal of Neuroscience*, 32(18), pp. 6183–6196. doi: 10.1523/JNEUROSCI.0343-12.2012.

Peng, Y. R. *et al.* (2017) 'Satb1 Regulates Contactin 5 to Pattern Dendrites of a Mammalian Retinal Ganglion Cell', *Neuron*. Elsevier Inc., 95(4), pp. 869-883.e6. doi: 10.1016/j.neuron.2017.07.019.

Pologruto, T. A., Sabatini, B. L. and Svoboda, K. (2003) 'ScanImage: Flexible software for operating laser scanning microscopes', *BioMedical Engineering Online*, 2, pp. 1–9. doi: 10.1186/1475-925X-2-13.

Richards, S. E. V. and Van Hooser, S. D. (2018) 'Neural architecture: From cells to circuits', *Journal of Neurophysiology*, 120(2), pp. 854–866. doi: 10.1152/jn.00044.2018.

Riemann, H. . W. and H. . J. . (1978) 'The Mosaic of Nerve Cells in the Mammalian Retina',

Proceedings of the Royal Society of London, 200(1141), pp. 441–461.

Rockhill, R. L., Euler, T. and Masland, R. H. (2000) 'Spatial order within but not between types of retinal neurons', *Proceedings of the National Academy of Sciences of the United States of America*, 97(5), pp. 2303–2307. doi: 10.1073/pnas.030413497.

Rosa, J. M. *et al.* (2016) 'Contributions of rod and cone pathways to retinal direction selectivity through development', *Journal of Neuroscience*, 36(37), pp. 9683–9695. doi: 10.1523/JNEUROSCI.3824-15.2016.

Sabbah, S. *et al.* (2017) 'A retinal code for motion along the gravitational and body axes', *Nature*. Nature Publishing Group, 546(7659), pp. 492–497. doi: 10.1038/nature22818.
Stuart, G. J. and Spruston, N. (2015) 'Dendritic integration: 60 years of progress', *Nature Neuroscience*, 18(12), pp. 1713–1721. doi: 10.1038/nn.4157.

Sun, L. O. *et al.* (2013) 'On and off retinal circuit assembly by divergent molecular mechanisms', *Science*, 342(6158). doi: 10.1126/science.1241974.

Tian, N. and Copenhagen, D. R. (2001) 'Visual deprivation alters development of synaptic function in inner retina after eye opening', *Neuron*, 32(3), pp. 439–449. doi: 10.1016/S0896-6273(01)00470-6.

Trenholm, S. *et al.* (2011) 'Parallel mechanisms encode direction in the retina', *Neuron*. Elsevier Inc., 71(4), pp. 683–694. doi: 10.1016/j.neuron.2011.06.020.

Trenholm, S. *et al.* (2013) 'Dynamic tuning of electrical and chemical synaptic transmission in a network of motion coding retinal neurons', *J Neurosci*, 33(37), pp. 14927–14938. doi: 10.1523/JNEUROSCI.0808-13.2013.

Vaney, D. I. and Taylor, W. R. (2002) 'Direction selectivity in the retina', *Current Opinion in Neurobiology*. Elsevier Ltd, pp. 405–410. doi: 10.1016/S0959-4388(02)00337-9.

Wei, W. *et al.* (2011) 'Development of asymmetric inhibition underlying direction selectivity in the retina.', *Nature*. Nature Publishing Group, 469(7330), pp. 402–406. doi: 10.1038/nature09600.

Wei, W., Elstrott, J. and Feller, M. B. (2010) 'Two-photon targeted recording of GFP-expressing neurons for light responses and live-cell imaging in the mouse retina', *Nature Protocols*. Nature Publishing Group, 5(7), pp. 1347–1352. doi: 10.1038/nprot.2010.106.

Wong, R. O. L. and Ghosh, A. (2002) 'Activity-dependent regulation of dendritic growth and patterning.', *Nature reviews. Neuroscience*, 3(10), pp. 803–812. doi: 10.1038/nrn941.

Woolsey, T. A. and Van der Loos, H. (1970) 'The structural organization of layer IV in the somatosensory region (S I) of mouse cerebral cortex. The description of a cortical field composed of discrete cytoarchitectonic units', *Brain Research*, 17(2), pp. 205–242. doi:

10.1016/0006-8993(70)90079-X.

Yao, X. *et al.* (2018) 'Gap Junctions Contribute to Differential Light Adaptation across Direction-Selective Retinal Ganglion Cells', *Neuron*. Elsevier Inc., 100(1), pp. 216-228.e6. doi: 10.1016/j.neuron.2018.08.021.

Yonehara, K. *et al.* (2011) 'Spatially asymmetric reorganization of inhibition establishes a motion-sensitive circuit.', *Nature*. Nature Publishing Group, 469(7330), pp. 407–410. doi: 10.1038/nature09711.

Yonehara, K. *et al.* (2016) 'Congenital Nystagmus Gene FRMD7 Is Necessary for Establishing a Neuronal Circuit Asymmetry for Direction Selectivity', *Neuron*, 89(1), pp. 177–193. doi: 10.1016/j.neuron.2015.11.032.

Zhang, L., Wu, Q. and Zhang, Y. (2020) 'Early visual motion experience shapes the gap junction connections among direction selective ganglion cells', *PLOS Biology*, 18(3), p. e3000692. doi: 10.1371/journal.pbio.3000692.

Rall, W. (1964). Theoretical significance of dendritic trees for neuronal input output relations. In Neural Theory and Modeling, R.F. Reiss, ed. (Stanford University Press), pp. 73–97.

KEY RESOURCES TABLE

REAGENT OR RESOURCE	SOURCE	IDENTIFIER
Antibodies		
Rabbit polyclonal anti-GFP	Invitrogen	Cat# A-11122; RRID: AB_221569
Goat polyclonal anti-Choline Acetyltransferase (ChAT)	Millipore	Cat# AB144P; RRID:AB_2079751
Donkey anti-rabbit Alexa Fluor 488	Invitrogen	Cat# A-21206; RRID:AB_2535792
Donkey anti-goat Alexa Fluor 594	Invitrogen	Cat# A-11058; RRID:AB_2534105
Chemicals, Peptides and Recombinant proteins		
Vectashield	Vector Laboratories	Cat# H-1400; RRID: AB_2336787
Neurobiotin	Vector Laboratories	Cat# SP-1120; RRID: AB_2313575
Streptavidin Alexa Fluor 594 conjugate	Invitrogen	Cat# S11227; RRID:
QX 314 Chloride	Tocris	Cat# 2313
Ames' Media	Sigma	Cat# A1420-10X1L
SR 95531 hydrobromide (gabazine)	Tocris	Cat# 1262
Experimental Models: Organisms/Strains		
Mouse: B6.Cg-Tg(Hlxb9-GFP)1Tmj/J (Hb9:GFP)	The Jackson Laboratory	RRID: IMST_JAX:005029
Software and Algorithms		
Simple Neurite Tracer FIJI plugin	NIH	https://imagej.net/Simple_Neurite_Tracer
FIJI	NIH	https://imagej.nih.gov/ij; RRID:SCR_003070
MATLAB	Mathworks	https://www.mathworks.com/products/matlab.html; RRID: SCR_001622
FIJI Dendrite analysis macro	This paper	
ScanImage4	(Pologruto, Sabatini and Svoboda, 2003)	http://scanimage.vidriotechnologies.com/display/SIH/ScanImage+Home; RRID: SCR_014307
Clampex 10.3	Molecular Devices	RRID: SCR_011323

FIGURE 1

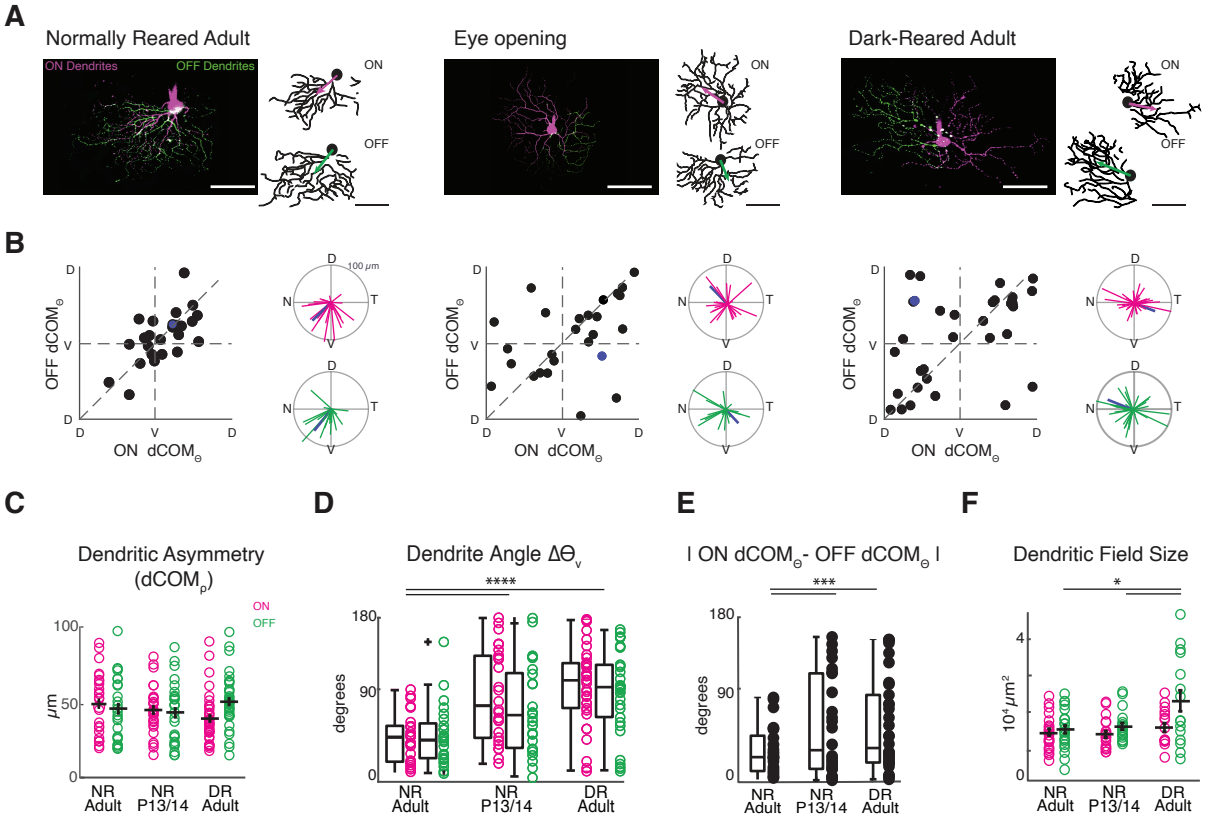
A
Normally Reared Adult
Eye opening
Dark-Reared Adult
ON Dendrites
OFF Dendrites
ON
OFF
B
OFF dCOM
ON dCOM
100 μm
C
Dendritic Asymmetry
(dCOM)
μm
NR Adult
NR P13/14
DR Adult
D
Dendrite Angle ΔΘ
degrees
****
E
I ON dCOM - OFF dCOM I
***
F
Dendritic Field Size
*

FIGURE 2

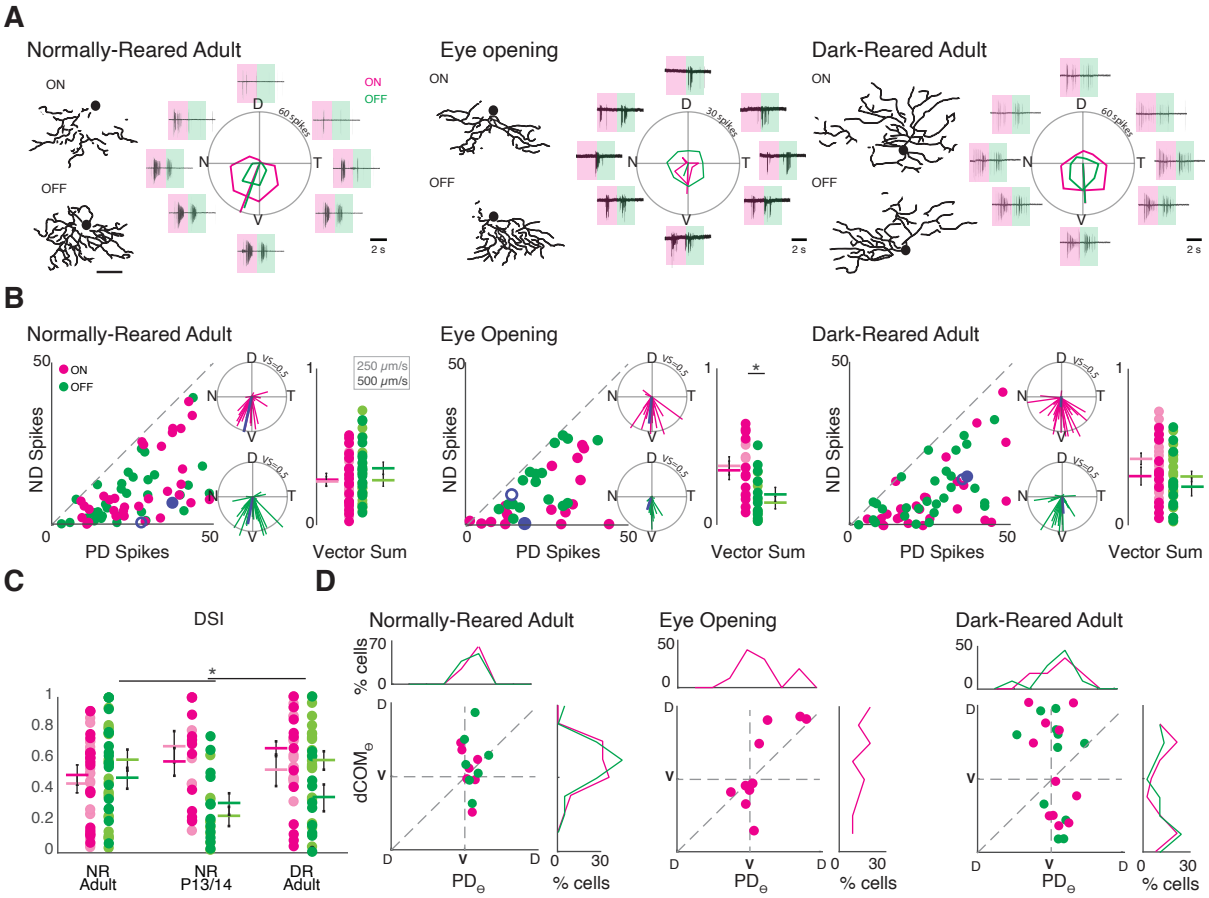
A
Normally-Reared Adult
Eye opening
Dark-Reared Adult
ON
OFF
B
Normally-Reared Adult
Eye Opening
Dark-Reared Adult
ND Spikes
PD Spikes
Vector Sum
250 μm/s
500 μm/s
C
DSI
NR Adult
NR P13/14
DR Adult
D
Normally-Reared Adult
Eye Opening
Dark-Reared Adult
% cells
dCOM
PD
% cells

FIGURE 3

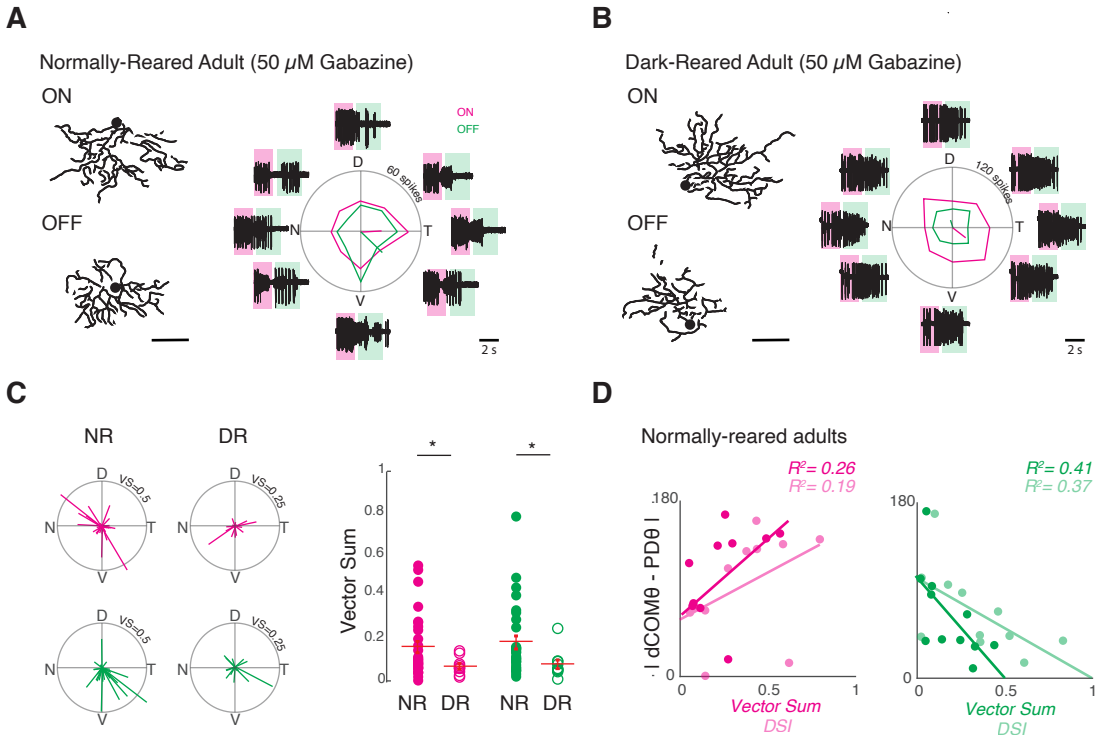
A
Normally-Reared Adult (50 μM Gabazine)
ON
OFF
ON
OFF
D
N
T
V
60 spikes
2 s
B
Dark-Reared Adult (50 μM Gabazine)
ON
OFF
120 spikes
2 s
C
NR
DR
VS=0.5
VS=0.25
Vector Sum
NR DR NR DR
D
Normally-reared adults
R²= 0.26
R²= 0.19
R²= 0.41
R²= 0.37
180
0
0.5
1
Vector Sum
DSI

FIGURE 4

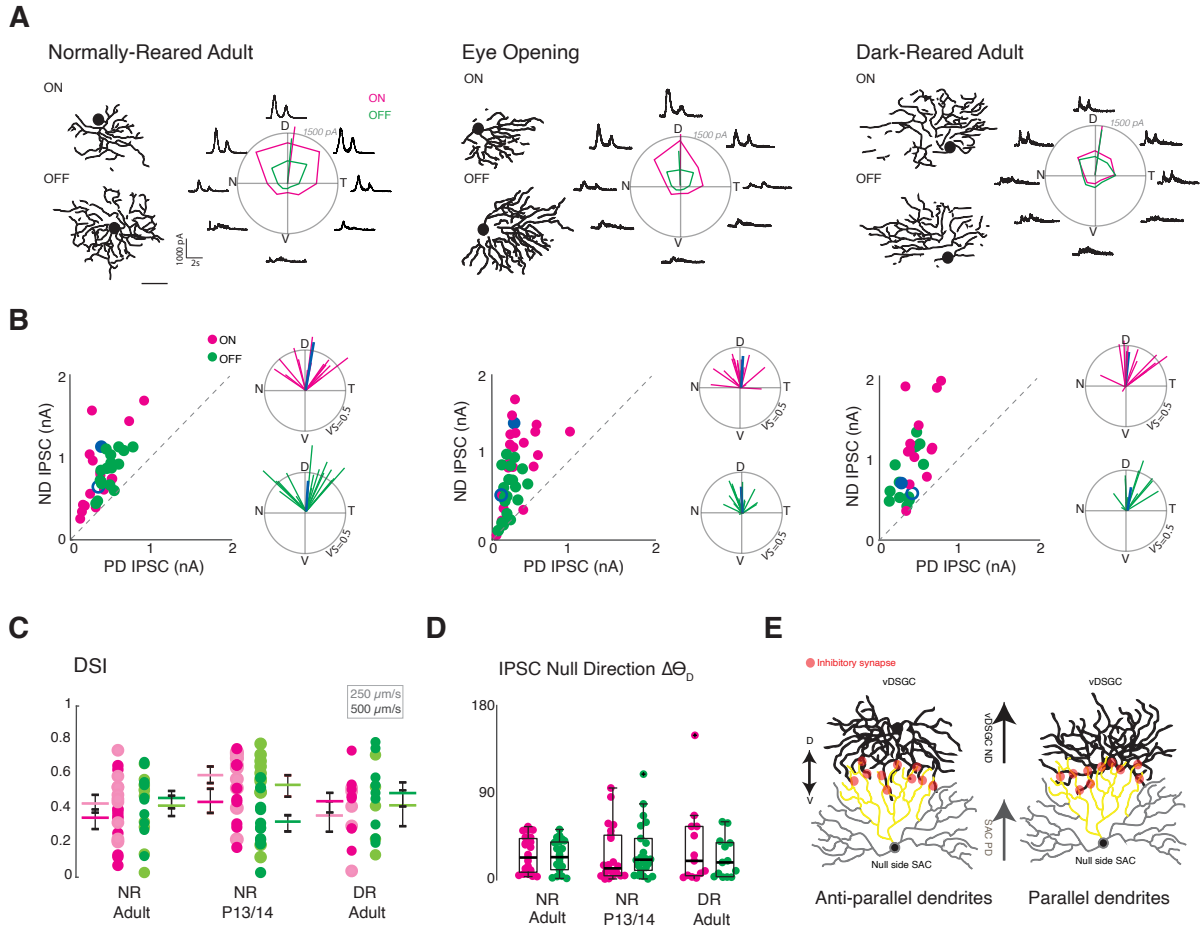
A
Normally-Reared Adult
Eye Opening
Dark-Reared Adult
ON
OFF
1500 pA
2s
B
ND IPSC (nA)
PD IPSC (nA)
VS=0.5
C
DSI
250 μm/s
500 μm/s
NR Adult
NR P13/14
DR Adult
D
IPSC Null Direction ΔΘD
E
Inhibitory synapse
vDSGC
Null side SAC
Anti-parallel dendrites
Parallel dendrites

FIGURE 5

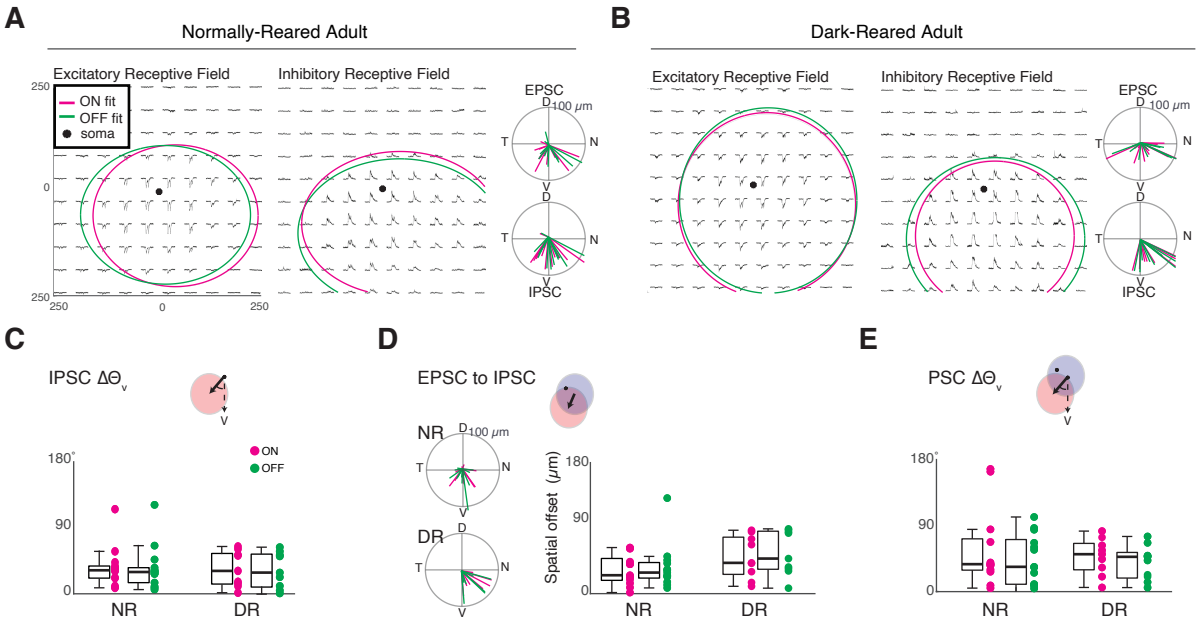
A
Normally-Reared Adult
Excitatory Receptive Field
Inhibitory Receptive Field
ON fit
OFF fit
soma
EPSC
IPSC
100 μm
B
Dark-Reared Adult
C
IPSC ΔΘv
ON
OFF
NR
DR
D
EPSC to IPSC
Spatial offset (μm)
E
PSC ΔΘv

Supplemental Figure 1

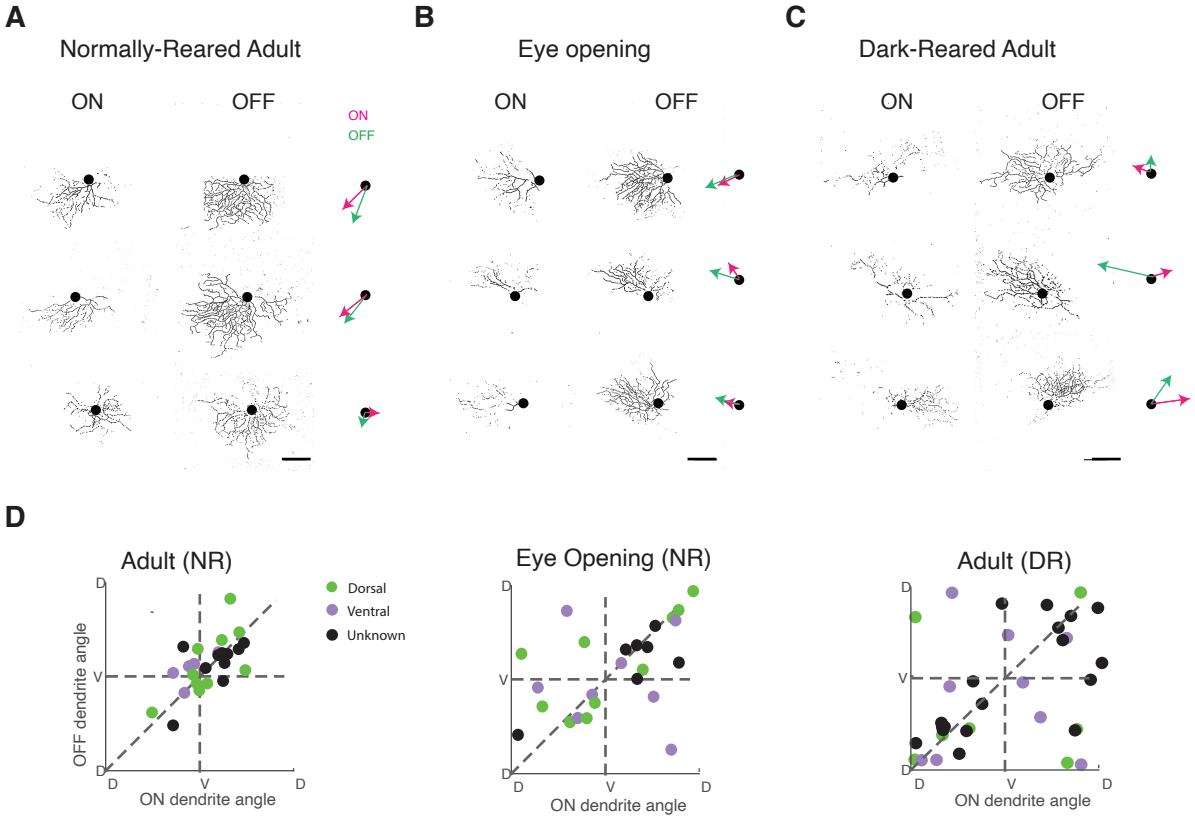

Figure S1: Dendritic Center of Mass (dCOM) as a measurement for dendrite orientation and asymmetry. Related to Figure 1.
(A-C) Three examples of ON and OFF skeletons of normally-reared adult (a) eye opening (b) and dark-reared adult (c) vDSGCs. Image scale bar = 100 µm. Right: magenta (ON) and green (OFF) vectors of dCOM about the soma. Note these dendritic skeletons are produced using a customized algorithm (see Methods) then used for analysis and they differ from the example dendrite skeletons shown in Figure 1. (D) Dendritic orientation in NR adults, at eye opening and in DR adults. Color indicates location on the retina. We do not observe an effect of location on the orientation of ON and OFF dendrites.

Supplemental Figure 2

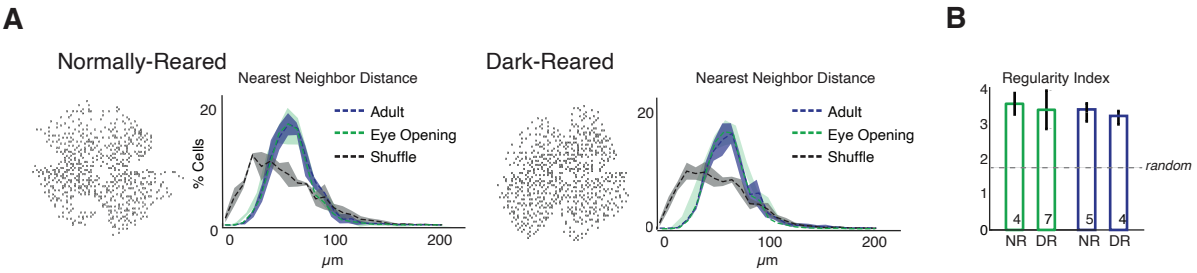

Figure S2: Visual experience does not alter mosaic organization of vDSGC somas. Related to Figure 1.

(A) Mosaic analysis of soma locations for normally reared vs dark reared adults . Left: binarized image marking soma locations across retina. Right: Nearest neighbor distance distributions (10 μm bins) for actual locations and for randomly shuffled distances. Significance assessed by one- way ANOVA, $p>0.05$.

(B) Regularity index shows that vDSGC somas are non-randomly distributed under all conditions. Numbers at the bottom of bar plot = number of retinas sampled. Random regularity index value obtained from a distribution of randomized distances.

Supplemental Figure 3

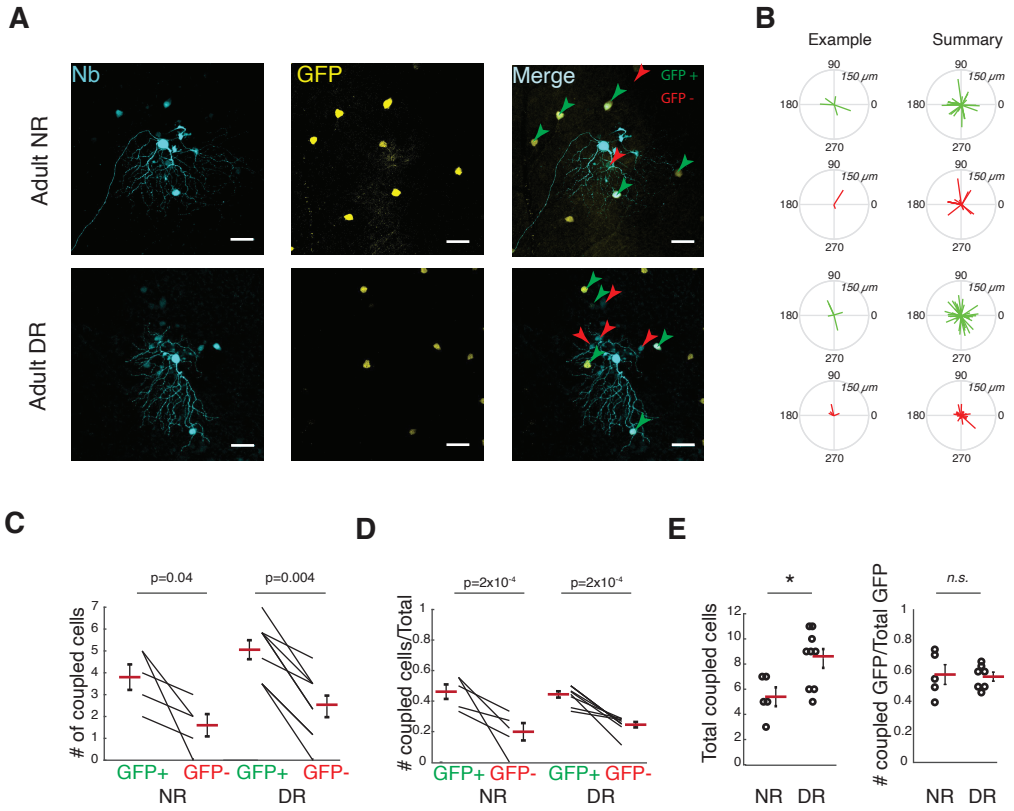

Figure S3: Dark rearing does not influence tracer coupling of vDSGCs. Related to Figure 1. (A) Confocal images of fixed retinas from normally-reared (NR - top row) and dark-reared (DR - bottom row) animals that are stained for neurobiotin (Nb - cyan, left) to label cells that are coupled to the injected cell and GFP (middle) to label vDSGCs. Merge channel shows coupled cells that are GFP positive (green arrowhead) and GFP negative (red arrowhead). Scale Bar = 50 μm. (B) Polar plots of the vector from the injected cell to each GFP positive (green) and GFP negative (red) coupled cell. Data for example cell (left) and population data (right) plotted separately. (C) Quantification of GFP positive and GFP negative coupled cells in normally-reared (NR) and dark-reared (DR) adult vDSGCs. Significance assessed by ANOVA, p =8.2x10-5, Tukey-Kramer test p-values shown on plot. Other relevant interactions are not statistically significant. (D) Quantification of the proportion of GFP positive and GFP negative coupled cells for normally-reared (NR) and dark-reared (DR) adult vDSGCs relative to the total number of coupled cells. Significance assessed by ANOVA, p =3.6x10-6, Tukey-Kramer test p-values shown on plot. Other relevant interactions are not statistically significant.
(E) Left: Quantification of the total number of coupled cells in normally-reared (NR) and dark-reared (DR) adult vDSGCs. Significance assessed by t-test, p=0.03 . Right: Quantification of the proportion of GFP positive coupled cells relative to the total number of GFP positive cells (both coupled and uncoupled). Significance assessed by t-test, p=0.93.

Supplemental Figure 4

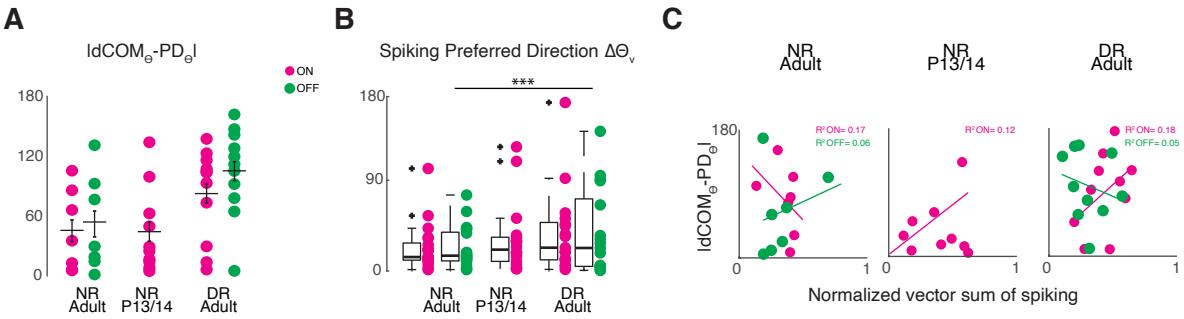

Figure S4: Ventral motion tuning is preserved in dark-reared mice despite altered vDSGC dendritic morphology. Related to Figure 2.

(A) Quantification of the alignment of dendrite orientation and preferred direction of vDSGCs. Data for ON (magenta) and OFF (green) plotted separately. Horizontal bar = mean, errors bars = SEM. Significance assessed by Kruskal Wallis test, p>0.05. Note, P13/14 OFF responses were excluded from this analysis due to weak tuning (See Figure 2c).

(B) Quantification of the alignment of vDSGC for ON (magenta) and OFF (green) spiking preferred direction to the ventral direction (ΔΘv). Horizontal bar = median. Significance assessed by Levene's test for absolute variance ***pOFF<0.002, pON>0.05. Note, P13/14 OFF responses were excluded from this analysis due to weak tuning.

(C) Comparison of the degree of alignment of dendrite orientation (dCOMΘ) and preferred direction (PDΘ) to the tuning strength of the vDSGCs based on the magnitude of the normalized vector sum of the tuning curve. Correlation of determination (R2) for ON (magenta) and OFF (green) values indicated on plot. Statistical significance of all correlation coefficients asessed using t-tests, p>0.05.

Supplemental Figure 5

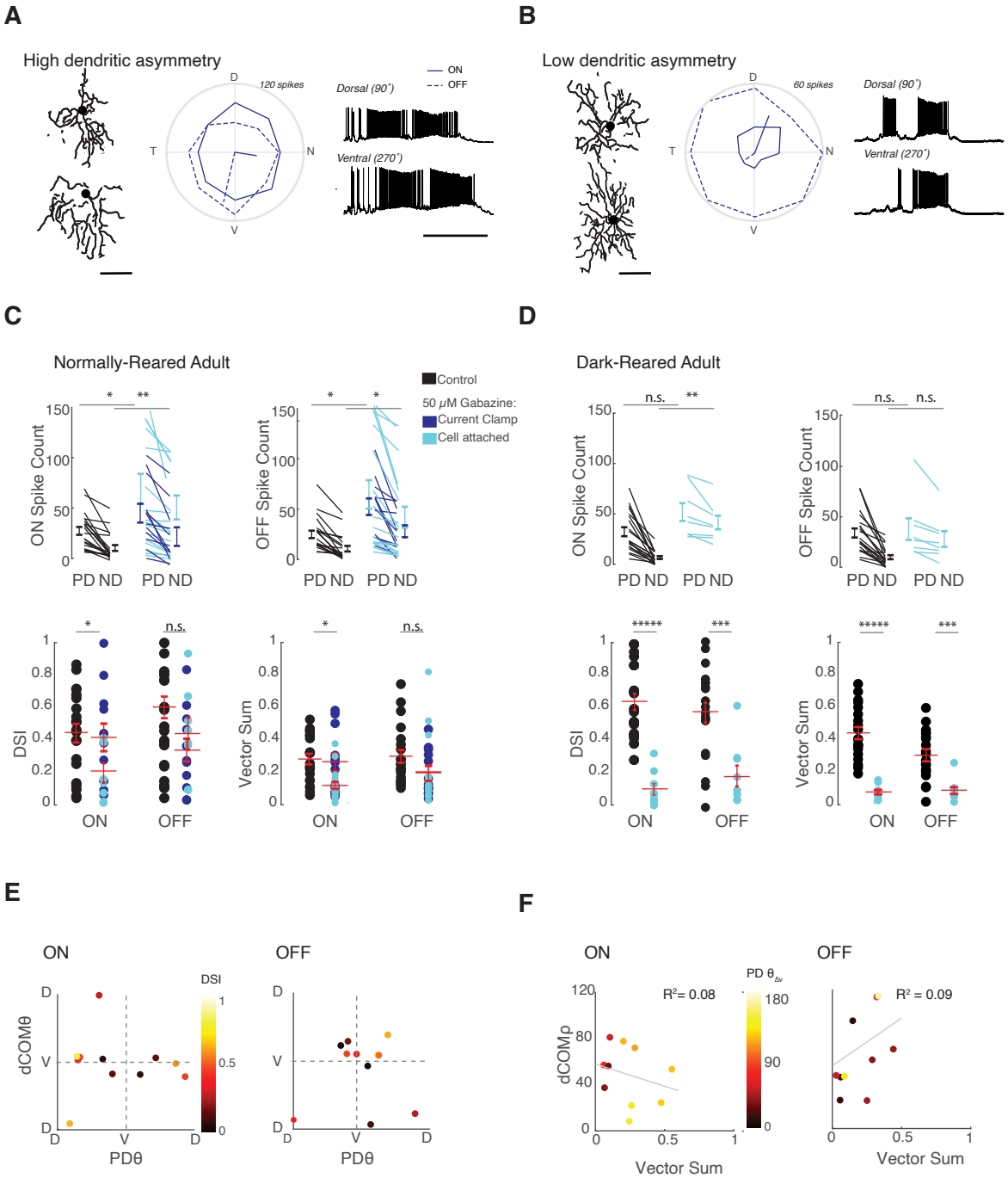

Figure S5: Dendritic alignment with preferred direction enhances strength of inhibition-independent directional tuning in normally-reared adult vDSGCs. Related to Figure 3.
(A) Left: example dendrite skeletons for ON and OFF dendritic segments for a normally-reared adult vDSGC that has dendrites with high dendritic asymmetry. Right: example average spike responses of the same cell in the presence of 50 µM gabazine in current clamp configuration. Tuning curves plotted in polar ON (solid line) and OFF (dashed line) responses. Radius of tuning curve =120 spikes. (B) Left: example dendrite skeletons for ON and OFF dendritic segments for a normally-reared adult vDSGC that has dendrites with low dendritic asymmetry. Right: example average spike responses of the same cell in the presence of 50 µM gabazine. Tuning curves plotted in polar ON (solid line) and OFF (dashed line) responses. Radius of tuning curve = 60 spikes.
(C)Top: Preferred (PD) vs. null (ND) direction spike counts for ON (left) and OFF (right) responses in normally-reared adult vDSGCs recorded in control conditions (black) and in 50 µM gabazine in current clamp configuration (navy) and cell attached configuration (cyan). Note control data replicated from cell-attached recordings in Figure 2 (250 µm/s bar). Bottom: Population data of spike tuning strength using DSI (left) and the magnitude of the vector sum of the tuning curve (Vector Sum - right) for ON and OFF spike responses in the presence of 50 µM Gabazine, recorded in current clamp (navy) and voltage clamp (cyan) configurations. Statistical significance assessed using t-tests.*$p<0.05$, **$p<0.01$, n.s. $p>0.05$. (D) Top: Preferred (PD) vs. null (ND) direction spike counts for ON (left) and OFF (right) responses in dark-reared adult vDSGCs recorded in control conditions (black) and in 50 µM gabazine in cell attached configuration (cyan). Note control data replicated from cell-attached recordings in Figure 2 (250 µm/s bar). Bottom: Population data of spike tuning strength using DSI (left) and the magnitude of the vector sum of the tuning curve (Vector Sum - right) for ON and OFF spike responses in the presence of 50 µM Gabazine, recorded in current clamp (navy) and voltage clamp (cyan) configurations. Statistical significance assessed using t-tests. **$p<0.01$, ***$p<0.001$, ****$p<0.0001$, n.s. $p>0.05$.
(E) Comparison of dendritic orientation (dCOMΘ) vs. spiking directional preference (PDΘ) , for normally-reared adult vDSGCs in the presence of 50 µM Gabazine. X and Y axes centered on ventral axis (V). ON (left) and OFF (right) morphology-physiology plotted separately. Data is color coded based on tuning strength (DSI).
(F) Comparison of the magnitude of dendritic asymmetry (dCOMρ) varies with the magnitude of the normalized vector sum of the tuning curve for normally-reared adult vDSGCs in the presence of 50 µM Gabazine. ON (left) and OFF (right) morphology-physiology plotted separately. Data is color coded based on deviation of spiking preferred direction from the ventral axis (PDΔv) .R2 value indicates fraction of the variance in tuning strength that is explained by the magnitude of dendritic asymmetry and vice-versa. Statistical significance of correlation coefficient assessed by t-test, pON & OFF > 0.05.

Supplemental Figure 6

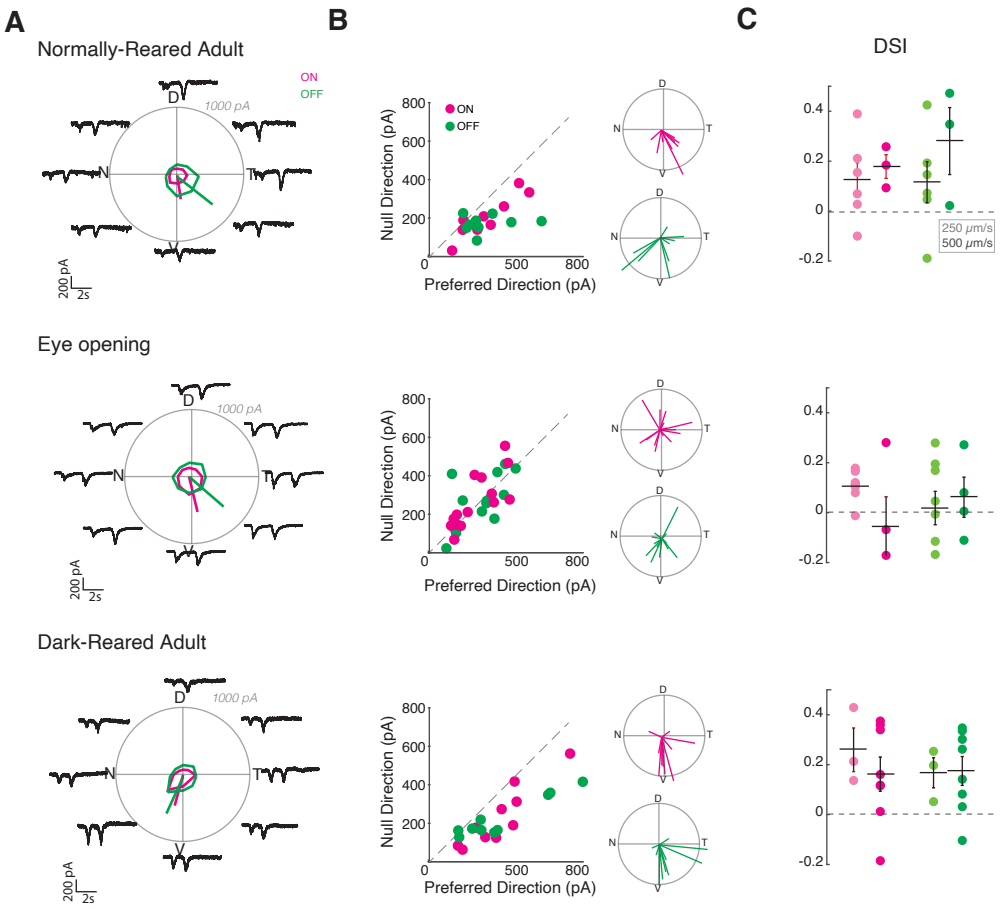

Figure S6: Adult vDSGCs exhibit weakly tuned excitatory input. Related to Figure 4.
(A) Example tuning curves of average ON (magenta) and OFF (green) excitatory currents of vDSGCs in normally-reared (top), at eye opening (middle row), and in dark-reared adults (bottom row) . Radius of polar plots = 1000 pA.
(B) Left: population data represented as peak amplitude of EPSC recorded for null direction (ND) vs. preferred direction (PD) stimulation in normally-reared adults (top) eye opening (middle) and dark reared (bottom) adults. Right: polar plot for normalized vector sums of population EPSC tuning curves. Note, radius of polar plot; Vector sum of the tuning curve = 0.25.
(C) Tuning strength of ON (magenta) and OFF (green) excitatory input of vDSGCs across two stimulus velocities (lighter shade: 250 μm/s; darker shade: 500 μm/s) quantified as the direction selectivity index (DSI) Horizontal bar = mean, errors bars = SEM. Significance assessed by t-tests.

Table S1: vDSGC dendritic morphology.
Related to Figure 1 and Supplemental Figure 1.

	Adult NR		Adult DR		Eye opening	
	ON	**OFF**	**ON**	**OFF**	**ON**	**OFF**
Orientation ($dCOM_\theta$)	235.7 ± 105.1	258.31 ± 86.5	177.3 ± 101.3	179.9 ± 121.4	182.4 ± 116.6	201.9 ± 110.2
|ON – OFF $dCOM_\theta$|	36.5 ±30.56		57.24 ± 48.15		56.22 ± 51.7	
Asymmetry ($dCOM_\rho$)	37.1± 20.4	34.1 ± 20.5	27.6 ±16.1	28.6 ±17.1	32.6 ± 16.1	30.7 ±19.7
Dendrite angle deviation from ventral ($\Delta\theta_v$)	54.1 ± 45.6	45.5 ±10.2	93.2±47.4	81.3 ± 46.1	92.5 ± 49.8	76.9 ± 48.1
	n=25	n=25	n=35	n=35	n=26	n=26

Table S2: vDSGC spike tuning.
Related to Figures 2,3 and Supplemental Figures 4,5.

	Adult NR		Adult DR		Eye opening	
	ON	**OFF**	**ON**	**OFF**	**ON**	**OFF**
500 µm/s						
Preferred direction (PD) spike count	31.0 ± 13.2	24.4 ± 12.1	26.7 ± 13.2	21.5 ± 12.1	22.7 ± 11.8	20.0 ± 7.4
Null direction (ND) spike count	12.9 ±11.1	8.2 ± 9.2	11.6 ± 13.4	12.4 ± 8.9	9.0 ± 9.7	11.8 ± 8.4
Spike DSI	0.50 ± 0.28	0.60 ± 0.29	0.54±0.35	0.35±0.30	0.58 ±0.31	0.31 ±0.24
	n=18	n=18	n=12	n=12	n=12	n=12
250 µm/s						
PD spike count	30.2 ± 17.8	25.5 ±16.9	32.5 ± 19.9	33.8 ± 20.2	20.8 ± 15.0	19.9 ± 11.7
ND spike count	13.2 ± 13.3	11.3 ± 12.8	6.8 ± 6.29	9.8 ± 12.8	3.2 ± 4.5	13.0 ± 9.1
Spike DSI	0.44 ± 0.26	0.48 ± 0.31	0.66 ±0.26	0.59 ± 0.21	0.68 ±0.30	0.23 ± 0.19
	n=21	n=21	n=20	n=20	n=9	n=9
PD angle deviation from ventral ($\Delta\theta_v$)	23.8 ±23.2	22.9 ±20.8	40.6 ± 43.8	42.6 ±44.1	31.6 ± 35.1	---
$\lvert PD_\Theta - dCOM_\Theta \rvert$	44.0 ±40.8	52.8 ±48.4	83.6 ±45.1	105.8± 43.8	44.6 ± 42.7	---
	n=12	n=12	n=16	n=16	n=18	n=18
250 µm/s						
PD spike count (gabazine)	63.8 ± 53.5	58.5 ± 49.2	46.0 ± 261	40.1 ± 28.2	---	---
ND spike count (gabazine)	43.4 ± 44.2	35.2 ± 36.4	37.0 ± 20.9	31.5 ± 22.8	---	---
Spike DSI (gabazine)	0.28 ±0.24	0.35 ±0.26	0.14 ± 0.17	0.15 ± 0.17	---	---
Spike Vector Sum Magnitude (gabazine)	0.16 ±0.15	0.18 ±0.17	0.07±0.04	0.08±0.07	---	---
	n=30	n=30	n=10	n=10	---	---

Table S3: Synaptic currents. ***Related to Figures 4 and 5.***

	Adult NR		Adult DR		Eye opening	
	ON	**OFF**	**ON**	**OFF**	**ON**	**OFF**
500 µm/s						
Preferred Direction (PD) IPSC amplitude	354 ± 228	252 ± 128	501.34 ± 169.18	296.71 ± 148.17	348.11 ± 231.25	226.57 ± 132.31
Null Direction (ND) IPSC amplitude	875.71 ± 474.8	651.67 ± 243.42	1279 ± 453.62	801.43 ± 261.50	861.60 ± 352.14	460.46 ± 271.92
IPSC DSI	0.43 ±0.17	0.45 ±0.16	0.42 ±0.18	0.47 ± 0.22	0.45 ±0.24	0.31 ± 0.16
	n=11	n=11	n=8	n=8	n=11	n=11
250 µm/s						
PD IPSC amplitude	451.3 ± 248.46	331.66 ± 358.72	381.39 ± 38.2	267.32 ± 128.54	193.10 ± 79.89	141.21 ± 56.71
ND IPSC amplitude	965.15 ± 509.15	642.27 ± 320.47	862.26 ± 327.87	629.08 ± 320.47	962.03 ± 469.65	573.59 ± 287.56
IPSC DSI	0.35 ± 0.78	0.41 ±0.18	0.34 ±0.19	0.39 ±0.23	0.60 ±0.16	054 ±0.21
	n=12	n=12	n=5	n=5	n=11	n=11
ND angle deviation from dorsal ($\Delta\theta_D$)	18.76 ± 10.66	20.93 ± 12.91	6.87 ± 26.91	3.45 ± 11.65	5.58 ± 14.5	5.14 ± 14.3
	n=7	n=7	n=5	n=5	n=10	n=10
RF Mapping						
EPSC peak amplitude	216.9 ± 100.0	194.6 ± 79.7	199.28 ± 85.83	167.44 ± 79.34	---	---
IPSC peak amplitude	484.5 ± 194.1	383.4 ± 133.1	489.6 ± 143.2	367.6 ± 106.3	---	---
Inhibition ($\Delta\theta_v$)	31.9 ± 27.0	31.6 ± 29.5	34.2 ± 25.2	32.9 ± 24.4	---	---
E-I distance	31.6 ± 20.7	35.0 ± 31.0	53.2 ± 29.3	58.6 ± 30.7	--	---
E-I Angle	239.4 ± 76.6	247.0 ± 85.6	276.9 ± 55.2	277.2 ± 28.0	---	---
E-I Angle ($\Delta\theta_v$)	54.5 ± 52.5	42.3 ± 33.5	47.0 ± 24.9	40.0 ± 23.6	---	---
	n=13	n=13	n=9	n=9	---	---

Chapter 3: Dendrite morphology minimally influences the synaptic distribution of excitation and inhibition in retinal direction selective ganglion cells.

Publication related to this work:
This chapter is a full reprint of El-Quessny & Feller (under review), of which I was the primary author. This work is included with permission from all authors.

SUMMARY

Throughout the nervous system, the organization of excitatory and inhibitory synaptic inputs within a neuron's receptive field shapes its output computation. In some cases, multiple motifs of synaptic organization can contribute to a single computation. Here, we compare two of these mechanisms performed by two morphologically distinct direction selective retinal ganglion cells (DSGCs): directionally tuned inhibition and spatially offset inhibition. Using drifting stimuli, we found that DSGCs that have asymmetric dendrites exhibited stronger directionally tuned inhibition than symmetric DSGCs. Using stationary stimuli to map receptive fields, we found that DSGCs with both symmetric and asymmetric dendrites exhibited similar spatially offset inhibition. Interestingly, we observed that excitatory and inhibitory synapses for both cell types were locally correlated in strength. This result indicates that in the mouse retina, dendritic morphology influences the amount of tuned inhibition attained through asymmetric wiring but does not dictate the synaptic organization of excitation relative to inhibition.

INTRODUCTION

Detecting the direction of moving stimuli is an essential part of sensory processing. In the mouse visual system, direction selectivity is first observed in the retina, where direction selective ganglion cells (DSGCs) fire many action potentials in response to motion in their preferred direction, and few to no action potentials in response to the opposite, or null, direction. Direction selective computations occur across many layers of the mammalian visual system from DSGCs of the retina, to the retino-recipent neurons of the dorsal lateral geniculate nucleus (dLGN) of the thalamus (Liang et al., 2018; Marshel et al., 2012), thalamo-recipient layer 4 neurons and intracortical circuits of the visual cortex (Rasmussen et al., 2020; Rossi et al., 2020). Additionally, direction selectivity has been shown to arise in nonvisual areas like the mouse whisker somatosensory cortex (Laboy-Juárez et al., 2019)and in the primary auditory cortex (Ye et al., 2010; Zhang et al., 2003).

Retinal direction selectivity is mediated primarily by inhibition through two non-mutually exclusive mechanisms. The first mechanism mediating direction selectivity is based on directional tuning of inhibition, where the amount of inhibitory input onto a DSGC is greater for null direction motion than for preferred direction motion. In the mammalian retina, this asymmetric inhibition is provided by starburst amacrine cells (SACs), where the combination of SAC centrifugal directional tuning (Ding et al., 2016; Gavrikov et al., 2006; Hausselt et al., 2007; Vlasits et al., 2016), and DSGC-SAC asymmetric wiring (Briggman et al., 2011; Rosa et al., 2016; Wei et al., 2011; Yonehara et al., 2011) ensures maximal spike suppression in response to null direction motion, compared to preferred direction motion. Though the role of asymmetric inhibition in tuning the direction selective circuit has been well established in the mouse and rabbit (Fried et al., 2002; Grama & Engert, 2012; Morrie & Feller, 2015; Taylor & Vaney, 2002; Wei et al., 2011; Yonehara et al., 2011), its dependence on the morphology of DSGCs has been unexplored.

The second mechanism is based on spatially offset inhibition - a term used to describe when excitatory and inhibitory receptive fields are spatially offset from each other such that, preferred direction motion elicits an excitatory response before the stimulus enters the inhibitory receptive field, thus a temporal delay is introduced into the inhibitory response. During null direction motion, the stimulus enters the inhibitory receptive field before it enters the excitatory receptive field, thus a temporal delay is introduced to the excitatory response and the inhibitory input effectively suppresses spiking output. This is the classical mechanism postulated to underlie direction-selective responses in both the retina (Fried et al., 2002; Yonehara et al., 2011) and in the visual cortex (Hubel & Wiesel, 1959, 1962; Priebe & Ferster, 2005; Rossi et al., 2020). Several studies have revealed temporal delays, consistent with spatially offset inhibition, play a role in the DS computation of the mouse retina (Hanson et al., 2019; Pei et al., 2015).

Here we explore whether directional tuning of inhibition or spatially offset inhibition are influenced by the dendritic morphology of two subsets of DSGCs. The first is a subset of DSGCs which prefer ventral motion (vDSGCs), which have asymmetric dendrites that are oriented toward their preferred direction (Trenholm et al., 2011), a configuration which contributes to their direction selectivity. The second is a subset of DSGCs which prefer nasal motion

(nDSGCs), which have symmetric dendrites that are not oriented in any particular direction. Multielectrode array data has shown that the spiking output of both vDSGCs and nDSGCs possesses similar directional tuning under bright stimulus conditions (Yao et al., 2018), however their dendritic differences imply different organization of inhibitory synapses (Figure 1). nDSGCs have symmetric dendrites (Rivlin-Etzion et al., 2011) that are more likely to overlap with SACs on their preferred side, we hypothesized that this may result in broader distribution of inhibitory synapses facilitating more spatially offset inhibition than vDSGCs. vDSGCs have asymmetric dendrites which point towards starburst amacrine cells located on the DSGC's null side, and hence there is relatively less overlap with SAC processes on their preferred side (Figure 1A) (Briggman et al., 2011; Wei et al., 2011). We hypothesized that this may result in greater inhibitory tuning due to a greater asymmetry in the distribution of inhibitory synapses on the vDSGC dendrites compared to nDSGCs. On the other hand, we recently used receptive field mapping to show that vDSGCs have both tuned inhibitory inputs and spatially offset inhibition and that neither of these circuit contributions were impacted by dramatic changes in the dendrite orientation due to dark-rearing (El-Quessny et al., 2020)(Figure 1B).

Here, we use whole cell voltage clamp to compare inhibitory tuning and spatial receptive fields of excitation and inhibition inputs to compare the synaptic organization of vDSGCs which have asymmetric dendrites to those of nDSGCs which have symmetric dendrites.

RESULTS

DSGCs with asymmetric dendrites exhibit greater directional tuning of inhibition than DSGCs with symmetric dendrites.

We first quantified the difference in dendritic asymmetry in vDSGCs vs. nDSGCs, by calculating the magnitude of the vector from the soma to the center of mass of the dendritic pixels. We found that both ON and OFF dendrites of vDSGCs were significantly more asymmetric than nDSGCs (*mean ± S.D.: vDSGCs: ON = 68.2 ± 25.0 µm, OFF = 65.2 ± 25.8 µm, n = 23*; nDSGCs*: ON = 44.3 ± 20.0 µm, OFF = 37.6 ± 17.5 µm, n = 16*) (Figure 2A). As reported previously, the asymmetry in the dendrites of nDSGCs are not consistently aligned with their preferred direction (Rivlin-Etzion et al. 2011).

To assess the impact of dendrite morphology on the tuning of inhibition, we conducted voltage clamp recordings of both vDSGCs and nDSGCs and isolated inhibitory postsynaptic currents (IPSCs) in response to a bar of light moving in eight different directions (Figure 2B). Asymmetric vDSGCs had a significantly higher direction selectivity index (DSI), compared to nDSGCs (DSI vDSGCs: ON = 0.47 ± 0.18, OFF= 0.55 ± 0.12; nDSGCs: ON =0.31 ± 0.13, OFF= 0.35± 0.10; Figure 2C). Hence vDSGCs with asymmetric dendrites had greater tuning of inhibition.

Previous studies have reported differences in the relative timing of excitatory and inhibitory synaptic inputs for preferred and null direction stimulation, consistent with the presence of spatially offset inhibition (Fried et al., 2002; Taylor & Vaney, 2002). Here, we report similar differences in timing, with inhibitory inputs delayed relative to excitatory input for preferred direction stimulation in symmetric, nDSGCs (E-I timing diff: ON =257± *134 msec, OFF= 173* ± 325 *msec*) and asymmetric vDSGCs (E-I timing diff *mean ± S.D.*: ON = 81± *262 msec, OFF= 292*± 468 *msec*), though there was greater variability during preferred direction motion for asymmetric vDSGCs due to the small amplitude of the inhibitory currents (Figure 2E). For both nDSGCs and vDSGCs, null direction motion elicited a much smaller temporal difference between the excitatory and inhibitory responses (Table 1). We also represented these timing differences as spatial offsets by multiplying by the velocity of our stimulus (250 µm/sec = 8.1˚/sec). These data suggest that, for both asymmetric vDSGCs and symmetric nDSGCs, spatially offset inhibition contributes to the DS computation.

Receptive field mapping of DSGCs reveals similar spatially offset inhibition for DSGCs with symmetric or asymmetric dendrites.

Previously, we showed that in asymmetric vDSGCs, the centers of mass of the spatial receptive fields for excitation and inhibition are both offset toward the preferred direction with inhibitory receptive fields further offset than the excitatory receptive fields (El-Quessny et al., 2020). However, for symmetric nDSGCs, the relative arrangement of excitatory and inhibitory receptive fields is unknown. Hence, we mapped the excitatory and inhibitory receptive fields by recording synaptic currents evoked by squares of light sequentially presented at 100 block-shuffled locations within a soma-centered grid (Figures 3A). We stimulated a 500x500 µm area spanned

by a 10x10 grid. We presented a 30x30 μm light flash within the center of each grid to prevent any blooming artifacts of the visual stimulus.

To characterize the relative position of excitatory and inhibitory receptive fields, we computed the center of mass for dendrites, excitatory receptive fields and inhibitory receptive fields (Figure 3B) and compared both the relative displacement and orientation of the inhibitory receptive field to the excitatory receptive field (Figures 3C). We found that the excitatory and inhibitory receptive fields of both vDSGCs and nDSGCs exhibited some spatial offset (Figure 3E). Though the relative magnitude of spatially offset inhibition (magnitude of the vector from excitation to inhibition) was slightly greater in nDSGCs (*mean* ± *S.D.* ON=38± 25 μm, OFF = 33 ± 26 μm), compared to vDSGCs (Figure 3E) (*mean* ± *S.D.* ON = 21± 15 μm, OFF = 20± 14 μm), we were surprised to find that they were comparable to each other despite their distinct dendritic morphologies. Moreover, we observed that the direction of the spatially offset inhibition on average clustered around the preferred direction but there was significant variance for both nDSGCs (Deviation from PD mean ± *S.D., ON: 7.9 ± 70˚; OFF: -4.9 ± 70˚),* and vDSGCs *(*Deviation from PD mean± *S.D., ON: -7.5 ± 87˚; OFF: -40 ± 72˚) (*Figure 3D and E).

Although we observed a shift in the position of inhibitory receptive fields relative to excitatory receptive fields in both cell types, there was also a striking correlation between them. First, we observed a strong positive correlation between the location of excitation and inhibition relative to the soma (Figure 3F). Note, this correlation was stronger in asymmetric vDSGCs (Table 2) consistent with previous findings (El-Quessny et al., 2020). Second, we observed a strong correlation between the strength of excitation and inhibition measured at each pixel (Figure 3G) where the amplitude of excitation explains on average 65% and 51% of the variance in the amplitude of inhibition in vDSGCs and nDSGCs, respectively (Figure 3H). This strong local correlation is consistent with a strong feedforward inhibitory circuit previously observed (Poleg-Polsky & Diamond, 2016).

To assess the impact along the preferred-null axis, we collapsed the synaptic currents recorded with the static stimulus along the axis orthogonal to their preferred direction and plotted the normalized distribution of excitation and inhibition (Figure 4A). These data indicate that both vDSGCs and nDSGCs exhibit a comparable skew in the spatial distribution of excitatory and inhibitory synapses towards their preferred directions (Figure 4B and C). Together, these data indicate that nDSGCs and vDSGCs exhibited similar spatially offset inhibition despite significant differences in their dendritic morphology.

DSGC dendritic morphology does determine the organization of spatial receptive fields

We next explored whether the small displacements for the EPSC and IPSC receptive field centers from the soma were correlated with variations in the spatial arrangement of the DSGC dendrites (Figure 5A). To do that, we compared the distance and orientation of the center of mass relative to the soma of the EPSC and the IPSC peak current amplitudes of the ON and OFF responses from the soma (Figure 3B),to those of the dendrites. Consistent with our previous study (El-Quessny et al., 2020), we found that the orientation of vDSGC dendrites (Angle mean ± SD, ON = 242 ± 42˚; OFF = 230 ± 41˚, n=20), excitatory receptive fields (Angle mean ± SD ON = 267 ± 45˚; OFF= 260± 45˚, n=17) and inhibitory receptive fields (Angle mean ± SD ON=

264 ± 41˚; OFF= 260± 43˚, n=20) were all ventrally pointing (ventral corresponds to 270˚) (El-Quessny et al., 2020) In contrast, nDSGC dendrites (Angle mean ± S.D. ON= 147 ± 67˚, OFF= 234 ± 76˚, n=20), excitatory receptive fields (Angle mean ± S.D. ON: 196 ± 65˚; OFF: 197± 61˚,n=15) and inhibitory receptive fields (Angle mean ± S.D.: ON= 296 ± 75˚; OFF = 278± 96˚,n = 20) did not exhibit a biased orientation toward the nasal direction (nasal corresponds to 0/360˚) (Figure 5B and C and Table 3). We also found that EPSC and IPSC receptive fields were significantly larger than the dendritic fields in both vDSGCs (EPSC/Dendrite Ratio mean ± SD: ON=1.9 ± 0.76, OFF = 1.9 ±0.93; IPSC/Dendrite: ON=1.6 ± 0.62, OFF = 1.9 ±0.91) and nDSGCs (EPSC/Dendrite Ratio mean ± SD: ON=2.1 ± 1.2, OFF = 2.6 ±1.4; IPSC/Dendrite: ON=2.1 ± 1.4, OFF = 3.1 ±1.6) (Figure 5D), contrary to previous studies in rabbit DSGCs (Brown et al., 2000; Yang & Masland, 1994).

In the above experiments, EPSCs are mediated by a combination of activation of nicotinic acetylcholine receptors (nAChRs) and glutamate receptors. In a subset of experiments, where we pharmacologically blocked cholinergic excitation, we found that the orientation of the glutamate receptive field in vDSGCs (Angle mean ± SD ON= 267 ± 47˚; OFF= 273± 54˚, n=6) was also ventrally oriented. In contrast, the orientation of the glutamate receptive field in nDSGCs was not oriented toward its preferred direction but rather, on average, was oriented towards the DSGCs' null direction (180˚) (mean ± SD ON= 200 ± 68˚; OFF= 220± 72˚, n=10) (Figures 6A and B). This is consistent with recent reports studying another nDSGC subtype, where interrupted stimuli reveal an asymmetry in glutamatergic synapses towards the DSGCs null direction (and the preferred-side SAC) (Table 4) (Ding et al. BioRXiV). Additionally, though glutamatergic receptive field were significantly larger than dendritic field size (Figure 6C), they were closer in area than mixed glutamatergic-cholinergic receptive field size (compare Figure 6C with 5D, left), indicating that cholinergic inputs from SACs contribute excitatory inputs outside of the DSGC dendrites. These data reveal that while the dendritic morphology of vDSGCs can predict the locations of their receptive fields, dendritic field size does not dictate the size of the inhibitory or mixed excitatory receptive fields in either vDSGCs or nDSGCs.

DISCUSSION

Dendritic morphology is thought to influence synaptic organization. Here, we show that dendritic morphology impacts the amount of tuned inhibition whereby DSGCs with asymmetric dendrites exhibit more strongly tuned inhibitory inputs than DSGCs with symmetric dendrites but both cell types exhibit comparable spatially offset inhibition. Moreover, we found in both cell types, that the receptive fields for excitation and inhibition are similarly oriented to each other and are locally correlated in strength. Finally, our results indicate that spatial receptive fields are significantly larger than dendritic fields and are not strongly dictated by the dendritic structure. Here, we discuss the implications of these findings for direction selectivity in the mouse retina.

Asymmetric dendrites lead to stronger tuning of inhibitory inputs with little impact on spatially offset of inhibition

Although vDSGCs and nDSGCs have been shown to exhibit similar spike tuning properties under our stimulus conditions (Yao et al., 2018), we found that vDSGCs had stronger inhibitory tuning than symmetric nDSGCs, indicating that fewer synaptic connections are made with SACs on the preferred side or that nDSGCs receive more contacts from nondirectionally selective GABAergic amacrine cells. This is consistent with several recent studies that have characterized the SAC-DSGC circuit in detail. Paired voltage clamp (Morrie & Feller, 2015; Wei et al., 2011) and serial EM reconstructions (Briggman et al., 2011; Poleg-Polsky et al., 2018) have implicated a stronger inhibitory input provided by SACs located on the null side, whose dendrites are oriented in the DSGC's null direction. However, SACs located on the preferred side still form synapses, though fewer in quantity (Figure 1). Hence, the absence of preferred side dendrites reduces the likelihood of these preferred side SAC-DSGC synapses.

Given this connectivity rule, it is still predicted that inhibition will be spatially offset. Paired voltage clamp recordings of DSGCs and SACs indicate that DSGCs preferentially wire with SACs whose somas are ~100-250 μm offset to the DSGC (Wei et al., 2011; Yonehara et al., 2011). However, several studies have indicated that computations within the SAC dendrites are localized (Koren et al., 2017; Morrie & Feller, 2018; Poleg-Polsky et al., 2018) and hence occur within the DSGC dendritic field (Jain et al., 2019). Furthermore, the high coverage factor of SAC processes (Sun et al., 2013) enables processes from nearby SACs to asymmetrically wire onto DSGCs. This is further supported by studies showing that decreases in the coverage factor of SAC dendritic arbors (Morrie & Feller, 2018) diminishes DS tuning, while increases in the coverage factor of SAC dendritic arbors increases DS tuning (Soto et al., 2019) in the mouse retina, indicating that the density of the SAC dendritic plexus is necessary for adequate asymmetric inhibition of DSGCs.

This is in contrast to recent studies implicating spatially offset inhibition in generating direction selectivity in the visual cortex (Rossi et al., 2020). In cortical circuits, spatially offset inhibition is facilitated by the diverse spiking patterns of cortical interneurons and their long-range processes, which enable inhibitory control of directionally selective neurons with marked spatiotemporal offset (Li et al., 2015; Wilson et al., 2018). In the retina, the dense SAC dendritic

plexus combined with their axon-less morphology and non-spiking physiology necessitates alternative methods for generating spatially offset inhibition.

Spatial receptive fields as a measure of spatially offset inhibition

Using receptive field mapping based on stationary stimuli, we find that overall, there was a shift in the inhibitory receptive field relative to the excitatory receptive field. This shift was on average less than 50 μm (Figure 3E), which is the resolution of our mapping. Interestingly, this spatial offset scales with that observed in the rabbit retina, which predicted spatial offsets of 150 microns, or roughly half the dendritic tree of rabbit DSGCs (Fried et al., 2002). Given the larger dendritic field of rabbit ON-OFF DSGCs (~ 600 μm diameter) (Oesch et al., 2005; Yang & Masland, 1994) compared to mouse ON-OFF DSGCs (~200 μm diameter) (Rivlin-Etzion et al., 2011), we believe that the observed spatial offset scales with dendritic field size across both species.

A spatial shift of less than 50 μm is comparable but a bit smaller than predicted by the temporal offsets induced by drifting bar (Figure 2E). Moreover, the small displacement of the inhibitory receptive field is smaller than that predicted by the temporal offsets previously reported for symmetric nDSGCs (270 msec at 500 μm/s corresponding to 135 μm, (Pei et al., 2015)). This may be due to different stimulus sizes leading to differential recruitment of lateral inhibitory circuits. Another difference is that stationary stimuli may more strongly activate symmetric sources of inhibition onto DSGCs that arise from non-starburst amacrine cells (Morrie & Feller, 2018; Wei, 2018).
In addition, the excitatory receptive fields are larger than dendritic fields because of the contribution of ACh from starburst amacrine cells. Paired recordings between SACs and DSGCs indicate that the strength of ACh synapses are symmetric, and likely mediated by diffuse release of ACh (Lee et al., 2010). Interestingly, motion stimuli may implicate asymmetric cholinergic excitation in the DS computation during low contrast stimuli (Poleg-Polsky & Diamond, 2016; Sethuramanujam et al., 2016). Indeed, optogenetic stimulation of SACs expressing channelrhodopsin leads to cholinergic excitation preceding GABAergic inhibition and exhibiting faster receptor kinetics, during preferred direction motion, with all other mechanisms of synaptic inputs blocked (Hanson et al., 2019; Pottackal et al., 2020). Hence temporal offsets in excitation and inhibition may be a more reliable measure of spatially offset inhibition than spatial receptive fields.

Local dendritic computations support direction selectivity in DSGCs

Though we observed spatial offsets for the center of mass of excitatory and inhibitory receptive fields, we observed a tremendous amount of correlation between them as well. For both vDSGCs and nDSGCs, inhibitory and excitatory receptive fields overlapped in spatial extent and orientation as well as exhibiting correlated synaptic strengths. However, we do not probe variations of the receptive field on a scale finer than 50 microns. For example, studies in DSGC indicate that local directional computations were performed within the dendritic tree ((Jain et al., 2019). Computational modeling showed that nonlinear conductance within the dendritic tree promotes a multi-compartmental model, allowing local interactions between excitation and inhibition to shape dendritic DS, while SAC ablation abolished DS. Despite our coarse mapping

of synaptic input distribution, our data supports this model whereby local balances in excitation and inhibition are computed at the level of the DSGC dendrite. A multi-compartmental model is specifically relevant for vDSGCs, whose form-function correlation enables them to nonlinearly integrate synaptic inputs along their dendrites (El-Quessny et al., 2020; Trenholm et al., 2011, 2013). This may explain how vDSGCs rely more heavily on asymmetric versus spatially offset inhibition, relative to nDSGCs which do not have a form-function relationship.

DSGC dendrites and the spatial organization of their receptive fields

Here we compare the size and asymmetric organization of DSGC dendrites to their spatial receptive fields. We found that both excitatory and inhibitory receptive fields are much larger than dendritic fields, extending beyond the dendritic trees (Figure 4). Our previous work has shown that vDSGCs exhibit ventrally offset inhibitory receptive fields, regardless of their altered morphology following dark (El-Quessny et al., 2020). However, unlike rabbit DSGCs, it is unknown whether the spiking receptive field for mouse DSGCs is restricted to the dendritic field (Brown et al., 2000; He et al., 1999). Hence, our data indicates that the synaptic inputs which expand beyond the dendritic tree contribute to its subthreshold responses including glutamatergic input from vglut3 amacrine cells (Lee et al., 2016), cholinergic input from SACs (Lee et al., 2010; Sethuramanujam et al., 2016) and symmetric GABAergic inputs from VIP- positive amacrine cells (Park et al., 2015).

Additionally, we find that the glutamatergic receptive field size is more correlated to the dendritic field size (Figure 6). This is consistent with the findings that the restricted geometry of bipolar cell terminals (Jain et al., 2019; Rasmussen et al., 2020; Sethuramanujam et al., 2018), confines the glutamatergic receptive field closer to the DSGC dendrite (Yang & Masland, 1994). Since we find that the inhibitory and the cholinergic excitatory receptive fields expand beyond the DSGC's dendritic tree, we postulate that the lateral arborization of SAC dendrites (Briggman et al., 2011; Lee et al., 2010; Sethuramanujam et al., 2016; Yonehara et al., 2011) allows the cholinergic excitation and inhibitory receptive fields to expand beyond the DSGC dendritic field. Another possibility not explored here is the role of gap junctions in expanding receptive field size as recently described for F-mini ON RGCs (Cooler & Schwartz, 2021)and in vDSGCs (Trenholm et al., 2013).

In conclusion, we show that DSGCs exhibit two parallel mechanisms for computing motion direction. The first is based on tuned inhibition, which we find is influenced by the morphology of the DSGC, and the second is based on spatially offset inhibition which is not influenced by the DSGCs' dendritic orientation, size or asymmetry.

FIGURE CAPTIONS

Figure 1: Schematic for synaptic distribution of excitation and inhibition in morphologically distinct DSGCs

A) Top: Schematic illustrating the distribution of inhibitory (magenta) and excitatory (green) synaptic inputs on an asymmetric DSGC, whose dendrites point towards it's preferred direction and towards the null oriented SAC dendrites (red) to which it is asymmetrically wired. Bottom: Schematic of the anatomical distribution of excitatory and inhibitory synaptic inputs along the DSGC's preferred direction (PD).

B) Same as A but for DSGCs with symmetric dendrites.

Figure 2: DSGCs with asymmetric dendrites exhibit more asymmetric inhibition but similar temporal offset to DSGCs with symmetric dendrites

A) Left: Skeletonized vDSGC (orange) and nDSGC (blue) showing asymmetry and ventral orientation of vDSGCs, in contrast to the symmetry of nDSGCs. Right: Summary data comparing dendritic asymmetry of vDSGCs (n=23) and nDSGCs (n=16) as measured by the magnitude of the vector from the soma to center of mass of the ON (filled) and OFF (open) dendrites. Red data points indicate the measurements for example cells on the left. Statistical significance assessed by one-way ANOVA (p=4x10-4) and Dunn-Sidak post-hoc test (**p<0.01).

B) Example tuning curve and mean traces of the inhibitory postsynaptic currents in vDSGCs (orange, left) and nDSGCs (blue, right) in response to a moving bar stimulus. ON (solid lines) and OFF (dashed lines) tuning curves and vector sums are based on peak current amplitudes in each direction.

C) Left: Scatter plot of the peak amplitude of IPSCs in response to preferred versus null direction motion in vDSGCs (orange) and nDSGCs (blue). SEM for ON (dark shade) and OFF (light shade) responses indicated on the plot. Right: Box plot summarizing the tuning of vDSGCs (orange) and nDSGCs (blue) as measured by the direction selectivity index. ON (filled) and OFF (open) responses separately. Unity line (grey dashed) indicating where preferred (PD) = null (ND) IPSC peak amplitude. Statistical significance assessed by Wilcoxon Rank-Sum test (** p<0.01, *** p<0.001).

D) IPSC and EPSC traces in response to the preferred direction (PD, top) and null direction (ND, bottom) for the example vDSGCs (orange) and nDSGCs (blue). Arrows indicating peak timing for IPSCs (magenta) and EPSCs (green) after applying an 80 ms moving average. Note, the small amplitude and complex kinetics of preferred direction IPSCs in vDSGC prevents a reliable calculation of the timing of the peak current. E) Summary data representing spatial offset based on the timing differences of the peak excitatory (E) and inhibitory (I) currents in response to preferred direction (PD) and null direction (ND) stimulation for ON (filled) and OFF (open) responses in vDSGCs (orange) and nDSGCs (blue). Statistical significance for nDSGCs assessed by paired t-test (p>0.05).

Figure 3: vDSGCs and nDSGCs have similar spatially offset inhibition and exhibit strong local correlations in excitation and inhibition.

A) Example vDSGC (top) and nDSGCs (bottom) receptive field displaying mean inhibitory and excitatory postsynaptic responses for each stimulus presentation. Asterisk in the center of the stimulus field denotes soma location. ON (cyan) and OFF (purple) dendritic skeletons are overlaid. Inset shows stimulus presentation of 30 x 30 μm light within a 50 x 50 μm area to evade scattering effects.
B) Heat map of dendritic density (left), the EPSC peak current amplitude (middle) and IPSC peak current amplitude (right) for ON (top) and OFF (bottom) responses of the example vDSGC (top row) and nDSGC (bottom row) to the left. Scale bar = 100 μm.
C) Summary data plotting the average IPSC (I) receptive field (vDSGCs, n=17; nDSGCs, n=15 cells), centered on the EPSC (E) receptive field center of mass (ECOM). ON (top) and OFF (bottom) responses are analyzed separately. Scale bar = 100 μm.
D) Summary data represented as polar plots of the vectors from the excitatory (center) to the inhibitory receptive fields in vDSGCs (orange, left) and nDSGCs (blue,right) for ON (solid) and OFF (dashed) responses.
E) Left: Summary data showing magnitude (left) of spatially offset inhibition (Vector from E to I) for vDSGCs (orange) and nDSGCs (blue). Spatial offset predicted from the temporal offset of excitation and inhibition during preferred direction motion of a moving bar stimulus (Figure 2) indicated in grey. Statistical Significance across cell types assessed with Wilcoxon Rank-Sum test (*$p<0.05$). Statistical significance between measured and predicted spatial offset determined by one-sided t-test (all p values< 0.001). Right: Summary data showing the angular deviation of spatially offset inhibition from the preferred direction of vDSGCs (orange) and nDSGCs (blue).
F) Summary data representing the orientation of the EPSC's receptive field relative to the orientation of the IPSC's receptive field in vDSGCs (orange, top) and nDSGCs (blue, bottom) for ON (filled) and OFF (open) responses. Peason's correlation coefficients presented in Table 2.
G) Example scatter plots of EPSC vs. IPSC amplitude per pixel in vDSGCs (orange, left) and nDSGCs (blue, right) for ON (filled) and OFF(open) responses. Trend lines computed using least squares regression. Pixels with current amplitude below 5% of the maximum were excluded. Inset: Coefficient of determination (R2) for each example cell.
H) Summary data of R2 values for each vDSGC (orange) and nDSGC (blue).

Figure 4: vDSGCs and nDSGCs display comparable distribution of synaptic inputs along their preferred-null axis.
A) Summary data displaying the normalized amplitude of the inhibitory (magenta) and excitatory (green) inputs along the null-preferred axis of vDSGCs (top, n=17 cells) and nDSGCs (bottom, n=15 cells). ON (left) and OFF (right) responses plotted separately.
B) Summary data representing the distribution of the locations of the peak inhibitory (magenta) and excitatory (green) inputs along the null-preferred axis of vDSGCs (top) and nDSGCs (bottom).
C) Summary data representing the locations of the peak excitatory (E) and inhibitory (I) inputs along the null-preferred axis of vDSGCs (orange, top) and nDSGCs (blue, bottom). Statistical Significance determined with a paired t-test ($p>0.05$).

Figure 5: Spatial organization of receptive fields differs from dendritic morphology.
A) Example vDSGC (left) and nDSGC (right) dendritic skeletons. Orientation on the retina indicated by arrows, with preferred direction in bold. Scale bar = 100 μm.

B) Summary data represented in polar plots of the vectors from the soma to the dendrites (left), the excitatory (middle) and the inhibitory (right) receptive field center of mass in vDSGCs (top, orange) and nDSGCs (bottom, blue). Data for ON (solid) and OFF (dashed) plotted separately.
C) Summary data displaying the relationship between the orientation of dendritic morphology and the orientation of the vector from the soma to the excitatory receptive field (EPSC) center of mass (left) and to the inhibitory receptive field (IPSC)(middle)in vDSGCs (orange) and nDSGCs (blue). Data for ON (filled circle) and OFF (open circle) plotted separately. Pearson's correlation coefficients determined no significant correlations between dendrite angle and EPSC or IPSC locations ($p > 0.05$).
D) Summary data comparing the relationship between dendritic area and EPSC (left)and IPSC (right) response areas within the receptive field, and the area of the dendrites for each vDSGC (orange) and nDSGC (blue). Data for ON (filled circle) and OFF (open circle) plotted separately. Statistical significance of the EPSC/Dendrite and IPSC/Dendrite ratio determined with one-sided t-test and compared to a ratio of 1 (PSC = Dendrite area) - All p values <0.001.

Figure 6: DSGC glutamatergic receptive field is more restricted to the dendritic field.
A) Left: Summary data represented as polar plots of the vectors from the soma to the excitatory glutamate receptive field center of mass in the presence of 100 µM Hexamethonium in vDSGCs (orange, top) and nDSGCs (blue, bottom) for ON (solid) and OFF (dashed) responses. Right: Summary data representing the deviation of the vector angle (right) from the vDSGC (orange, top) and nDSGC (blue, bottom) preferred direction. Data for ON (filled circle) and OFF (open circle) plotted separately.
B) Summary data displaying the relationship between the orientation of the vector from the soma to the glutamatergic excitatory receptive field ($EPSC_{Glu}$) center of mass, relative to the orientation of the dendritic center of mass in vDSGCs (orange, n=5 cells) and nDSGCs (blue, n=9 cells).
C) Summary data comparing the relationship between dendritic area and the glutamatergic excitatory (EPSCGlu) response areas within the receptive field, and the area of the dendrites for each vDSGC (orange) and nDSGC (blue). Data for ON (filled circle) and OFF (open circle) plotted separately. Statistical significance of the $EPSC_{Glu}$/Dendrite ratio determined with one-sided t-test and compared to a ratio of 1 ($EPSC_{Glu}$=Dendrite area) - All p values <0.001.

METHODS

Experimental model and test subject details

Mice used in this study were aged from p30-60 and were of both sexes. Animals used in experiments had not previously been involved in other experiments or exposed to any drugs. Animal health was monitored daily and only healthy animals were used in experiments. To target ventral preferring DSGCs, we used Hb9::GFP (Arber et al., 1999) mice, which express GFP in a subset of DSGCs (Trenholm et al., 2011). To target nasal preferring DSGCs, we used Trhr::GFP (Rivlin-Etzion et al., 2011). All experiments involved recording from 1-7 cells from at least 2 animals of either sex. All animal procedures were approved by the UC Berkeley Institutional Animal Care and Use Committee and conformed to the NIH Guide for the Care and Use of Laboratory Animals, the Public Health Service Policy, and the SfN Policy on the Use of Animals in Neuroscience Research.

Retina Preparation

Mice were anesthetized with isoflurane and decapitated. Retinas were dissected from enucleated eyes in oxygenated (95% O2/5% CO2) Ames' media (Sigma) for light responses or ACSF (in mM, 119 NaCl, 2.5 KCl, 1.3 MgCl2, 1 K2HPO4, 26.2 NaHCO3, 11D-glucose, and 2.5 CaCl2) for paired recordings. Retinal orientation was determined as described previously (Wei et al., 2010). Isolated whole retinas were micro-cut at the dorsal and ventral halves to allow flattening, with dorsal and ventral mounted over two 1–2 mm2 hole in nitrocellulose filter paper (Millipore) with the photoreceptor layer side down and stored in oxygenated Ames' media or ACSF until use (maximum 10 h). All experiments were performed on retinas in which dorsal-ventral orientation was tracked.

Visual Stimulation

For visual stimulation of DSGCs, visible light (420– 530 nm) were generated using a computer running 420-520 nm light through a digital micro-mirror device (DLI Cel5500) projector with a light emitting diode (LED) light source generated using MATLAB software with the Psychophysics Toolbox. Visual stimuli are focused on the photoreceptor layer using a condenser in the DMD path to the chamber.

Moving stimuli

Drifting bars were presented (velocity = 250 μm/s, length =600 μm width =350 μm over a 700 μm radius circular mask) in 8 block shuffled directions, repeated 3 times, with each presentation lasting 6 s and followed by 500 msec of grey screen). A 20X water-immersion objective (Olympus LUMPlanFl/IR 360/1.0 NA) was used to target cells for electrophysiological recording. The illumination radius on the retina was 1.4 mm to limit modulation of DSGC responses by inhibitory wide-field amacrine cells (Chen et al., 2016).

The directionally selective index (DSI) was calculated for spike responses as: PD-NDPD+ND where PD is the number of spikes in the preferred direction and ND is the number of spikes in the null direction. We also used the magnitude of the vector sum of the spike responses as another measurement of directional tuning (Vector Sum = 1-Circular Variance of the spike responses (Mazurek et al., 2014)).

Static stimuli for receptive field mapping
To map excitatory and inhibitory receptive fields of DSGCs, visual stimuli were generated using a computer running 420-520 nm light through a digital micro-mirror device (DLI Cel5500) projector with a light emitting diode (LED) light source through a 20X objective (UMPlanFL 0.5NA W). Stimuli (30 x 30 μm) at an intensity of 3.1 x 10^5 R*/s/rod and 96% Michealson's contrast were presented in a pseudorandom order, in a 10x10 grid, onto a stimulus field of 500 x 500 μm, with the DSGC soma located in the center of the stimulus field (See Figure 3). Voltage clamp recordings were simultaneously acquired using methods described below.

Two-photon targeted whole-cell voltage-clamp recordings
Oriented retinas were placed under the microscope in oxygenated Ames' medium at 32–34˚C. Identification and recordings from GFP+ cells were performed as described previously (Wei et al., 2010). In brief, GFP+ cells were identified using a custom-modified two-photon microscope (Fluoview 300; Olympus America) tuned to 920 nm to minimize bleaching of photoreceptors. The inner limiting membrane above the targeted cell was dissected using a glass electrode. Cell attached voltage clamp recordings were performed with a new glass electrode (4-5 MW) filled with internal solution containing the following (in mM): 110 CsMeSO4, 2.8 NaCl, 20 HEPES, 4 EGTA, 5 TEA-Cl, 4 Mg-ATP, 0.3 Na_3GTP, 10 Na_2Phosphocreatine, QX-Cl (pH = 7.2 with CsOH, osmolarity = 290, ECl^- = -60 mV). Whole cell recordings were performed with the same pipette after obtaining a GW seal. Holding voltages for measuring excitation and inhibition after correction for the liquid junction potential (10 mV) were 0 mV and -70 mV, respectively. Signals were acquired using Clampex 10.4 recording software and a Multiclamp 700A amplifier (Molecular Devices), sampled at 10 kHz, and low pass filtered at 6 kHz.

Two-photon microscopy and morphological reconstruction
After physiological recordings of DSGCs were completed, Alexa-594-filled DSGCs were imaged using the two-photon microscope at 800 nm. At this wavelength, GFP is not efficiently excited but Alexa 594 is brightly fluorescent. 480x 480 μm Image stacks were acquired at z intervals of 1.0 μm and resampled fifteen times for each stack using a 20X objective (Olympus LUMPlanFl/IR 2x digital zoom, 1.0 NA) 30kHz resonance scanning mirrors covering the entire dendritic fields of the DSGCs. Image stacks of DSGCs were then imported to FIJI (NIH) and a custom macro was used to segment ON and OFF dendrites based on their lamination depth in the inner plexiform layer (ON layer 10-30 μm, OFF layer 35-65 μm depth). Following ON and OFF dendritic segmentation, another custom FIJI macro uses the local maximum values of fluorescent pixels to binarize and skeletonize ON and OFF dendritic segments for morphological analyses.

Pharmacology
For experiments conducted in Hexamethonium (Millipore Sigma), we diluted 100 μM in AMES media, and allowed it to perfuse for 5-10 mins at a perfusion rate of 1 mL/min.

QUANTIFICATION AND STATISTICAL ANALYSIS

Statistical Tests

Mean ± standard deviations for all angles performed using circular mean and circular standard deviations. Details of statistical tests, number of replicates, and p values are indicated in the figures and figure captions. P values less than 0.05 were considered significant.

Whole cell recordings

For voltage clamp recordings during moving stimuli, traces were first average across the 3 trials for each direction and inspected to ensure consistency of responses. Average traces were baseline subtracted based on the last 500 msec of recording or a user defined interval after manual inspection. Peak currents were calculated from average baseline subtracted traces and were the maximal (IPSC) or minimal (EPSC) points during the 1.9 s window described above. The peak currents were used to calculate the vector sum of the current responses. For timing analysis, PSC traces were low pass filtered using an 80 msec moving average, and peak time for excitation and inhibition was extracted for ON and OFF responses. Preferred directions for both ON and OFF responses used to calculate peak responses and were defined as 180˚ - the angle of the vector sum of ON and OFF peak IPSCs, or the angle of the vector sum of ON and OFF peak EPSCs if IPSCs were not recorded in that cell.

For voltage clamp recordings during static stimuli, we first divided each trace into the ON and OFF response based on the stimulus we present. Next, we calculated the center of mass of the peak current amplitudes of the stimulus field. To measure the displacement and orientation of the receptive fields relative to the soma, we calculated the magnitude and angle, respectively, of vector from the soma to the center of mass of the receptive field.
To quantify spatially offset inhibition, we calculated the vector from the center of mass of the excitatory to the center of mass of the inhibitory receptive fields.

Quantification of synaptic inputs onto dendrites We started by characterizing the anatomical receptive field of a subtype of nasally preferring DSGCs (nDSGC) labelled under the Trhr-GFP mouse line (Rivlin-Etzion et al., 2011). This cell type has been characterized to show nasal directional preference, asymmetric inhibition in response to null (temporal) direction motion, symmetric excitation in response to all directions, with fairly symmetric dendrites that are not oriented in a particular direction. In figure 3A we show the responses of an example vDSGC and nDSGC recorded in control conditions. We calculated the center of mass (COM) of the peak amplitude of the ON and OFF excitatory and inhibitory responses. We then calculated the vector from the soma to the center of mass of the receptive field; the magnitude of the vector indicates the magnitude of spatial offset of the receptive field relative to the soma, while the angle of the vector indicates the orientation of the receptive field relative to the soma.

REFERENCES

Arber, S., Han, B., Mendelsohn, M., Smith, M., & Jessell, T. M. (1999). Requirement for the Homeobox Gene Hb9 in the Consolidation of Motor Neuron Identity. *Neuron*, *23*, 659–674.

Briggman, K. L., Helmstaedter, M., & Denk, W. (2011). Wiring specificity in the direction-selectivity circuit of the retina. *Nature*. https://doi.org/10.1038/nature09818

Brown, S. P., He, S., & Masland, R. H. (2000). Receptive field microstructure and dendritic geometry of retinal ganglion cells. *Neuron*, *27*(2), 371–383. https://doi.org/10.1016/S0896-6273(00)00044-1

Chen, Q., Pei, Z., Koren, D., & Wei, W. (2016). Stimulus-dependent recruitment of lateral inhibition underlies retinal direction selectivity. *ELife*, *5*, 1–19. https://doi.org/10.7554/eLife.21053

Cooler, S., & Schwartz, G. W. (2021). An offset ON–OFF receptive field is created by gap junctions between distinct types of retinal ganglion cells. *Nature Neuroscience*, *24*(1), 105–115. https://doi.org/10.1038/s41593-020-00747-8

Ding, H., Smith, R. G., Poleg-Polsky, A., Diamond, J. S., & Briggman, K. L. (2016). Species-specific wiring for direction selectivity in the mammalian retina. *Nature*. https://doi.org/10.1038/nature18609

El-Quessny, M., Maanum, K., & Feller, M. B. (2020). Visual Experience Influences Dendritic Orientation but Is Not Required for Asymmetric Wiring of the Retinal Direction Selective Circuit. *Cell Reports*, *31*(13), 107844. https://doi.org/10.1016/j.celrep.2020.107844

Fried, S. I., Mü nch, T. A., & Werblin, F. S. (2002). *Mechanisms and circuitry underlying directional selectivity in the retina*. www.nature.com/nature

Gavrikov, K. E., Nilson, J. E., Dmitriev, A. V., Zucker, C. L., & Mangel, S. C. (2006). Dendritic compartmentalization of chloride contransporters underlies directional responses of starburst amacrine cells in retina. *Proceedings of the National Academy of Sciences of the United States of America*, *103*(49), 18793–18798. https://doi.org/10.1073/pnas.0604551103

Grama, A., & Engert, F. (2012). Direction selectivity in the larval zebrafish tectum is mediated by asymmetric inhibition. *Frontiers in Neural Circuits*, *6*(SEPTEMBER), 1–9. https://doi.org/10.3389/fncir.2012.00059

Hanson, L., Sethuramanujam, S., de Rosenroll, G., Jain, V., & Awatramani, G. B. (2019). Retinal direction selectivity in the absence of asymmetric starburst amacrine cell responses. *ELife*, *8*. https://doi.org/10.7554/eLife.42392

Hausselt, S. E., Euler, T., Detwiler, P. B., & Denk, W. (2007). A dendrite-autonomous mechanism for direction selectivity in retinal starburst amacrine cells. *PLoS Biology*. https://doi.org/10.1371/journal.pbio.0050185

He, S., Jin, Z. F., & Masland, R. H. (1999). The nondiscriminating zone of directionally selective retinal ganglion cells: Comparison with dendritic structure and implications for mechanism. *Journal of Neuroscience*, *19*(18), 8049–8056. https://doi.org/10.1523/jneurosci.19-18-08049.1999

Hubel, D. H., & Wiesel, T. (1959). Receptive fields of single neurons in the cat's striate cortex. *Journal of Physiology*, 574–591.

Hubel, D. H., & Wiesel, T. (1962). Receptive Fields, Binocular Interaction and Functional Architecture in the cat's visual cortex. *Journal of Physiology*, 106–154.

Jain, V., Murphy-Baum, B. L., deRosenroll, G., Sethuramanujam, S., Delsey, M., Delaney, K., & Awatramani, G. B. (2019). The functional organization of excitation and inhibition in the

dendritic arbors of retinal direction-selective ganglion cells. *BioRxiv*, 1–23. https://doi.org/10.1101/718783

Koren, D., Grove, J. C. R., & Wei, W. (2017). Cross-compartmental Modulation of Dendritic Signals for Retinal Direction Selectivity. *Neuron*, *95*(4), 914-927.e4. https://doi.org/10.1016/j.neuron.2017.07.020

Laboy-Juárez, K. J., Langberg, T., Ahn, S., & Feldman, D. E. (2019). Elementary motion sequence detectors in whisker somatosensory cortex. *Nature Neuroscience*, *22*(9), 1438–1449. https://doi.org/10.1038/s41593-019-0448-6

Lee, S., Kim, K., & Zhou, Z. J. (2010). Role of ACh-GABA Cotransmission in Detecting Image Motion and Motion Direction. *Neuron*. https://doi.org/10.1016/j.neuron.2010.11.031

Lee, S., Zhang, Y., Chen, M., & Zhou, Z. J. (2016). Segregated Glycine-Glutamate Co-transmission from vGluT3 Amacrine Cells to Contrast-Suppressed and Contrast-Enhanced Retinal Circuits. *Neuron*, *90*(1), 27–34. https://doi.org/10.1016/j.neuron.2016.02.023

Li, Y. T., Liu, B. H., Chou, X. L., Zhang, L. I., & Tao, H. W. (2015). Strengthening of direction selectivity by broadly tuned and spatiotemporally slightly offset inhibition in mouse visual cortex. *Cerebral Cortex*, *25*(9), 2466–2477. https://doi.org/10.1093/cercor/bhu049

Liang, L., Fratzl, A., Goldey, G., Ramesh, R. N., Sugden, A. U., Morgan, J. L., Chen, C., & Andermann, M. L. (2018). A Fine-Scale Functional Logic to Convergence from Retina to Thalamus. *Cell*, *173*(6), 1343-1355.e24. https://doi.org/10.1016/j.cell.2018.04.041

Marshel, J. H., Kaye, A. P., Nauhaus, I., & Callaway, E. M. (2012). Anterior-Posterior Direction Opponency in the Superficial Mouse Lateral Geniculate Nucleus. *Neuron*, *76*(4), 713–720. https://doi.org/10.1016/j.neuron.2012.09.021

Mazurek, M., Kager, M., & Van Hooser, S. D. (2014). Robust quantification of orientation selectivity and direction selectivity. *Frontiers in Neural Circuits*, *8*(AUG), 1–17. https://doi.org/10.3389/fncir.2014.00092

Morrie, R. D., & Feller, M. B. (2015). An Asymmetric Increase in Inhibitory Synapse Number Underlies the Development of a Direction Selective Circuit in the Retina. *Journal of Neuroscience*. https://doi.org/10.1523/JNEUROSCI.0670-15.2015

Morrie, R. D., & Feller, M. B. (2018). A Dense Starburst Plexus Is Critical for Generating Direction Selectivity. *Current Biology*, *28*(8), 1204-1212.e5. https://doi.org/10.1016/j.cub.2018.03.001

Oesch, N., Euler, T., & Taylor, W. R. (2005). Direction-selective dendritic action potentials in rabbit retina. *Neuron*, *47*(5), 739–750. https://doi.org/10.1016/j.neuron.2005.06.036

Park, S. J. H., Borghuis, B. G., Rahmani, P., Zeng, Q., Kim, I. J., & Demb, J. B. (2015). Function and circuitry of VIP+ interneurons in the mouse retina. *Journal of Neuroscience*, *35*(30), 10685–10700. https://doi.org/10.1523/JNEUROSCI.0222-15.2015

Pei, Z., Chen, Q., Koren, D., Giammarinaro, B., Acaron Ledesma, H., & Wei, W. (2015). Conditional Knock-Out of Vesicular GABA Transporter Gene from Starburst Amacrine Cells Reveals the Contributions of Multiple Synaptic Mechanisms Underlying Direction Selectivity in the Retina. *The Journal of Neuroscience : The Official Journal of the Society for Neuroscience*, *35*(38), 13219–13232. https://doi.org/10.1523/JNEUROSCI.0933-15.2015

Poleg-Polsky, A., & Diamond, J. S. (2016). Retinal circuitry balances contrast tuning of excitation and inhibition to enable reliable computation of direction selectivity. *Journal of Neuroscience*, *36*(21), 5861–5876. https://doi.org/10.1523/JNEUROSCI.4013-15.2016

Poleg-Polsky, A., Ding, H., & Diamond, J. S. (2018). Functional Compartmentalization within

Starburst Amacrine Cell Dendrites in the Retina. *Cell Reports*, *22*(11), 2898–2908. https://doi.org/10.1016/j.celrep.2018.02.064

Pottackal, J., Singer, J. H., & Demb, J. B. (2020). Receptoral Mechanisms for Fast Cholinergic Transmission in Direction-Selective Retinal Circuitry. *Frontiers in Cellular Neuroscience*, *14*(November). https://doi.org/10.3389/fncel.2020.604163

Priebe, N. J., & Ferster, D. (2005). Direction selectivity of excitation and inhibition in simple cells of the cat primary visual cortex. *Neuron*, *45*(1), 133–145. https://doi.org/10.1016/j.neuron.2004.12.024

Rasmussen, R., Matsumoto, A., Dahlstrup Sietam, M., & Yonehara, K. (2020). A segregated cortical stream for retinal direction selectivity. *Nature Communications*, *11*(1). https://doi.org/10.1038/s41467-020-14643-z

Rivlin-Etzion, M., Zhou, K., Wei, W., Elstrott, J., Nguyen, P. L., Barres, B. A., Huberman, A. D., & Feller, M. B. (2011). Transgenic Mice Reveal Unexpected Diversity of On-Off Direction-Selective Retinal Ganglion Cell Subtypes and Brain Structures Involved in Motion Processing. *Journal of Neuroscience*. https://doi.org/10.1523/JNEUROSCI.0564-11.2011

Rosa, J. M., Morrie, R. D., Baertsch, H. C., & Feller, M. B. (2016). Contributions of rod and cone pathways to retinal direction selectivity through development. *Journal of Neuroscience*, *36*(37), 9683–9695. https://doi.org/10.1523/JNEUROSCI.3824-15.2016

Rossi, L. F., Harris, K. D., & Carandini, M. (2020). Spatial connectivity matches direction selectivity in visual cortex. *Nature*, *2019*(January 2019). https://doi.org/10.1038/s41586-020-2894-4

Sethuramanujam, S., Awatramani, G. B., & Slaughter, M. M. (2018). Cholinergic excitation complements glutamate in coding visual information in retinal ganglion cells. *Journal of Physiology*, *596*(16), 3709–3724. https://doi.org/10.1113/JP275073

Sethuramanujam, S., McLaughlin, A. J., deRosenroll, G., Hoggarth, A., Schwab, D. J., & Awatramani, G. B. (2016). A Central Role for Mixed Acetylcholine/GABA Transmission in Direction Coding in the Retina. *Neuron*. https://doi.org/10.1016/j.neuron.2016.04.041

Soto, F., Tien, N. W., Goel, A., Zhao, L., Ruzycki, P. A., & Kerschensteiner, D. (2019). AMIGO2 Scales Dendrite Arbors in the Retina. *Cell Reports*, *29*(6), 1568-1578.e4. https://doi.org/10.1016/j.celrep.2019.09.085

Sun, L. O., Jiang, Z., Rivlin-Etzion, M., Hand, R., Brady, C. M., Matsuoka, R. L., Yau, K.-W., Feller, M. B., & Kolodkin, A. L. (2013). On and Off Retinal Circuit Assembly by Divergent Molecular Mechanisms. *Science*, *342*(6158). https://doi.org/10.1126/science.1241974

Taylor, W. R., & Vaney, D. I. (2002). Diverse synaptic mechanisms generate direction selectivity in the rabbit retina. *The Journal of Neuroscience : The Official Journal of the Society for Neuroscience*, *22*(17), 7712–7720. https://doi.org/22/17/7712 [pii]

Trenholm, S., Johnson, K., Li, X., Smith, R. G., & Awatramani, G. B. (2011). Parallel mechanisms encode direction in the retina. *Neuron*. https://doi.org/10.1016/j.neuron.2011.06.020

Trenholm, S., Schwab, D. J., Balasubramanian, V., & Awatramani, G. B. (2013). Lag normalization in an electrically coupled neural network. *Nature Neuroscience*. https://doi.org/10.1038/nn.3308

Vlasits, A. L., Morrie, R. D., Tran-Van-Minh, A., Bleckert, A., Gainer, C. F., DiGregorio, D. A., & Feller, M. B. (2016). A Role for Synaptic Input Distribution in a Dendritic Computation of Motion Direction in the Retina. *Neuron*. https://doi.org/10.1016/j.neuron.2016.02.020

Wei, W. (2018). Neural mechanisms of motion processing in the mammalian retina. *Annual Review of Vision Science*, *4*, 165–192. https://doi.org/10.1146/annurev-vision-091517-034048

Wei, W., Elstrott, J., & Feller, M. B. (2010). Two-photon targeted recording of GFP-expressing neurons for light responses and live-cell imaging in the mouse retina. *Nature Protocols*. https://doi.org/10.1038/nprot.2010.106

Wei, W., Hamby, A. M., Zhou, K., & Feller, M. B. (2011). Development of asymmetric inhibition underlying direction selectivity in the retina. *Nature*. https://doi.org/10.1038/nature09600

Wilson, D. E., Scholl, B., & Fitzpatrick, D. (2018). Differential tuning of excitation and inhibition shapes direction selectivity in ferret visual cortex. *Nature*, *560*(7716), 97–101. https://doi.org/10.1038/s41586-018-0354-1

Yang, G., & Masland, R. H. (1994). Receptive fields and dendritic structure of directionally selective retinal ganglion cells. *Journal of Neuroscience*, *14*(9), 5267–5280. https://doi.org/10.1523/jneurosci.14-09-05267.1994

Yao, X., Cafaro, J., McLaughlin, A. J., Postma, F. R., Paul, D. L., Awatramani, G., & Field, G. D. (2018). Gap Junctions Contribute to Differential Light Adaptation across Direction-Selective Retinal Ganglion Cells. *Neuron*, *100*(1), 216-228.e6. https://doi.org/10.1016/j.neuron.2018.08.021

Ye, C. Q., Poo, M. M., Dan, Y., & Zhang, X. H. (2010). Synaptic mechanisms of direction selectivity in primary auditory cortex. *Journal of Neuroscience*, *30*(5), 1861–1868. https://doi.org/10.1523/JNEUROSCI.3088-09.2010

Yonehara, K., Balint, K., Noda, M., Nagel, G., Bamberg, E., & Roska, B. (2011). Spatially asymmetric reorganization of inhibition establishes a motion-sensitive circuit. *Nature*, *469*(7330), 407–410. https://doi.org/10.1038/nature09711

Zhang, L. I., Tan, A. Y. Y., Schreiner, C. E., & Merzenich, M. M. (2003). Topography and synaptic shaping of direction selectivity in primary auditory cortex. *Nature*, *424*(6945), 201–205. https://doi.org/10.1038/nature01796

FIGURE 1

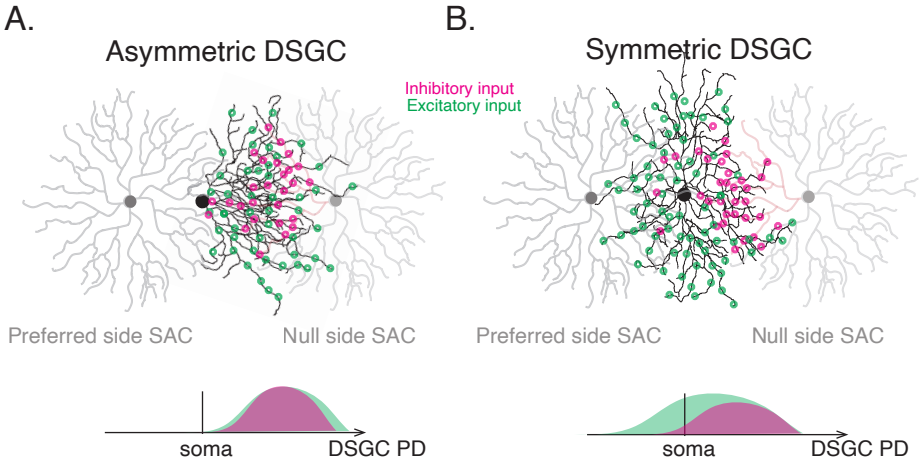
A.
Asymmetric DSGC
Inhibitory input
Excitatory input
Preferred side SAC
Null side SAC
soma
DSGC PD
B.
Symmetric DSGC
Preferred side SAC
Null side SAC
soma
DSGC PD

FIGURE 2

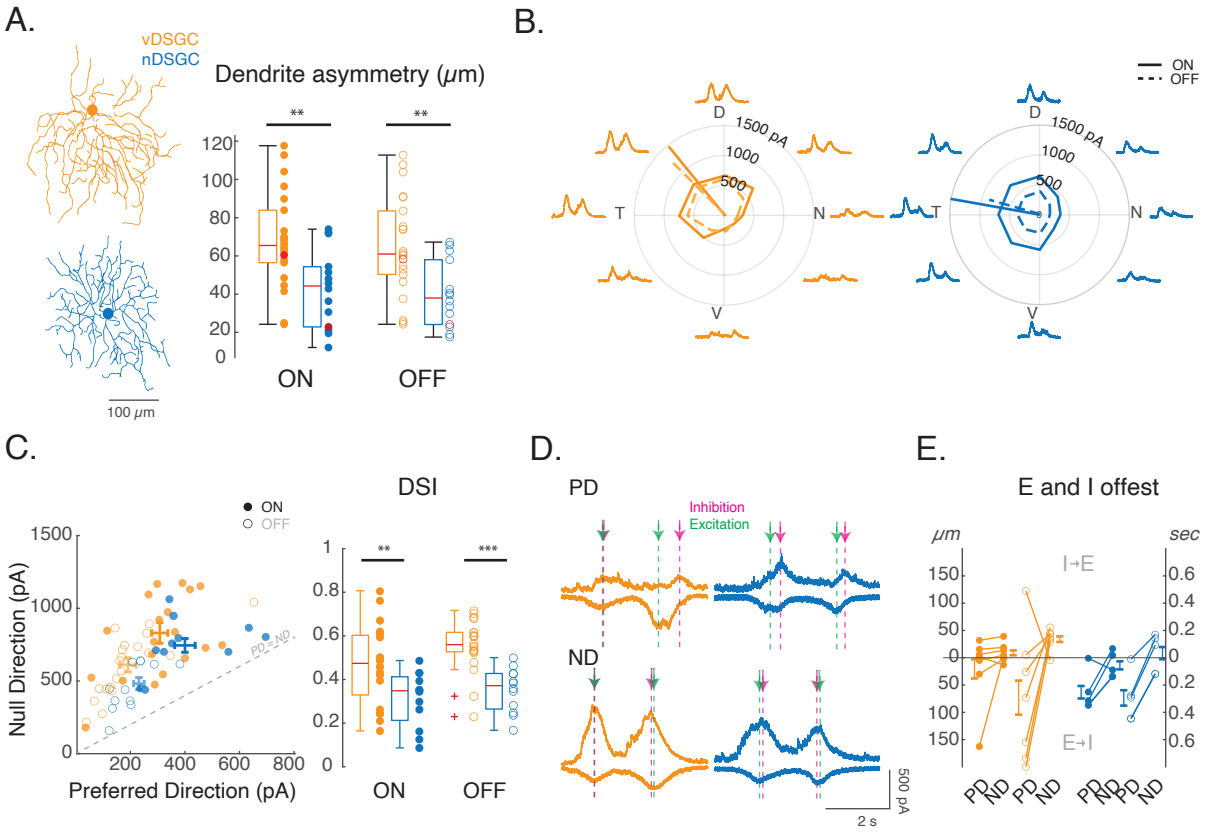
A.
vDSGC
nDSGC
100 μm
Dendrite asymmetry (μm)
**
**
120
100
80
60
40
20
0
ON
OFF
B.
ON
OFF
D
1500 pA
1000
500
T
N
V
C.
DSI
ON
OFF
1500
1000
500
0
Null Direction (pA)
200
400
600
800
Preferred Direction (pA)
PD = ND
1
0.8
0.6
0.4
0.2
0
**
***
ON
OFF
D.
PD
Inhibition
Excitation
ND
500 pA
2 s
E.
E and I offest
μm
sec
150
100
50
0
50
100
150
I→E
E→I
0.6
0.4
0.2
0
0.2
0.4
0.6
PD
ND
PD
ND
PD
ND
PD
ND

FIGURE 3

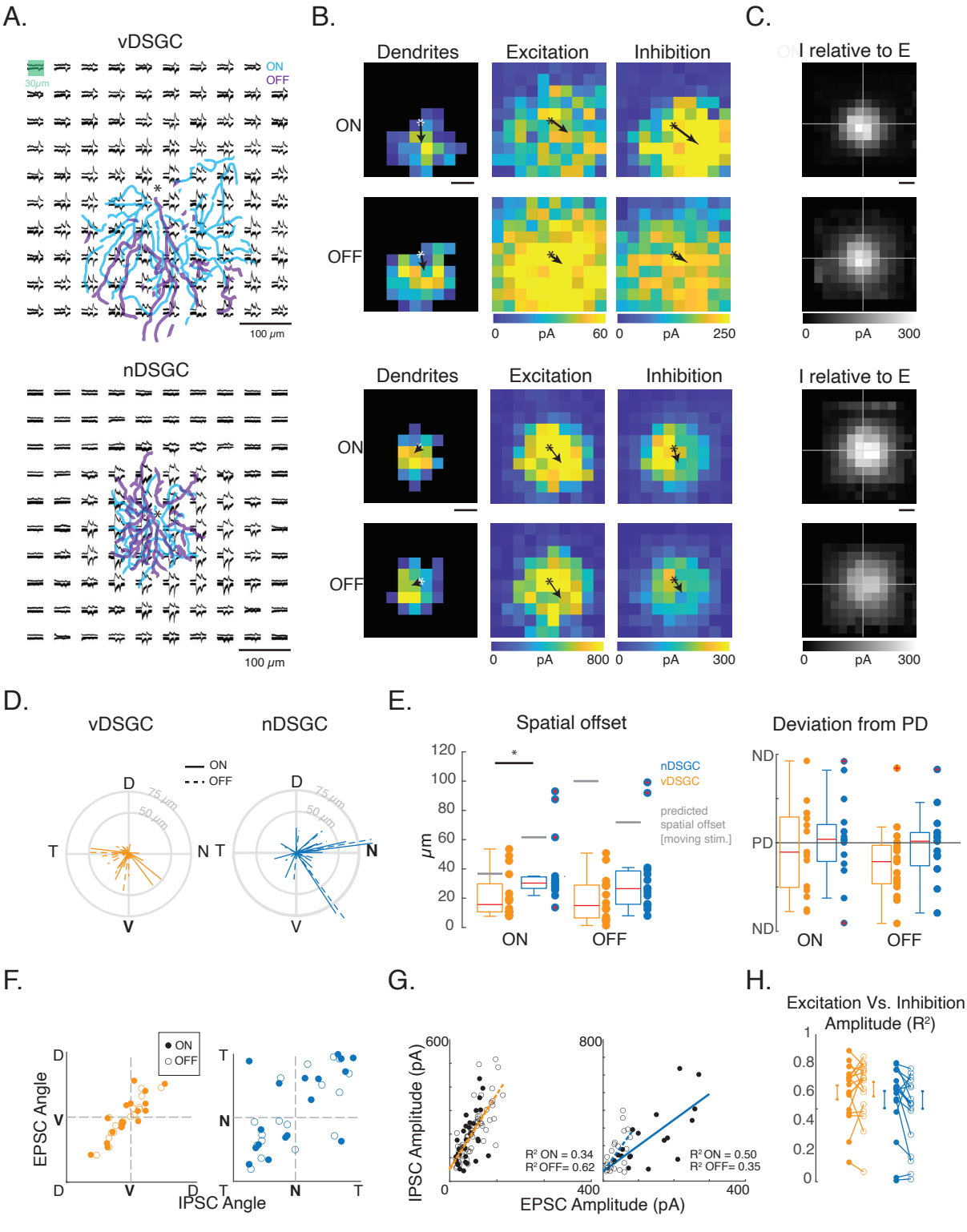
A.
vDSGC
ON
OFF
30μm
100 μm
nDSGC
100 μm
B.
Dendrites
Excitation
Inhibition
ON
OFF
0 pA 60
0 pA 250
0 pA 800
0 pA 300
C.
I relative to E
0 pA 300
D.
vDSGC
nDSGC
ON
OFF
D
T
N
V
75 μm
50 μm
E.
Spatial offset
nDSGC
vDSGC
predicted spatial offset [moving stim.]
μm
ON
OFF
Deviation from PD
ND
PD
F.
EPSC Angle
IPSC Angle
G.
IPSC Amplitude (pA)
EPSC Amplitude (pA)
R² ON = 0.34
R² OFF= 0.62
R² ON = 0.50
R² OFF= 0.35
H.
Excitation Vs. Inhibition Amplitude (R²)

FIGURE 4

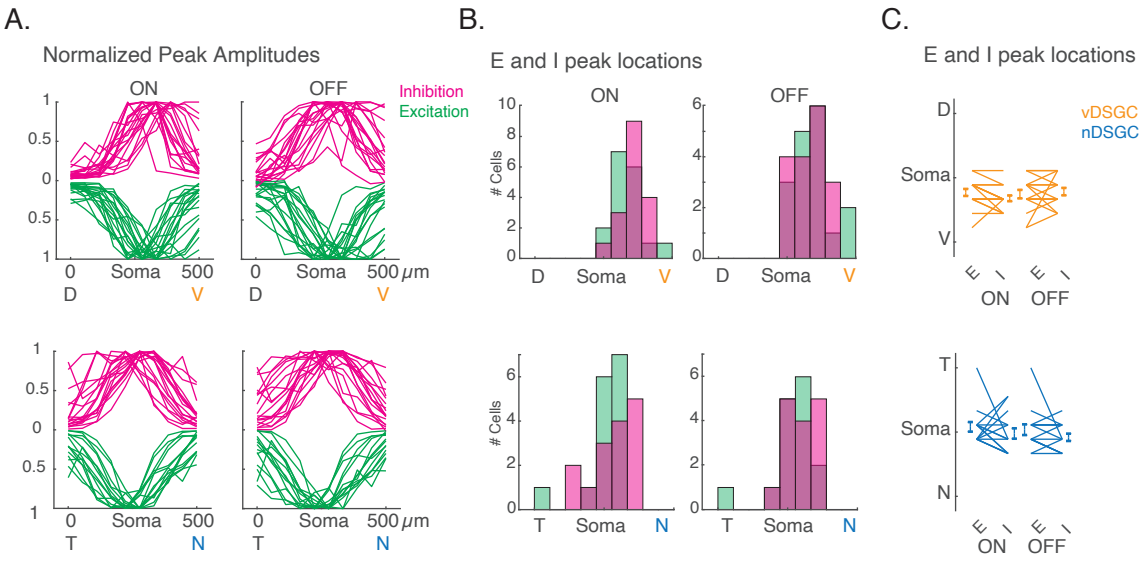
A.
Normalized Peak Amplitudes
ON
OFF
Inhibition
Excitation
1
0.5
0
0.5
1
0
Soma
500
500 μm
D
V
T
N
B.
E and I peak locations
ON
OFF
Cells
10
8
6
4
2
0
D
Soma
V
T
N
C.
E and I peak locations
vDSGC
nDSGC
D
Soma
V
T
N
E
I
ON
OFF

FIGURE 5

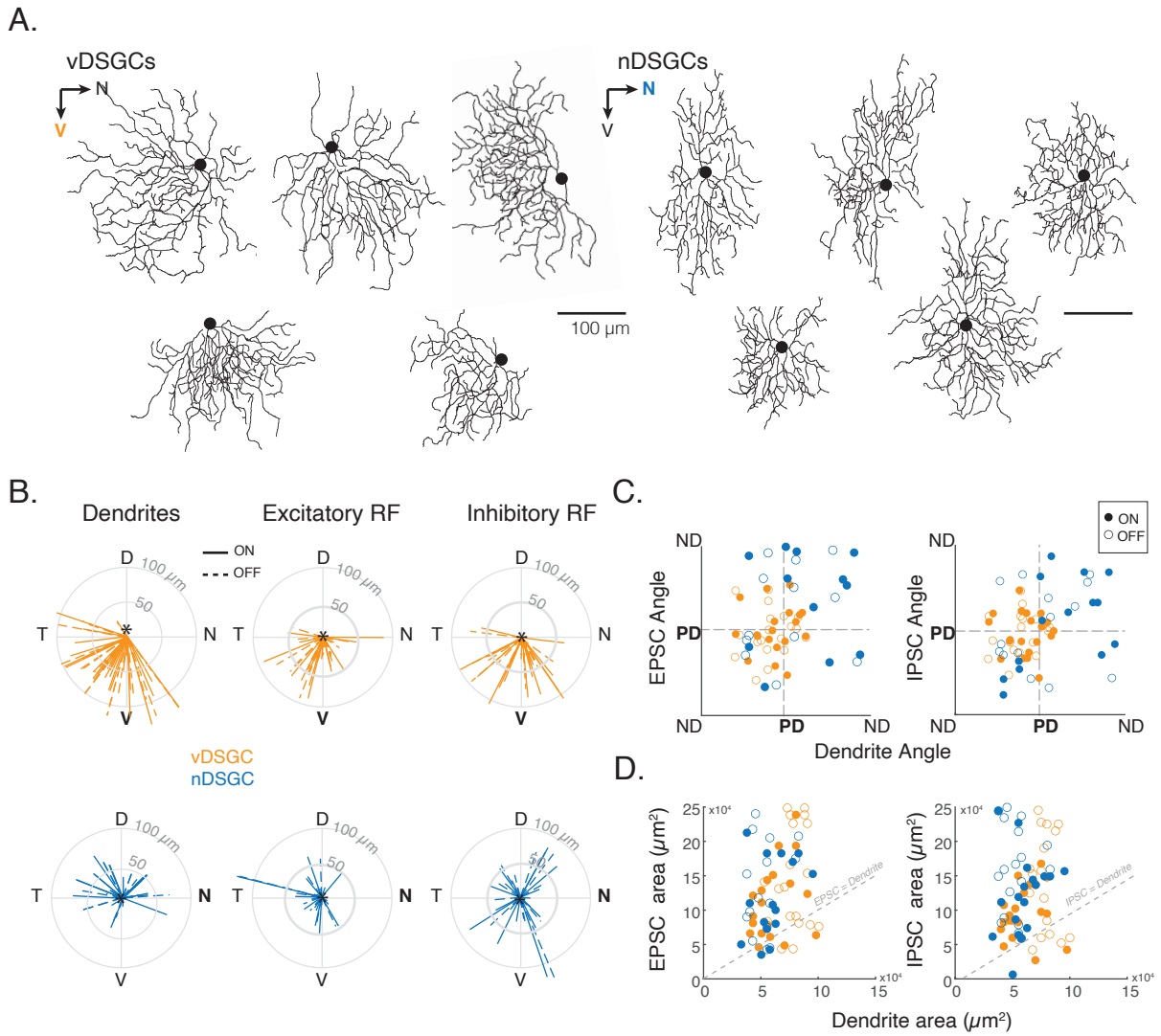
A.
vDSGCs
N
V
nDSGCs
N
V
100 µm
B.
Dendrites
Excitatory RF
Inhibitory RF
ON
OFF
D
T
N
V
100 µm
50
vDSGC
nDSGC
C.
ND
PD
EPSC Angle
IPSC Angle
Dendrite Angle
ON
OFF
D.
EPSC area (µm²)
IPSC area (µm²)
Dendrite area (µm²)
EPSC = Dendrite
IPSC = Dendrite
x10⁴

FIGURE 6

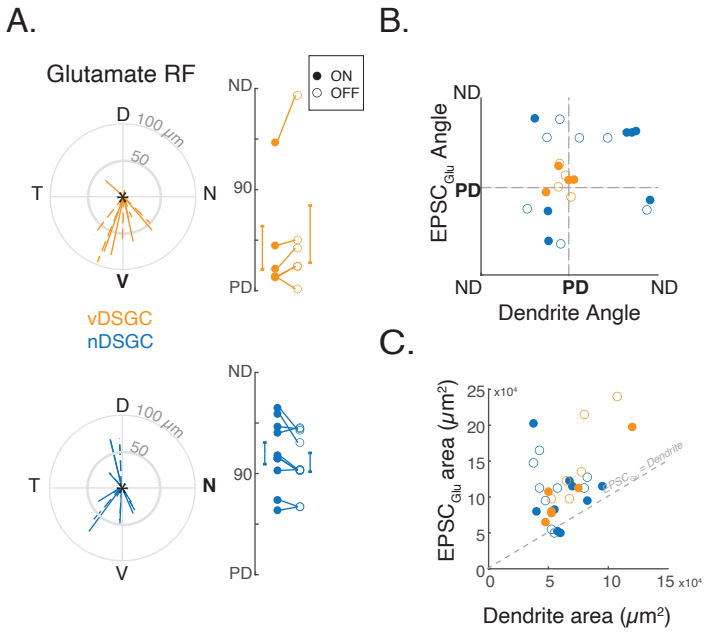

Figure 6: DSGC glutamatergic receptive field is more restricted to the dendritic field.
A) Left: Summary data represented as polar plots of the vectors from the soma to the excitatory glutamate receptive field center of mass in the presence of 100 μM Hexamethonium in vDSGCs (orange, top) and nDSGCs (blue, bottom) for ON (solid) and OFF (dashed) responses. Right: Summary data representing the deviation of the vector angle (right) from the vDSGC(orange,top) and nDSGC (blue,bottom) preferred direction. Data for ON (filled circle) and OFF (open circle) plotted separately.
B) Summary data displaying the relationship between the orientation of the vector from the soma to the glutamatergic excitatory receptive field ($EPSC_{Glu}$) center of mass, relative to the orientation of the dendritic center of mass in vDSGCs (orange, n=5 cells) and nDSGCs (blue, n=9 cells).
C) Summary data comparing the relationship between dendritic area and the glutamatergic excitatory ($EPSC_{Glu}$) response areas within the receptive field, and the area of the dendrites for each vDSGC (orange) and nDSGC (blue). Data for ON (filled circle) and OFF (open circle) plotted separately. Statistical significance of the $EPSC_{Glu}$/Dendrite ratio determined with one-sided t-test and compared to a ratio of 1 ($EPSC_{Glu}$=Dendrite area) - All p values <0.001.

TABLE 1 (Related to figure 2)	ON Responses				OFF Responses			
	vDSGCs		nDSGCs		vDSGCs		nDSGCs	
	Mean ± SD		Mean ± SD		Mean ± SD		Mean ± SD	
Dendrite Asymmetry (µm)	66.67	25.50	43.08	20.51	65.83	25.40	39.98	17.32
Dendrite Angle (˚)	242.11	41.70	146.87	67.12	230.80	40.56	234.14	76.06
IPSC Amplitude (ND) (pA)	794.60	309.80	665.99	146.30	574.92	181.10	449.37	102.50
IPSC Amplitude (PD) (pA)	290.70	136.81	325.75	101.98	173.58	88.61	212.96	63.23
IPSC DSI	0.48	0.19	0.34	0.14	0.56	0.11	0.31	0.17
E - I Timing difference (ND) (msec)	0.0360	0.0673	-0.0531	0.0924	0.1362	0.0764	0.0397	0.1449
E - I Timing difference (PD) (msec)	-0.0816	0.2621	-0.2576	0.1343	-0.2924	0.4675	-0.1735	0.3251
E - I Spatial Offset (ND) (µm)	13.32	13.07	21.77	12.73	35.31	16.23	33.52	5.58
E - I Spatial Offset (PD) (µm)	36.04	57.12	64.39	33.57	109.55	76.79	74.67	44.58

TABLE 2 (Related to Figure 3)	ON Responses				OFF Responses			
	vDSGCs Mean ± SD		**nDSGCs** Mean ± SD		**vDSGCs** Mean ± SD		**nDSGCs** Mean ± SD	
RF Spatial offset magnitude (E-I) (µm)	20.796	15.537	38.140	23.394	19.831	14.490	33.716	27.010
RF Spatial offset deviation from PD (˚)	-7.532	86.592	7.895	86.951	-40.793	72.278	-4.971	70.196
	R	p value	R	p value	R	p value	R	p value
EPSC angle Vs. IPSC angle Pearson's Correlation	0.83	2.70E-05	0.67	5.00E-03	0.92	1.60E-09	0.67	6.30E-03

TABLE 3 (Related to Figure 5)	ON Responses				OFF Responses			
	vDSGCs		**nDSGCs**		**vDSGCs**		**nDSGCs**	
	Mean ± SD		Mean ± SD		Mean ± SD		Mean ± SD	
Soma to EPSC COM vector magnitude	50.795	25.043	37.012	29.581	42.039	20.210	31.505	28.828
Soma to EPSC COM vector Angle (˚)	267.380	45.426	195.732	65.676	260.717	44.738	196.601	60.523
Soma to IPSC COM vector magnitude	62.997	27.202	45.048	29.685	53.888	20.794	37.503	31.937
Soma to IPSC COM vector Angle (˚)	264.889	41.454	295.957	74.892	259.792	42.779	279.538	75.550
EPSC area/Dendrite area	1.931	0.764	2.273	1.193	1.904	0.929	2.865	1.347
IPSC area/Dendrite area	1.643	0.620	2.323	1.302	1.860	0.911	3.313	1.542
	R	p value	R	p value	R	p value	R	p value
EPSC angle Vs. Dendrite angle Pearson's Correlation	0.09	0.72	0.49	0.1	0.084	0.73	0.4	0.19
IPSC angle Vs. Dendrite angle Pearson's Correlation	-0.08	0.74	0.78	0.0006*	0.24	0.31	0.39	0.17
EPSC area Vs. Dendrite area Pearson's Correlation	0.35	0.14	0.35	0.24	0.13	0.59	0.21	0.5
IPSC area Vs. Dendrite area Pearson's Correlation	0.13	0.6	0.13	0.62	0.11	0.66	-0.05	0.83

COM = center of mass.

TABLE 4 **(Related to Figure 6)**	ON Responses				OFF Responses			
	vDSGCs		**nDSGCs**		**vDSGCs**		**nDSGCs**	
	Mean ± SD		Mean ± SD		Mean ± SD		Mean ± SD	
Soma to $EPSC_{Glu}$ COM vector magnitude (µm)	58.283	22.436	41.088	24.233	52.304	30.230	39.739	19.977
Soma to $EPSC_{Glu}$ COM vector Angle (˚)	266.943	47.114	200.467	67.992	272.876	53.750	220.879	71.833
$EPSC_{Glu}$ area/Dendrite area	1.611	0.279	1.830	1.396	1.975	0.432	2.148	1.127
	R	p	R	p	R	p	R	p
$EPSC_{Glu}$ area Vs. Dendrite area Pearson's Correlation	0.96	0.003	-0.14	0.7	0.88	0.02	-0.12	0.76

COM = center of mass.

CHAPTER 4: Conclusions and Future Directions

Visual experience influences the orientation of DSGC dendrites

In this thesis, we demonstrate that visual experience, following eye opening, is required for asymmetric ventral preferring DSGCs (vDSGCs) to orient their dendrites ventrally, and that proper orientation is prevented by dark rearing. How might sensory activity influence dendritic orientation? One clue comes from examples of other neurons in the nervous system, whose asymmetric dendritic arbors are oriented towards their presynaptic partners. This includes ganglion cells in the zebrafish retina (Choi et al., 2010), layer IV Stellate cells in the somatosensory cortex (Greenough & Chang, 1988; Nakazawa et al., 2018; Woolsey & Van der Loos, 1970), mitral cells of the rodent olfactory bulb (Blanchart et al., 2006; Hinds & Ruffett, 1973), among others (*for review see* Wong and Ghosh, 2002). In these examples, altering afferent activity through sensory deprivation similarly alters dendritic orientation.

Despite the prevalence of this form-function relationship across the nervous system, we still know very little about the mechanisms by which sensory activity, or patterned afferent input, can influence the dendritic cytoskeleton. Recent studies have revealed that sensory experience may be required for the establishment of dendritic orientation through mechanisms that influence gene transcription. In the rodent somatosensory cortex, in situ hybridization has revealed that the transcription factor BTBD3 is highly localized to the whisker barrels during development and that activity-dependent nuclear translocation of BTBD3 is required for the orientation of stellate neuron dendrites towards the barrel hollows. Similarly, BTBD3 is implicated in the orientation of dendrites in ferret visual cortex towards the center of ocular dominance columns whereby monocular enucleation and BTBD3 shRNA knock-down lead to misorientation of layer IV excitatory neuron dendrites (Matsui et al., 2013). Further investigations into the activity-dependent regulation of gene expression in DSGCs of normal vs. visually deprived animals would lend us a deeper mechanistic understanding of how activity influences the orientation of asymmetric DSGCs.

What aspects of visual experience influence the direction selective network? A recent study using trained visual experience paradigms has shown an increase in gap junction coupling in vDSGCs of animals only experience upward (preferred direction) motion and display synchronized population spike responses (Zhang et al., 2020). Null direction training had no effect on coupling, and neither did changing contrast, luminance and temporal frequency regimes of the training stimulus. Gap junction networks between vDSGCs are hypothesized to enable motion detection at scotopic light levels and motion discrimination at high light levels (Yao et al., 2018). Although we find that gap junction coupling between vDSGCs are unchanged in dark-reared animals, this suggests that structured visual experience and synchronized network function, provided by sequential activation of gap junction networks and presynaptic inputs may play a key role in mediating the orientation of vDSGC dendrites towards their preferred direction. Further dissection of vDSGC gap junction networks, combined with pharmacologic and transgenic manipulation of the specific connexin proteins expressed in vDSGCs, will enable a greater understanding in whether network synchronization mediates dendritic remodeling, or whether dendritic orientation facilitates network synchronization.

Dendritic morphology plays a role in post synaptic mechanisms for directional tuning

Thus far, vDSGCs are the only DSGC subtype to exhibit directional tuning in the absence of inhibitory input (Trenholm et al., 2011). In the presence of the $GABA_A$ receptor antagonist gabazine, other subtypes of anterior and posterior preferring DSGCs lose their directional tuning (Ackert et al., 2009; Bos et al., 2016; Rivlin-Etzion et al., 2011; Wei et al., 2011). However, we find that it is the precise correlation of dendritic orientation and preferred direction that enables normally-reared adult vDSGCs to possess postsynaptic mechanisms for encoding motion direction, while dark-reared vDSGCs that no longer exhibit this correlation, lose their directional tuning.

Computational modeling experiments have shown that vDSGCs may possess nonlinear conductances, like voltage gated sodium channels, at their distal dendrites, that mediate efficient active integration of excitatory inputs during preferred direction motion (Trenholm et al. 2011). However, future experimental investigation of the sources of active nonlinear integration are necessary for a mechanistic understanding of a) why postsynaptic mechanisms for DSGC tuning exist given the robust presynaptic circuit tuning, and b) whether unoriented dendrites in dark-reared vDSGCs still possess active conductances, or whether visual experience influences their expression.

Dendritic morphology does not influence presynaptic mechanisms for directional tuning

Elucidating the wiring maps of neuronal circuits provides a conceptual framework for understanding the various computations of the nervous system. Despite our comprehensive knowledge of neuronal circuitry, the fundamental process by which a neuron selectively connects with its targets remains largely unknown. However, across the nervous system, dendritic morphology is thought to influence synaptic organization. To this end, this thesis adds a piece to this puzzle. Namely, that the shape of a DSGC's dendrite does not dictate the organization of its presynaptic excitatory and inhibitory inputs relative to each other in order to mediate its directional computation.

The interaction of complementary recognition tags expressed by pre- and postsynaptic partners (Sperry, 1963) has long been invoked as the main strategy to explain the process of synaptic specificity. This strategy implies the existence of an intricate recognition code that establishes connection selectivity, but in many brain regions it has been difficult to determine the identity and logic of cellular recognition determinants (Zipursky & Sanes, 2010). Future investigations of the link between hard-wired cellular recognition molecules and activity-dependent determinants of gene expression will elucidate the molecular cues that determine synaptic specificity retina as well as the role of sensory-evoked and spontaneous activity in synaptic targeting.

REFERENCES

Ackert, J. M., Farajian, R., Völgyi, B., & Bloomfield, S. A. (2009). GABA blockade unmasks an off response in on direction selective ganglion cells in the mammalian retina. *Journal of Physiology*, *587*(18), 4481–4495. https://doi.org/10.1113/jphysiol.2009.173344

Blanchart, A., De Carlos, J. A., & López-Mascaraque, L. (2006). Time frame of mitral cell development in the mice olfactory bulb. *Journal Comparative and General Neurology*, *543*(August 2006), 496–529. https://doi.org/10.1002/cne

Bos, R., Gainer, C., & Feller, M. B. (2016). Role for visual experience in the development of direction-selective circuits. *Current Biology*. https://doi.org/10.1016/j.cub.2016.03.073

Choi, J. H., Law, M. Y., Chien, C. Bin, Link, B. A., & Wong, R. O. L. (2010). In vivo development of dendritic orientation in wild-type and mislocalized retinal ganglion cells. *Neural Development*. https://doi.org/10.1186/1749-8104-5-29

Greenough, W. T., & Chang, F. L. F. (1988). Dendritic pattern formation involves both oriented regression and oriented growth in the barrels of mouse somatosensory cortex. *Developmental Brain Research*, *43*(1), 148–152. https://doi.org/10.1016/0165-3806(88)90160-5

Hinds, J. W., & Ruffett, T. L. (1973). Mitral cell development in the mouse olfactory bulb: Reorientation of the perikaryon and maturation of the axon initial segment. *Journal of Comparative Neurology*, *151*(3), 281–305. https://doi.org/10.1002/cne.901510305

Matsui, A., Tran, M., Yoshida, A. C., Kikuchi, S. S., Mami, U., Ogawa, M., & Shimogori, T. (2013). BTBD3 Controls Dendrite Orientation Toward Active Axons in Mammalian Neocortex. *Science*, *342*(November), 1114–1118.

Nakazawa, S., Mizuno, H., & Iwasato, T. (2018). Differential dynamics of cortical neuron dendritic trees revealed by long-term in vivo imaging in neonates. *Nature Communications*, *9*(1). https://doi.org/10.1038/s41467-018-05563-0

Rivlin-Etzion, M., Zhou, K., Wei, W., Elstrott, J., Nguyen, P. L., Barres, B. A., Huberman, A. D., & Feller, M. B. (2011). Transgenic Mice Reveal Unexpected Diversity of On-Off Direction-Selective Retinal Ganglion Cell Subtypes and Brain Structures Involved in Motion Processing. *Journal of Neuroscience*. https://doi.org/10.1523/JNEUROSCI.0564-11.2011

Sperry, R. W. (1963). Chemoaffinity in the orderly growth of nerve fiber patterns and connections. *Proceedings of the National Academy of Sciences*, 703–710.

Trenholm, S., Johnson, K., Li, X., Smith, R. G., & Awatramani, G. B. (2011). Parallel mechanisms encode direction in the retina. *Neuron*. https://doi.org/10.1016/j.neuron.2011.06.020

Wei, W., Hamby, A. M., Zhou, K., & Feller, M. B. (2011). Development of asymmetric inhibition underlying direction selectivity in the retina. *Nature*. https://doi.org/10.1038/nature09600

Woolsey, T. A., & Van der Loos, H. (1970). The structural organization of layer IV in the somatosensory region (S I) of mouse cerebral cortex. The description of a cortical field composed of discrete cytoarchitectonic units. *Brain Research*, *17*(2), 205–242. https://doi.org/10.1016/0006-8993(70)90079-X

Yao, X., Cafaro, J., McLaughlin, A. J., Postma, F. R., Paul, D. L., Awatramani, G., & Field, G. D. (2018). Gap Junctions Contribute to Differential Light Adaptation across Direction-Selective Retinal Ganglion Cells. *Neuron*, *100*(1), 216-228.e6.

https://doi.org/10.1016/j.neuron.2018.08.021
Zhang, L., Wu, Q., & Zhang, Y. (2020). Early visual motion experience shapes the gap junction connections among direction selective ganglion cells. *PLoS Biology*, *18*(3), 10–13. https://doi.org/10.1371/journal.pbio.3000692
Zipursky, S. L., & Sanes, J. R. (2010). Review Chemoaffinity Revisited : Dscams , Protocadherins , and Neural Circuit Assembly. *Cell*, *143*(3), 343–353. https://doi.org/10.1016/j.cell.2010.10.009